University of New Mexico
UNM Digital Repository

Chemical and Biological Engineering ETDs | Engineering ETDs

Fall 11-10-2016

Dielectric Characterization of Mylar and The Effects of Doping Processes

Cami B. Belcher
University of New Mexico

Follow this and additional works at: https://digitalrepository.unm.edu/cbe_etds

 Part of the Chemical Engineering Commons

Recommended Citation
Belcher, Cami B.. "Dielectric Characterization of Mylar and The Effects of Doping Processes." (2016).
https://digitalrepository.unm.edu/cbe_etds/56

This Thesis is brought to you for free and open access by the Engineering ETDs at UNM Digital Repository. It has been accepted for inclusion in Chemical and Biological Engineering ETDs by an authorized administrator of UNM Digital Repository. For more information, please contact disc@unm.edu.

Cami Beth Belcher
Candidate

Chemical and Biological Engineering
Department

This thesis is approved, and it is acceptable in quality and form for publication:

Approved by the Thesis Committee:

Fernando Garzon, Chairperson

Leah Appelhans

Richard Kemp

DIELECTRIC CHARACTERIZATION OF MYLAR AND THE EFFECTS OF DOPING PROCESSES

by

CAMI BETH BELCHER

B.S., CHEMISTRY, UNIVERSITY OF NEW MEXICO, 2014

THESIS

Submitted in Partial Fulfillment of the
Requirements for the Degree of

Master of Science

Chemical Engineering

The University of New Mexico
Albuquerque, New Mexico

December 2016

ACKNOWLEDGEMENTS

I would first like to thank my mentor Leah Appelhans for the endless support, guidance and knowledge she has imparted. The abilities that I have acquired through this experience will carry me forward and prove instrumental in my career. I would also like to thank my advisor and committee chair Dr. Fernando Garzon for his support through this process as well as Rick Kemp for serving as a member on my committee. I would also like to thank Pat Finnegan, Alex Robinson and Ted Parson for their support of the work in this thesis and their contributions to sample preparation and instrumentation design. I am also extremely thankful for the vast knowledge and skills I have gained from my colleagues at Sandia National Laboratories, including Departments 1853 and 2632.

I would like to thank Sandia National Laboratories for funding this research. Sandia National Laboratories is a multi-program laboratory managed and operated by Sandia Corporation, a wholly owned subsidiary of Lockheed Martin Corporation, for the U.S. Department of Energy's National Nuclear Security Administration under contract DE-AC04-94AL85000. SAND2016-11533 T.

DIELECTRIC CHARACTERIZATION OF MYLAR AND THE EFFECTS OF DOPING PROCESSES

By

Cami Beth Belcher

B.S., Chemistry, University of New Mexico, 2014
M.S., Chemical Engineering, University of New Mexico, 2016

ABSTRACT

Mylar® polymer is a bi-axially oriented polyethylene terephthalate (PET) polymer film used widely as a dielectric, specifically in capacitors. The dielectric characteristics of Mylar have been well studied and documented over the years; however, many of the mechanisms responsible for dielectric breakdown and failure are not understood for modified versions of the material. Previous studies on Mylar confirm that factors such as temperature, humidity, and voltage ramp rates can also have a significant effect on the dielectric properties and measurement of the dielectric properties. This study seeks to determine how dielectric properties, including permittivity, dielectric loss, and breakdown strength, are affected by doping of the polymer. To do this, two types of Mylar films, virgin film and film doped with a small-molecule electron-acceptor, are tested. Both types of materials are tested under a variety of environmental and experimental conditions, including testing at elevated temperatures, varying relative humidity, and varying ramp rates in dielectric breakdown testing. Analysis of permittivity, dielectric loss, and breakdown strength will be presented comparing virgin and doped Mylar to gain insight into the effects of doping with electron-acceptor molecules on dielectric properties under these varying environmental and test conditions.

Table of Contents

Introduction:

Polyethylene terephthalate (PET), also known by the DuPont trade name, Mylar®, is a condensation polymer commonly synthesized by the transesterification/polycondensation reaction shown in Figure 1. PET was originally synthesized by the direct reaction of terephthalic acid and ethylene glycol, however the synthetic mechanism shown in Figure 1, using the dimethyl ester, is preferred for industrial manufacture. [5] Mylar films are produced by extrusion, followed by biaxial orientation of the film with heat setting to reinforce that orientation. Biaxial orientation has been found to significantly improve the mechanical properties of the material. [5, 48]

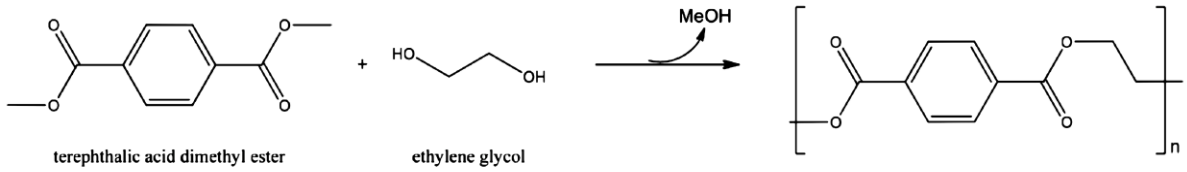

Figure 1: Synthesis of PET

When PET was first utilized in its fiber form in the 1950's its potential as a dielectric material was recognized and the production of DuPont's electrical grade PET films, Mylar C, for dielectric uses began. [3-4] Early dielectric characterization carried out by Amborski [4] reported an AC dielectric strength of 1770 kV/cm in a 50 micron Mylar C film at a frequency of 60Hz. The DuPont electrical characterization data sheet from 2003 reports a value of 7 kV/mil for a film tested with the same experimental conditions. This change in dielectric strength could be due to the improved film quality

and processing techniques, as improvements in chemical synthesis and processing techniques of PET have improved over the last 70 years. This is important to note when attempting to compare data obtained from different studies; film quality, treatment and production techniques can significantly change the dielectric properties of the material. In addition the test methods used may also significantly affect the measured results from dielectric testing.

While there has been thorough research completed on virgin Mylar since the realization of its value as a dielectric material, there is relatively little understanding of the dielectric properties and breakdown mechanisms of materials that have been modified with a dopant. The doped material is altered with a small-molecule electron-acceptor; this modification can affect the movement of electrons and charge carriers within the material, in turn potentially altering the dielectric properties and breakdown mechanisms relative to the virgin material. The goal of this study is to investigate the dielectric properties of both virgin Mylar and modified Mylar to determine the effects of the dopant and possible defects introduced to the material by the doping process on the electrical properties. A set of experiments examining the permittivity, dielectric loss and breakdown strength of the two materials over a range of environmental and test conditions has been devised to identify differences, if any, between virgin and modified Mylar.

Objective of thesis:

A large body of work has been completed on Mylar for dielectric applications, but there is still a need to understand the effect of dopants and doping processes on the dielectric properties. In order to establish a reliable control by which to compare doped materials, it is important to create a collection of Mylar data using the same test conditions used for the doped material. Both virgin and modified Mylar were tested under a variety of test conditions to determine the best methods and procedures, as well as to determine if the two types of films behave differently under any of the varying test conditions. These tests included elevated temperatures both above and below T_g, DC voltage ramp rate, humidity effects, effects of varying electrode areas, single electrode testing compared to multi-electrode samples, and finally a short-term aging study. The data collected enables comparison of the materials on a broad spectrum of conditions.

Another important aspect of dielectric materials characterization is lifetime prediction and failure testing, also known as highly accelerated life testing (HALT), and highly accelerated stress screening (HASS). HALT/HASS confirms that the product and material are designed properly and verified by a series of tests, ensuring reliable products with predictable lifetimes. However, accelerated aging can activate degradation mechanisms that are different from those seen in field aging and it is unknown if these occurs in Mylar. As part of an ongoing aging study to determine lifetime predictability and reliability, this thesis investigates the effects of temperature on the materials over short time periods. Short-term aging and testing completed at elevated temperatures, combined with previous long-term aging studies will enable future studies comparing accelerated aging methods to real-time aging that occurs in the field.

Overall the hypothesis of this thesis is: what effect does temperature, humidity, electrode area, DC voltage ramp rate, and doping processes have upon on the dielectric properties of virgin Mylar and doped Mylar. Conclusions from the data collected are the first step in beginning to understand material lifetime, failure mechanisms, and consistency of accelerated aging tests such as HALT/HASS with failure of field-aged dielectrics.

Chapter 1: Dielectric Properties, Breakdown Phenomena and Experimental Design Considerations

1.1: Dielectric Properties- Capacitance, Permittivity and Dielectric Loss

1.1.1: Capacitor Basics

The function of a capacitor is to store and release electric charge efficiently. Capacitors are widely used as reliable power sources over a variety of applications due to their efficiency, reliability and customizability. Capacitors can vary widely in shape, size, and design but the simplest form of a capacitor is the parallel plate capacitor, composed of two conductors separated by an electrically insulating material known as the dielectric. The construction of this design is shown below in Figure 1. A few of the common properties used to determine the quality and performance of the dielectric material used in the capacitor include capacitance, permittivity, dielectric loss, and dielectric breakdown strength. Capacitance, C, (Equation 1) is the amount of charge that can be stored in a capacitor and mathematically it is defined as the amount of stored charge, Q, divided by the voltage difference between the two conducting plates, ΔV. Equation 2 represents the capacitance for a parallel plate in terms of relative permittivity, ε_r, permittivity of vacuum, ε_0, electrode area, A, and dielectric thickness, d. Capacitance for a parallel plate is dependent on three main factors: 1) electrode area 2) dielectric thickness 3) the permittivity of the dielectric material. One of the most important components of a capacitor is the dielectric material utilized; the material's dielectric properties can define and limit the capacitor's capabilities.

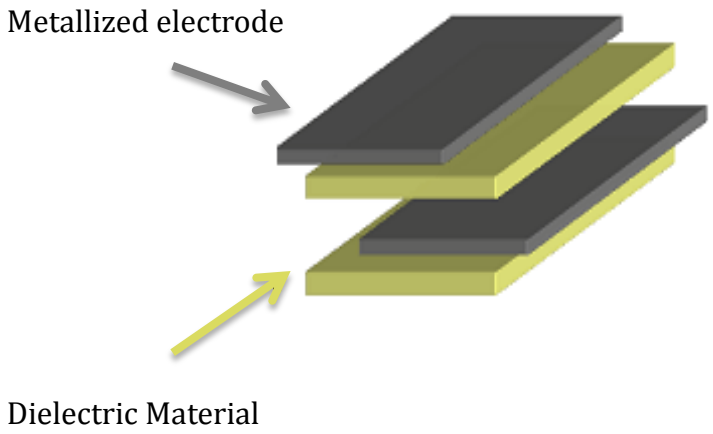

Figure 2: Parallel-Plate Capacitor Configuration

$$C = \frac{Q}{\Delta V}$$

Equation 1: Capacitance

$$C = \frac{\varepsilon_r \varepsilon_0 A}{d}$$

Equation 2: Capacitance for a parallel plate

Dielectric materials are insulators that store energy by means of polarization. When a field is applied to a material, the charges or dipoles do not flow through the material but slightly shift from their average equilibrium positions, leading to a dielectric polarization. Polarization of the dielectric produces an electric field opposing the field between the conductive plates, enabling more charge storage in the capacitor. The dielectric constant, also referred to as relative permittivity, characterizes the reduction of the effective electric field due to the polarization; increased polarization results in greater permittivity and thus greater capacitance values. The dielectric performance of these materials can be characterized by different properties; however, in this work three

dielectric properties: permittivity, dielectric loss, and dielectric breakdown strength are measured.

1.1.2: Dielectric polarization and permittivity

The defining property of a dielectric material is the dielectric constant, often referred to as the relative permittivity, denoted as ε_r, and measured relative to the permittivity of free space, ε_0, in Equation 3. Permittivity is a measurement of the reduction of the effective electric field between the two conducting plates of the capacitor due to the polarization of the medium.

There are four main types of polarization that can occur in dielectric materials: electronic, ionic, orientational, and interfacial polarization. These polarization mechanisms are frequency dependent and contributions to the overall polarization diminish as frequency is increased. Electronic polarization is electron displacement relative to the positive charges in the nucleus and remains active at the highest frequencies. [6] Displacement of electrons due to electronic polarization results in a relatively small contribution to the permittivity relative to other mechanisms. Ionic polarization is common to materials with ions located in defined lattice sites and remains active at high frequencies. In an ionic material, the field can displace ions relative to their equilibrium lattice positions. The effect of this change can be a net dipole moment and result in polarization of the medium. Orientational polarization is the shifting of natural dipoles, which are usually randomly oriented within a material that is not under field, to align with the applied field. [6] This polarization mechanism is active at mid-range frequencies. The contribution of orientational polarization is comparatively small relative to ionic polarization mechanisms. However, it is the main polarization mechanism of

most polymers and can create significant differences in dielectric properties between different materials. Interfacial polarization occurs whenever there is an accumulation of charge at an interface between two surfaces, grain boundaries, or interphase boundaries and it is seen in low to mid-range frequencies. It can contribute significantly in solid dielectrics due to the interfaces of the conducting plates and the dielectric medium. Interfacial polarization is also often seen due to the trapping of electrons or holes at defects at the surface. [9]

Figure 3 is a representative plot showing polarization mechanisms that are active over a range of frequencies. The specific frequency ranges shown in Figure 3 are material dependent. The top plot, labeled ε_r', shows the permittivity and the mechanisms active. The lower plot, labeled ε_r'', is the dielectric loss. As is evident from Figure 3, dielectric loss is at a maximum when the frequency of the external field coincides with the relaxation frequency of a polarization mechanism. When perturbation frequencies exceed the relaxation frequency for a polarization mechanism, that particular mechanism cannot couple with the oscillating field and no longer contributes to the polarization of the material, leading to decreases in permittivity and in some cases increasing loss.

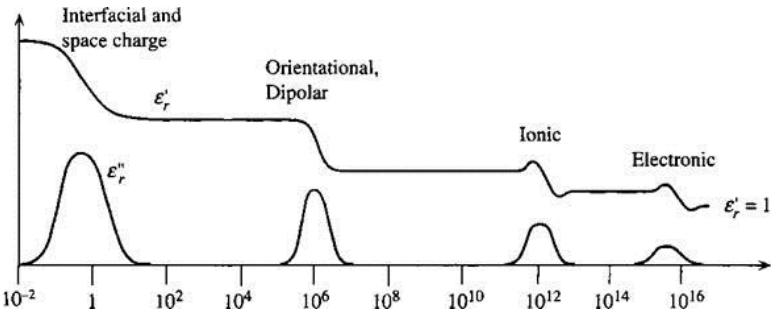

Figure 3: Polarization mechanisms over a range of frequencies

http://chemwiki.ucdavis.edu/u_Materials/Optics/Dielectric_Polarization

1.1.3: Dielectric Loss

Dielectric loss is a measurement of the dissipation of energy within a dielectric material. In an ideal dielectric material, there would no dissipation of energy, however, real-world materials experience loss for a variety of reasons, leading to non-ideal material properties. When loss mechanisms are not active within a dielectric, the current leads the voltage by 90 degrees. However, when loss does occur, a phase lag is introduced, as the dipoles are no longer able to immediately follow the changes of the field. The resultant phase angle will now be less than 90 degrees. The difference between the actual phase angle and 90 degrees is referred to as the loss angle. This is represented in Figure 4.The value of tanδ is the dissipation factor, defined at the energy lost per cycle divided by the energy stored per cycle. Dielectric loss, as mentioned previously, is a material-specific property and it varies with frequency. [8] At lower frequencies, the material can more easily achieve full polarization in each cycle. However, at frequencies specific to the material the dielectric is unable to align with the field and a phase lag is introduced, resulting in dielectric loss. Dielectric loss is especially high around the resonant frequencies of the polarization mechanisms mentioned earlier in this section. Dielectric loss is important to understanding the performance of a capacitor and the dielectric medium. It is desirable to minimize losses to increase performance of a dielectric material; loss can also lead to dielectric heating within the material, degrading the insulating properties and increasing the risk for failure.

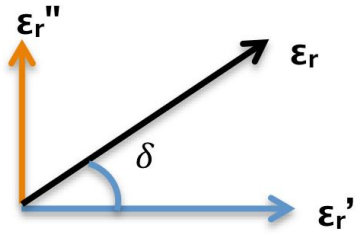

$$tan\delta = \frac{\varepsilon_r{}''}{\varepsilon_r{}'} = Df = \frac{Energy\ lost\ per\ cycle}{Energy\ stored\ per\ cycle}$$

Figure 3: Loss tangent and derivation of dissipation factor

1.2: Dielectric Failure, Breakdown Phenomena, and Conduction in Polymers

The application of an electric field on a dielectric material can cause the movement of free charge carriers and charge injection, resulting in space charge formation at interfaces. A combination of these factors causes electrical stresses within the material, which can lead to dielectric failure. All dielectric materials have a maximum applied field at which they fail and begin to conduct charge rather than insulate. This failure limit is referred to as the dielectric breakdown strength of the material. Failure is experimentally defined by the onset of current flow above a certain value. Breakdown strengths can vary from an array of interrelated factors such as; charge injection, trap depth and density, electron-hole mobility, and Poole-Frenkel emission within the material. Breakdown strength can also be influenced by experimental factors such as temperature, electrode area, dielectric thickness, voltage ramp rate, and self-clearing; all of which are studied in this thesis.

The last century has given rise to many advances in the understanding of dielectric breakdown; however this phenomena and its exact mechanism are still not well understood, particularly in polymer dielectrics. Experimental evidence has shown that

dielectric failure is complex and usually involves a combination of several different, interrelated breakdown mechanisms. [9] These mechanisms can be divided broadly into three different categories: electrical, thermal, and electromechanical.

Electronic breakdown arises from the movement of charge carriers within the dielectric material. These charge carriers can arise from collision ionization, Poole-Frenkel emission, or Schottky emission from the electrode interface. [9] Theoretical descriptions of electronic breakdown vary based on the source of the charge carrier and the interactions of the carrier within the dielectric. Electronic breakdown mechanisms are by far the most difficult mechanisms to pinpoint in a failure event, as it is the highest breakdown value a material can achieve after eliminating all other known secondary effects. [9]

Thermal breakdown is a result of dielectric and/or Joule heating of the bulk material by loss/conduction mechanisms due to the application of an electric field. Thermal failure can occur when the rate at which heat is generated by loss or conduction mechanisms exceeds the rate at which the heat can be dissipated to the surroundings. This thermal imbalance increases the temperature of the material, which in turn increases the dielectric loss and conduction. This cycle continues, resulting in a thermal runaway. Heat generated within the bulk material can be proportional to the frequency in AC field applications; in this case thermal breakdown is of greater concern at high frequencies.

Electrically stressed materials may also fail by mechanical collapse before they experience thermal or electronic breakdown. In high field applications, there are electrostatic forces between the conductors, causing an attractive force between the conductors that compresses the dielectric and creates a field enhancement at the location

of electromechanical stress. This compression from the electrostatic forces leads to physical deformations of the polymer and compromise the electrical integrity of the dielectric.

In real materials, breakdown processes often include contributions from two, or all three of these mechanisms. Electrical breakdown often occurs as a result of thermal damage, such as bond cleavage and decomposition and thermal exposure can also lead to weakening of the mechanical properties of the polymer. As a result it can be difficult to pinpoint a single mechanism that is responsible for failure.

1.3 Dopants, chemical impurity and defects introduced

Doping agents, compounds added to a substance in very low concentrations, are introduced into many materials in order to modify the electrical, optical or mechanical properties of a material, such as PVA, TiO_2, and silica. The introduction of a dopant into the insulator can greatly affect the trap depth [54] and accumulation of space charge. [32] Although research has shown that dopants can enhance charge carrier migration and mobility [32], this is dependent upon the type and properties of the dopant used. Research completed on small-molecule electron accepting dopants in Mylar suggests that the dielectric breakdown strength of the doped material increases slightly from that of the virgin material. [38-41] Previous work concluded that a dopant can create a higher density of deep electron traps, which diminishes mobile charge carrier density and contributes to the increased breakdown strength. It also revealed that doping above a specified concentration could decrease the breakdown strength, as the density of deep traps would be sufficiently high to allow range-limited hopping, or narrowing of the band structure. [54]

There are two types of traps discussed in the literature for semi-crystalline materials such as Mylar: deep and shallow traps. These trap depths are defined by the amount of energy required to remove an electron from the trap. It is also concluded that trap depth, especially near the surface, may vary from sample to sample based on its chemical, thermal and physical treatment. [42] Other studies [54] have shown a clear relationship between increasing trap depths, due to doping, and increases in the breakdown strength of the dielectric. However, the authors do state that doping above specified concentrations can make it more difficult for trapped charges to escape the localized states, severely distorting the electric field within the bulk material causing premature failure. [54]

1.4: Previous dielectric studies and dielectric characterization of Mylar

1.4.1: Dielectric Properties of PET- Permittivity and Dielectric Loss

Permittivity

The dielectric properties of PET have been extensively studied and documented since its realization as a suitable dielectric. DuPont has characterized and provided the data for Mylar C, their dielectric grade material. DuPont has reported a dielectric constant value for Mylar over a range of frequencies. [14] Values of the dielectric constant have been reported for frequencies of 60Hz to 1GHz at room temperature, tested at ASTM standards. It was also reported [5] that there is a decrease in permittivity with increasing frequency. As the frequency of the field increases, the lag in dielectric polarization increases, consequently lowering the permittivity and increasing the loss. Table 1 lists typical dielectric properties of Mylar for the 48G thickness. [14]

Table 1: Typical dielectric properties of electrical grade Mylar

Typical Electrical Properties of Mylar (PET)		
DC Dielectric Strength (48G)	Permittivity (1kHz) at 25°C	Dissipation Factor (1kHz) at 25° C
4.9 kV/mil	3.25	0.0050

Temperature and Humidity

DuPont [14] has also characterized varying environmental effects on the dielectric properties of Mylar. They reported an increase in dielectric constant with increasing temperature over a range of 25°C to 80°C. Studies completed by Coburn and Boyd, who completed a thorough investigation of dielectric relaxation in PET, found similar results with permittivity values ranging from 3.0 to 3.2. [15] Literature studies examining the effects of temperatures from from 0°C to 80°C each reported increased permittivity values with increasing temperature, which is in agreement with data provided by DuPont.[3,5,15] Significant changes take place in the physical properties of the material at the glass transition temperature- T_g of the material, which in turn affects the dielectric properties as well. Polymers transition from a hard, glassy material to a softer, rubber-like material at the glass transition temperature. As the temperature approaches the T_g, 80°C, there is a very sharp increase in the permittivity values. At room temperature, DuPont reported that the dielectric constant at 100Hz and 1kHz increased by 3% at room temperature as the relative humidity increased from 20 to 80% for films above 2mil thick. Lightfoot and Xu [17] suggest that the increase in permittivity is due to the water

molecules forming clusters at terminal –OH groups of PET, which can sustain an effective dipole, contributing to the overall polarization and thus permittivity.

Dielectric Loss

There have also been studies on dielectric loss values for PET, as well as the effects of varying environmental conditions on loss values. DuPont reports dissipation factors for frequencies of 60Hz-1GHz at room temperature, tested under ASTM D150 standards. The dissipation factor increases steadily up to 100kHz, at which point there is a sharp increase in dissipation factor. Dissipation factors continue to increase until very high frequencies, above 3GHz, where they begin to decrease. The same trend is seen in the early data reported on the comparison of the dielectric properties of amorphous and crystalline PET. [3]

Temperature and Humidity

Temperature studies [5, 15] reported a decrease in loss as temperature was increased up to the T_g of the material. Above the T_g of the material, 80°C, the loss begins to increase and continues to rise with increasing temperatures. [14] The decrease in loss with increasing temperature below the T_g is attributed to the enhanced dipole mobility, allowing the material to readily align with the applied field. However, above the T_g the temperatures are sufficiently high enough that the polymer chains begin vibrating and moving from their ordered, crystalline positions, allowing dipoles to easily misalign with the field, contributing to increases in loss. Above the T_g, loss can also be a result of the dissipation of heat within the dielectric.

There is an increase in dielectric loss with increasing humidity. [3, 5, 18] At room temperature, DuPont reported that the dielectric constant at 100Hz and 1kHz increased by 3% as the relative humidity increased from 20 to 80%. Lightfoot and Xu [17] suggest that the increase in loss is due to the water molecules forming clusters at terminal –OH groups of PET, which can sustain an effective dipole but are much less mobile, increasing the activation energy and loss.

1.4.2: Breakdown Strength of Mylar

In studying and reporting dielectric breakdown strengths, it is important to understand how different parameters impact the breakdown strength. In addition to the intrinsic material properties, test parameters and environmental conditions can also influence the measured dielectric breakdown strength and must be well understood and controlled in order to obtain consistent results and compare different test groups to each other. Environmental changes, such as humidity and temperature can activate different breakdown mechanisms, affecting the breakdown strength. Test parameters including voltage type and ramp rate, as well as electrode spacing, area, geometry and metallization thickness, can significantly influence the measured breakdown strengths.

Temperature and Humidity

In most polymer dielectrics it is found that an increase in temperature will lead to a decrease in dielectric breakdown strength, this trend holds true for PET as well. Studies [15, 16] have shown that breakdown strength decreases with increasing temperature in the range of -196°C to 25°C for both AC and DC measurements. DuPont's electrical

characterization data sheet shows similar trends in breakdown strength as temperature increases above room temperature. [13] This decrease in breakdown strength can be attributed to a variety of factors. Specifically, as temperature increases, particularly above the T_g of the polymer, thermal breakdown pathways, mentioned in Section 2, may become active compromising the dielectric integrity of the material. Increasing the temperature also increases the mobility of free electrons and charge carriers in the polymer; this may result in an increase in conductivity within the polymer. [15, 16] Increased conduction can lead to higher localized Joule heating which in turn further increases carrier mobility and conduction; this cycle continues and can result in thermal runaway, contributing to dielectric failure.

Another environmental factor that can strongly influence the breakdown strength of polymer dielectrics is relative humidity. Previous studies by DuPont report a decrease in breakdown strength as a function of humidity. Films above 2mil thick decreased in dielectric strength by ~10% as humidity was increased from 20% to 80%. [5] These decreases in breakdown strength due to increased relative humidity are a result of new breakdown pathways that are introduced into the Mylar films. Previous work hypothesizes when sufficient amounts of water are present in the polymer, they can assist in the dissociation of impurities under electrical stress, increasing electrical conduction. Increased conduction can lead to higher localized Joule heating, which in turn increases carrier mobility and conduction; the cycle continues, leading to a thermal runaway which can result in breakdown at lower fields. [47] Thin films, like the 48G (12μm) samples used in this study, are especially susceptible to humidity and can quickly equilibrate to

ambient conditions. Humidity control during testing and storage is highly important for test consistency and reproducibility.

Voltage Type and Ramp Rate

It is well known that the dielectric strength of polymers tends to be higher when measured with DC voltage and lower when measured with AC voltage. This is partly due to the increase in dielectric heating in an AC field; the AC field is alternating, as the field alternates the molecules rotate, which causes collisions with other molecules, creating energy that is dispersed among the adjacent molecules as heat. [18, 20] It is also hypothesized that the injected charges at the electrode surface are annihilated during the pole reversal of AC fields and the energy generated by the recombination may contribute to bond breaking and dielectric failure. [19] It has been suggested in a study of low density polyethylene (LDPE) [20] that there is a greater amount of deeply trapped space charge under AC voltage, as space charge arises from charge injection into the material. Charge injection is a result of the injection of carriers at the electrodes as well as ionization within the material itself. Field switching can enhance charge injection experienced by the material. The increased charge injection can lead to field enhancement within the dielectric and decrease the breakdown strength under AC fields. Typical differences for Mylar between AC and DC breakdown strengths are usually on the order of approximately 100kV/cm. [5, 21, 22]. Older studies have found a much greater difference between AC and DC breakdown strengths for Mylar, even up to 300kV/cm. [19] However, there was not sufficient experimental detail to determine if these differences were due to methodology differences or other factors. Again, it is

important to note these differences when trying to interpret data comparisons as they can lead to inaccurate conclusions. In this thesis, DC breakdown is studied exclusively. It is important to keep the voltage type in mind when drawing conclusions or making comparison in dielectric breakdown data of Mylar.

Voltage ramp rate is the rate at which the applied voltage is increased during dielectric breakdown experiments. The ramp rate can vary due to different rates of voltage application or to different sample thicknesses, which changes the field ramp of the material. Ramp rates can be applied as a continuous ramp or in stepped increments. A continuous ramp is increased continuously, where as a stepped ramp is increased stepwise with the field being increased by a designated amount at discrete time points. There have been no studies that have focused specifically on the effect of ramp rates on the breakdown strength of PET. However, a study [55] that examined the effects of varying material thickness on the breakdown strength at a constant ramp rate suggest the slower ramp rates may result in lower breakdown strengths. There have been some studies on the effect of ramp rate on the breakdown strength of polypropylene and there were no reported significant effects on the dielectric strength. [29, 52] However, it is predicted for PET that space-charge effects at the electrode-polymer interface should be dependent on the ramp rate [53], and previous studies on ceramic dielectrics have shown a dependence of dielectric breakdown strength on ramp rate. [49] Further investigations on the effects of ramp rate will provide useful information on the breakdown strength of poly(ethylene terephthalate) and if the modified material responds to ramp rates differently than Mylar.

Sample Test Volume (Electrode Area)

In general it is noted that the dielectric strength, for a capacitor of a defined area, decreases with increasing film thickness, which is usually attributed to the defect density within the polymer and the greater number of defects present within a sample of larger volume. Studies of PET by Laihonen *et al* [22] have shown however, that an increase in volume due to area and increases in volume due to thickness do not yield proportionate effects on the breakdown strength. This work found no correlation between the breakdown strength and thickness in films from 8-20μm, but this study did report a significant decrease in breakdown strength with increased area due to larger electrode diameters. [22] This implies that an increase in electrode diameter yields a greater increase in number of defects present. However, there could be a significant difference if the film thicknesses differed by a greater amount; the thickness range examined may have been too small to produce an effect. It is also important to note that defects and defect density can vary greatly based on film manufacturer, processing methods and film thickness as well.

This thesis will further investigate the effect of various electrode sizes on the dielectric properties of Mylar and modified Mylar to determine if electrode area effects are dependent upon material type/doping processes.

Electrode Spacing and Self-Clearing

For metallized dielectric films, self-clearing is a process that results in the clearing of defects within the film, which can delay catastrophic failure. [34, 35] The self-clearing process begins with a breakdown event within the sample. The breakdown

releases energy which can result in arcing or current across the film, and this energy can vaporize the metallized electrode and remove defects within the film that may have been present. Self-clearing is known to occur in metallized capacitors, and it is hypothesized that it may occur between adjacent electrodes in multi-electrode test samples. Although self-clearing can be a desirable property in some dielectric applications, it can also distort the measured breakdown strength by increasing the apparent breakdown strengths of self-cleared electrodes. The extent of self-clearing may also be dependent on metallization thickness [35] and electrode-to-electrode distances. In order to provide more representative measurement of breakdown strengths of uncleared materials, a study on the effect of metallization thickness as well as single-electrode versus multi-electrode samples was performed to determine the influence of self-clearing on the measured breakdown strength values. A study of single electrode samples reduces possibility of self-clearing; a comparison of single electrode sample to multi-electrode samples can help to determine if self-clearing events do occur more readily in multi-electrode films and how they affect the measurement results.

1.5 Mylar Aging and Lifetime Reliability Studies

A vital part of dielectric research is being able to understand, predict and prevent failure processes, especially those incurred by field aging. Often accelerated aging techniques are utilized to try to predict the effects of long-term field aging on the dielectric properties of the capacitor. However, a major concern with the prediction of lifetime reliability of these materials is how accurately accelerated aging reproduces the effects of field-aging and simulates true lifetime performance of the material. It is

possible that accelerated aging, due to the higher temperatures and/or electrical stresses, introduces new degradation mechanisms that do not occur in field-aged materials, and degradation mechanisms may differ over the acceleration range. It is important to determine if and how accelerated aging differs from field-aged material performance.

Previous aging studies have measured dielectric properties of thermally aged polymers. Both virgin and doped Mylar were measured at time points from 30 days to 549 days. These studies have shown that thermal sample aging for virgin Mylar and modified Mylar does have a significant effect on permittivity and dielectric loss with the majority of the changes occurring within the first 30 days of aging. [32] However, there were no further changes in the properties from 30 to 549 days that were consistent over all the time points. [32] Since the biggest changes to properties occurred within the first 30 days a short-term aging study was designed to elucidate the behavior in the less than 30 day time period. The long-term study also examined the dielectric breakdown strength of thermally aged samples at the same temperatures and aging time points as in the permittivity and loss study. It was determined dielectric breakdown strength did not significantly change due to thermal aging, although there was sample-to-sample variability within aging groups. A short-term aging study, less than 30 days, could be helpful to providing insight to the changes that occur in the permittivity and loss samples. The dielectric breakdown strengths at these short-term aging time points will also be examined for completeness.

In addition to the short-term aging study this thesis will also continue studies on the effect of temperature on dielectric properties. Permittivity, loss and breakdown will be measured in samples while the sample is equilibrated to elevated temperature to

determine if there are changes that occur during testing at elevated temperature. This will allow for understanding about other stresses that the materials experience if exposed to both field and thermal stresses during the accelerated aging process, that may not captured by thermal aging studies alone.

Chapter 2: Methods and Materials

2.1 Sample Preparation

Films samples are cut from 48G Mylar (12μm) rolls with a scalpel, or any other cutting device that will not rip, tear or distort the samples during the harvest process. The samples were cut to size in order to accommodate 24-30 individual electrode test areas; sufficient sample dimensions are approximately 3" by 2.25".

The films are then coated with the desired amount of gold by evaporative deposition. The back of the film is a continuous, gold coating over the entire sample area. The front deposition consists of 30 individual circular electrodes of 6.3mm diameter. In the case of the electrode area studies, samples are also coated with 9mm, 12.65mm, or 18.97mm diameter electrodes. It has been determined that the spacing shown in Figure 5 does result in some contribution from self-healing during breakdown testing, as discussed in Section 1. The 6.3mm 30 electrode mask (shown in Figure 5) was used in this study to allow comparison to previous results obtained with the same spacing. A margin of at least 4mm is maintained between the outer electrodes and the edge of the film sample. Deposition thickness of 50nm was utilized in all metallized samples, except where otherwise indicated for the metallization thickness studies.

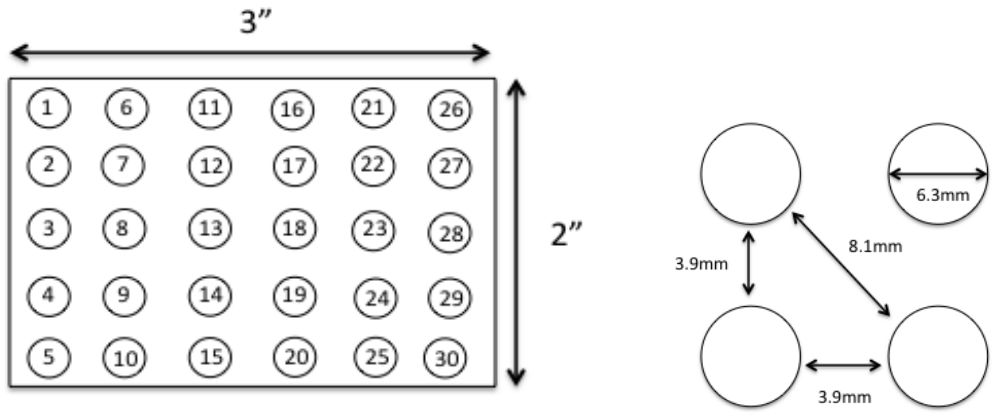

Figure 4: Electrode configuration for 6.3mm diameter

After samples have been coated, thickness measurements are recorded for each film with a Measure It All LE1000-2 digital thickness gauge. Thickness corrections are made for the 200nm metallized samples by subtracting the total amount of metallization, 400nm, from the measured thickness before calculation of dielectric properties from gathered data. Corrections are currently not made for the 50nm metallized samples to allow for comparison to other tests that have been previously conducted on this material, tests in which thickness corrections were not made. [32-33]

2.2 Humidity Control

Storage

All stock sources (*i.e.* bulk rolls or sheets of film from which samples are obtained) are stored in ambient laboratory environments in standard, plastic zip-closure bags. After samples are harvested and sent for evaporative deposition, they are stored in a desiccator with Drierite desiccant and their exposure to ambient conditions is closely monitored. All samples are stored in desiccators for 12 days after exposure to ambient conditions before they are tested or measured to ensure completely dry films. This time

period was determined by previous studies of humidity exposure and breakdown strength [50].

Testing

It is also important to control humidity for the duration of testing procedures. After thickness measurements are taken, films are desiccated for 12 days prior to undergoing anymore testing, as humidity is not controlled during thickness measurements. For permittivity and dielectric loss testing, the samples are removed from the desiccator and immediately placed under a nitrogen blanket setup to ensure a dry environment of <10% relative humidity. The nitrogen blanket setup, Figure 6, consists of ¼" Tygon tubing attached to a glass diffuser inside a 10cm diameter plastic powder funnel with house nitrogen flowing at a rate of 30psig. Relative humidity is monitored for the duration of testing by a Measurement Computing LCD-502_LCD humidity logger.

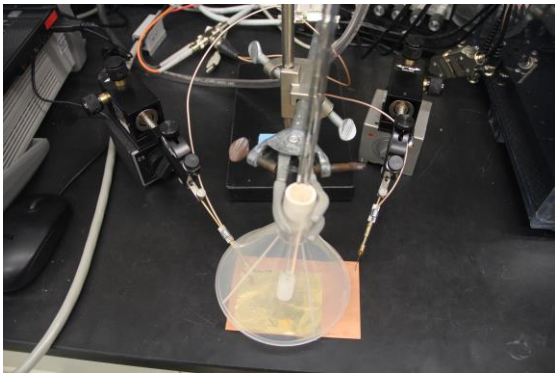

Figure 6: Nitrogen blanket setup

Dielectric breakdown testing is performed in Fluorinert FC-40, a dielectric fluid. Samples are removed from the desiccator and immediately submerged in Fluorinert. Previous testing has shown that films that are submerged in Fluorinert are relatively well protected from ambient humidity for the duration of the breakdown testing. [50] The

breakdown strengths of films tested in this manner are consistent with the storage humidity and not significantly affected by the ambient humidity during testing.

Relative Humidity Chamber

The chamber, shown in Figure 7, is equipped with a Thorlabs DDSM100 Travel Direct Drive Stage apparatus, which includes the ground plate and test probes connected to an LCR meter. A Labview program mechanically drives the stage to each electrode position for testing where the Labview program records capacitance and dielectric loss measurements. The Drive Stage is enclosed by an 11”x11” PVC Static-Dissipative chamber, with a top-opening lid. The relative humidity of the chamber is controlled by use of a rotameter, which controls the flow rates of humid and dry air into the chamber.

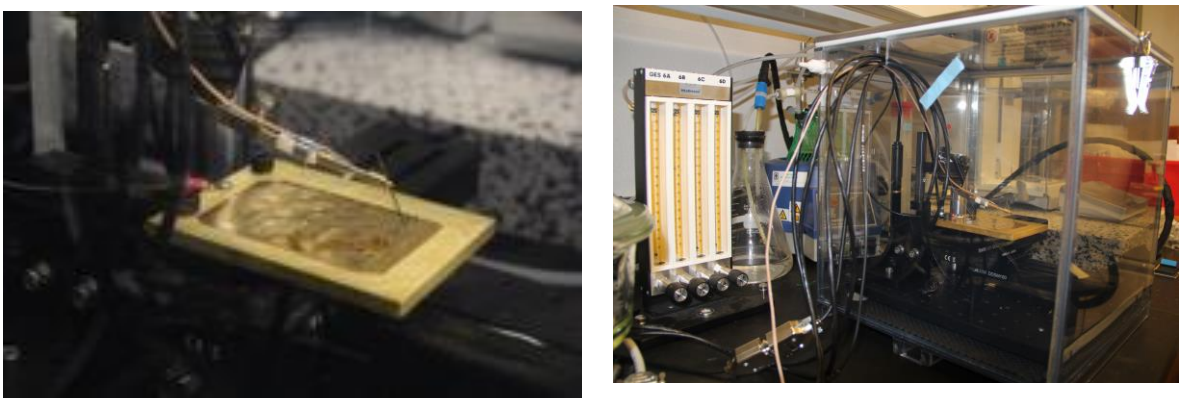

Figure 5: Controlled Relative Humidity Chamber setup

2.3 Permittivity and Dielectric Loss Measurements

Dielectric permittivities and dissipation factors were measured using a calibrated Agilent LCR meter (Model E 4980A) and a probe/plate setup. The probe/plate apparatus consists of a ground probe that is connected to a copper plate by surface contact. The source probe is then placed on top of the electrode to be tested, and probe height is

adjusted so that there is enough force to allow the electrode to firmly contact the sample and the copper plate. The ground and source probes are Signatone S-725 micropositioners with BNC connections equipped with Signatone SE TB Tungsten 20 mil diameter probe tips, which are bent to provide a smooth curved surface for film contact. The samples are tested under a nitrogen blanket or in a controlled humidity chamber as described in section 2.2. Permittivity and loss are recorded at 20 Hz, 250 Hz, 1 kHz, 10 kHz, 100 kHz, and 1 MHz. Before testing begins, a short correction and an open correction to the test circuit are performed using the built-in LCR meter correction function. These corrections are stored and applied at each frequency. Capacitance and dielectric loss data is measured at each frequency and is recorded by a Labview program, which outputs the data into a text file for each individual electrode. Dielectric loss is output directly from the LCR meter. Permittivity values are calculated, as shown in Equation 3, from the capacitance values output by the LCR meter and the electrode diameter and thickness data for each individual electrode.

$$\kappa \equiv \varepsilon_r = \frac{Cd}{A\varepsilon_0}$$

Equation 3: Permittivity calculation from measured capacitance

Rejection of Values

Occasionally poor contact between the test probe and the sample occurs within the test setup, resulting in capacitance and dissipation values that are statistical outliers for one electrode when compared to the rest of the electrode data from the same film. If this is the case, the electrode is retested to ensure that good contact was made. If the retesting show that poor contact was the reason for the outlier value, then the retested

value may be substituted for data analysis. If the retesting does not change the measured capacitance and dissipation factor then the original data is used.

For some data sets there outliers are excluded to enable better comparison of the average performance. Any data that has been excluded from data plots is noted prior to the presentation of results in each section. The same plots without any data points excluded from the plot area as well as tables with the data of those exclusions are available in the Appendices.

2.4 Dielectric Breakdown Strength Testing

The parallel-plate method described earlier for capacitance and dissipation factor measurements is also utilized for dielectric breakdown strength testing. However, in this setup the samples are submerged in Fluorinert, a fluorocarbon dielectric fluid, to prevent arcing as dielectric breakdown strength testing is completed at high voltages.

Sample films are prepared for testing by metallization of electrodes onto the films as previously described, with the humidity control parameters discussed in section 2.2. A copper plate that has been cleaned with water, mild detergent and rinsed with isopropanol is allowed to dry overnight at ambient conditions; the plate is then dried under nitrogen flow as described in section 2.2 is placed into a flat evaporating dish and immersed in Fluorinert approximately 1-1.5cm deep. Once carbon residue deposited during breakdown becomes visible, usually after about 10 samples, the copper plate is turned over to continue testing on the clean side of the plate. When the second side of the plate shows carbon residue, approximately another 10 samples, the plate is removed and cleaned to remove residue where breakdown events have occurred from testing. The

Fluorinert is removed from the evaporation plate and gravity filtered with qualitative Grade 2 filter paper to remove any particles and contaminants from breakdown events. The evaporating dish is also wiped clean and washed with isopropanol to remove soot and carbon residues; it is dried thoroughly before refilling with clean or filtered Fluorinert.

The ground electrode probe is connected to the copper plate by direct surface contact, the metallized sample is immersed in Fluorinert with insulated metal weights to help keep the film immobilized and fully immersed during testing. The source electrode is then placed on top of the electrode to be tested. The probe height is carefully adjusted such that the probe firmly contacts the electrode and plate. The breakdown setup is shown below in Figure 8.

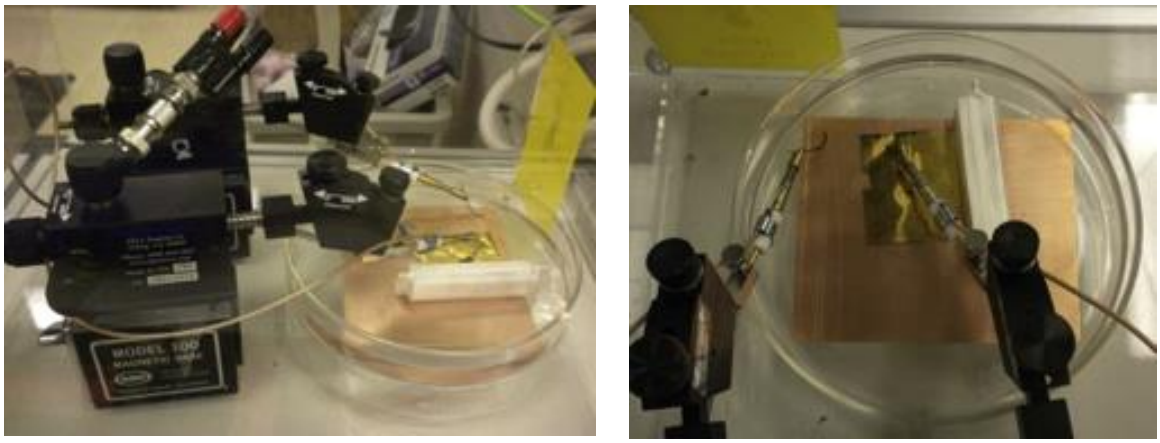

Figure 6: Dielectric breakdown strength test setup

The ground and source electrodes are Signatone S-725 micropositioners with BNC connections equipped with Signatone SE TB Tungsten 20 mil diameter probe tips. The end of the probe tips are bent to provide a smooth, rounded surface for contact to the film and ground, as shown in Figure 9 (a). The voltage source is a Trek High Voltage

Amplifier Model 30/20A paired with an Agilent LCR meter (Model E 4980A) used for the input signal. In the case of temperature studies above the T_g, it was necessary to use a ball-plane probe setup, as shown in Figure 9 (b) to avoid damages that may be caused by the wire tip probe above the glass transition. The steel ball at the end of the probe, which is 0.5" in diameter and weighs 8.3 g, makes contact with the film as the source probe. The ball-plane probe is approximately 3.0" long and 1.0" in diameter and weighs a total of 71.5 g, exerting a calculated force of 0.7N on the sample.

(a) 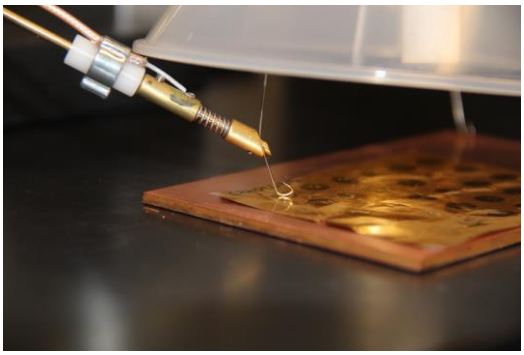 (b) 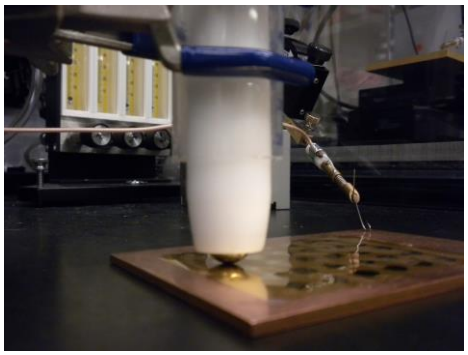

Figure 9: (a) Wire tip probe contact on parallel plate configuration (b) Ball-plane probe configuration

A Labview program is paired with an LCR meter with a data acquisition module, DAQ 6009, which is the interface that converts electrical signals received from the amplifier into readable data for the computer. A Trek High Voltage Amplifier is used to amplify the voltage output from the LCR meter. For all breakdown tests, which the exception of the ramp rate experiments, a 500 V/s stepped ramp rate is utilized, with a 50 V step size per 100 milliseconds. It is important to note that for continuous ramp rate breakdown tests, a DAQ 6216 was used, as the DAQ 6009 could not achieve the faster sampling rate for continuous ramp rate data collection. Calibration measurements were

taken for both programs and DAQ boxes to ensure comparability of data collected and can be found in Appendix A. Breakdown events are detected by monitoring the current with the internal current detection circuit within the Trek high voltage amplifier, which is current limited at 5 mA. The Labview program detects breakdown and turns off the voltage source when the current exceeds 1 mA. When breakdown occurs, the time, source voltage, and current data are written into a raw data file for each individual electrode. The breakdown voltage is the highest voltage recorded prior to the spike in current.

Statistical Treatment of Data

Dielectric breakdown strength data is analyzed by the use of Weibull statistics, which are customarily used in failure analysis studies. Equation 4, below, defines the Weibull probability of failure distribution, where *F(t)* is the probability of failure after time *t.* The α parameter represents the dielectric breakdown strength, which is the field at which 63.2% of the samples have failed. The 63.2% failure point is used because this is the only point at which the α parameter is independent of the shape parameter, β. The β parameter represents the data dispersion within the sample set; a high β parameter corresponds to lower dispersion. The threshhold parameter, γ, is taken to be zero for calculations in this thesis. A non-zero γ parameter assumes that there is a threshhold field below which no failures will occur. The Weibull distribution is extremely flexible, fitting a variety of data sets and best models end of life data which often have a low failure tail.

$$F(t) = 1 - e^{-\left(\frac{t-\gamma}{\alpha}\right)^{\beta}}$$

Equation 4: Weibull Probability of Failure

Rejection of Values

It has been seen that occasionally poor contact between the test probe and the sample or other external interferences can result in breakdown values that are statistical outliers from the other electrodes within the film sample. If these outliers are due to operator errors during testing or pre-identified defects in the electrodes due to sample harvesting or preparation they can be excluded. Data points may also be excluded at very low breakdown field strength values <250kV/cm to allow for better comparison between groups so that the statistics are not highly skewed by a single low failure data point. Any data points that are excluded from plots are noted in the appendix and are clearly stated in the discussion of results in Chapters 3 and 4.

2.5 Variable Environmental and Experimental Conditions

2.5.1 Variable Temperature

Permittivity and Dielectric Loss

When testing dielectric properties and breakdown strength at elevated temperatures some changes are made to the test process and setup. For permittivity and dissipation factor measurements, the samples are heated by use of a Signatone S-1060 Series Thermal Chuck paired with the LCR meter and probe setup described previously in section 2.3. The Signatone hot chuck maintains the desired temperature throughout the test process, which is confirmed by the use of a type K National Instruments thermocouple. The hot chuck is turned on 30 minutes prior to measurements being taken to ensure target temperature equilibration. Once the system has reached and equilibrated at the target temperature, films are placed on the hot chuck and allowed to equilibrate to

target temperature, the test procedure follows as described previously in section 2.3 with humidity control by a nitrogen blanket.

Dielectric Breakdown Strength

For breakdown strength testing at elevated temperatures, an evaporation dish filled with silicone oil is placed on top of a hot plate with a layer of insulating film between the hotplate and the evaporation dish; see Figure 10. Silicone oil is utilized as the dielectric fluid in place of Fluorinert FC-40 for elevated temperatures as it has a much lower vapor pressure than Fluorinert. The hot plate is set to the target temperature and allowed to equilibrate for 30 minutes prior to testing. Temperature is monitored by a thermocouple placed in the silicon oil bath. Once the setup has equilibrated at the target temperature, the film is placed into the bath and allowed to equilibrate to the target temperature for approximately 10 minutes, testing is then performed as described in section 2.4. For above T_g temperature studies, a ball-plane probe was utilized in place of the wire tip probe at the electrode contact to prevent damage from the force of the wire tip probe. A comparison of data obtained with each probe type is discussed in Chapter 4.

As the testing temperature exceeds the T_g of the material, it is necessary to consider probe force effects on the dielectric properties of the films. Breakdown testing of these samples is completed with a ball-plane probe configuration on metallized samples, as discussed previously in section 2.4. The ball-plane probe setup was compared to the wire-tip test setup with control Mylar films to ensure comparability between the two techniques prior to testing samples above the T_g with the ball-plane probe technique.

This comparison is presented in chapter 3 with the discussion of the above T_g breakdown strength results. All other test parameters followed those described in section 2.5.

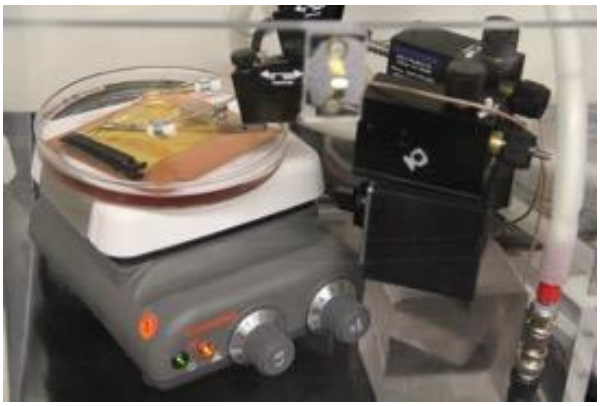

Figure 10: Elevated temperature dielectric breakdown setup

2.5.3 DC Voltage Ramp Rate Effects on Dielectric Breakdown Strength

DC ramp rate studies investigate a range of rates from 50V/s to 3000V/s, with both stepped ramp rate and continuous ramp rates on sample sizes of 2x15 electrode, unmetallized films. Tests are completed with ramp rates of 50V/s, 250V/s, 500V/s, 1000V/s and 3000V/s are conducted as described in section 2.4, with a ball-plane probe setup. Because the LCR meter does not output a continuous voltage waveform, continuous ramp rate measurements utilize a LeCroy WaveStation 2052 50MHz Waveform Generator in place of the LCR meter. The LeCroy generates a continuous DC waveform, which serves as the DC source for the voltage amplifier. A Labview program also controls the waveform generator, amplifier function, and data collection in the continuous ramp rate experiments. As mentioned in section 2.4, DC ramp rate tests are completed with the use of a faster sampling DAQ 6216 data acquisition box and LeCroy Wavefunction Generator, which has been calibrated with the test setup for comparison of

data obtained from the same setup with the DAQ6009/LCR meter setup (see section 4.3 and Appendix A).

2.5.4 Variable Humidity Testing

Permittivity and Dielectric Loss

For humidity effect experiments, there are two types of experiments that are completed for permittivity and dielectric loss. The first experiment is kinetic in nature; dry samples are placed into the humidity chamber, described in section 2.2, which has been equilibrated to the target relative humidity. The samples are then tested 6 times over a 24-hour period to observe the change in permittivity and loss as the films equilibrate to the chamber humidity. In the second experiment, the target humidity levels are achieved by the use of saturated salt baths with water to salt ratios obtained from literature [33] for each targeted relative humidity level.

Table 2 shows salt bath compositions used to achieve target humidity levels. The true humidity levels of the humidity chambers measured by a Measurement Computing DAQ humidity and temperature logger can be found in Appendix A for each target humidity.

Table 2: Target Humidity Storage Chamber Salt-Water ratios

Target % RH	Measured %RH	Salt Type	Amount of Salt (g)	Water (mL)
25	27	Potassium Acetate	200	65
50	50	Magnesium	200	30

		Nitrate		
75	69	Sodium Chloride	200	60

Metallized, 6.3mm electrode samples are stored in controlled humidity chambers with the salt baths for 1 week prior to testing to ensure desired humidity levels are achieved within the samples. Permittivity testing takes place in the adjustable humidity chamber, described in section 2.2, which is equilibrated to the same target humidity level as the equilibration chambers. The one-week humidity exposure samples for permittivity and loss measurements were stored inside the salt bath humidity chambers prior to testing.

Dielectric Breakdown Strength

Metallized, 6.3mm electrode samples for dielectric breakdown testing were also stored in humidity chambers with the same salt baths for 12 days. After the 12 day storage period to ensure equilibration to desired humidity levels, samples were removed and tested in Fluorinert as described in section 2.4. The same small humidity chambers and target humidity levels were used for permittivity/loss and dielectric breakdown studies, shown in Table 2.

2.5.5 Electrode Area

Area effect tests were completed with the same methods described previously (sections 2.3 and 2.4), however, three different deposited electrode diameters are used, shown in Figure 11. To test the effect electrode area has on dielectric properties and strength, measurements are completed on 9mm, 13mm and 19mm diameter samples, with

50nm Au deposition thickness. Figure 11 illustrates the electrode measurements and spacing for each different diameter, see Figure 5 for 6.3 mm diameter electrode spacing dimensions. Sample sizes of 24-30 electrodes were utilized for the electrode area experiments, as the larger electrode sizes require more sample films than the smaller 6.3mm electrodes.

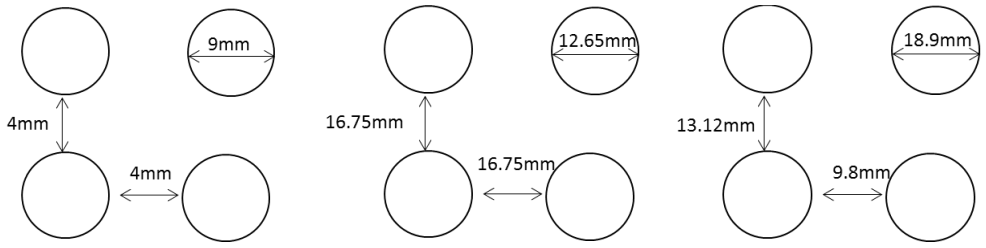

Figure 7: 9mm, 12.65mm and 18.97mm electrode mask dimensions

2.5.5 Single Electrode

Single electrode testing was performed to determine the effects, if any, of self-clearing at adjacent electrodes on the measured dielectric breakdown strength of the samples. In order to test the theory of self-clearing occurring at adjacent electrodes in these samples, the films were cut up into 30 individual 6.3mm electrodes after deposition and thickness measurements were recorded, then desiccated for 12 days. Film preparation prior to separation of the individual electrodes followed the methods set in section 2.1. These individual electrodes were tested by the same techniques for k/DF and breakdown as described in sections 2.3 and 2.4, in the same order with the exception that each electrode was tested individually. During testing, all untested electrodes are removed from the desiccator and stored in a separate Fluorinert bath to maintain dryness and easily access the samples without exposing them to ambient humidity.

2.5.6 Short-term Aging Study

Evaluation of the effects of short-term thermal aging on the dielectric properties of virgin and modified Mylar was carried out by evaluating the dielectric properties, including capacitance, dielectric loss and permittivity, and dielectric breakdown strength of films that had been thermally aged in laboratory grade ovens at a temperature range from 40°C to 124°C, and time periods ranging from 1 to 29 days. Each aging time point has its own corresponding sample film for both Mylar and modified Mylar.

Table 3 shows the accelerated aging time points and the time for which the samples were aged. The films were aged prior to metallization. After aging, the films were prepared as described in section 2.1 and testing of dielectric properties and breakdown strength were evaluated according to sections 2.3 and 2.4.

Table 3: Accelerated Aging time points

Time point	Days at temperature	Aging Temperatures
T1	24 hrs	40°C, 64°C, 80°C, 109°C, 124°C
T2	3 days	
T3	7 days	
T4	29 days	

Chapter 3: Effects of variable test conditions on dielectric performance of Mylar

3.1: Variable Temperature

A variable temperature study was completed on sample sizes of 3x30 electrode films for Mylar and 3x24 electrode films for modified Mylar, while the control set for modified Mylar only had 2x24 electrode films. The study was completed on films with two different metallization thicknesses, one with 50nm Au deposition on each side and another with 200nm Au depositions. In this section only temperature effects will be discussed, later sections address the effects of different metallization thicknesses. The temperature range examined for the 50nm Au metallized films were 20°C, 43°C, 73°C 80°C, and 100°C. The temperatures examined for 200nm Au metallized films were 20°C, 33°C, 43°C, 53°C, 63°C, and 73°C. Data was collected for permittivity, loss and dielectric breakdown strength. There were a small number of data points excluded from the analysis due to their extreme outlying values making comparisons between the typical performance of the groups difficult. Plots with these outliers are in Appendix B, Mylar data, and Appendix C, Modified Mylar data.

Permittivity and Dielectric Loss

200nm Au Metallized samples

The 200nm Au metallized samples are measured at temperatures up to 73°C. As temperature increases the permittivity increases as well, shown in Figure 12 (a) and (b). In modified Mylar there are no significant changes between room temperature and 63°C, but there is a significant increase in the permittivity measured at 73°C. Permittivity increases with increasing temperature are likely due to increased dipole mobility,

allowing the dipoles to move freely and align more readily. The magnitude of increase in permittivity from room temperature to 73°C is the same in both materials, suggesting that the doping process has no significant effect on the material's response to temperature with respect to permittivity. The loss decreases with increasing temperature, Figure 13 (a) and (b) clearly show a decrease in loss as temperature is increased in both modified and virgin materials deposited with 200nm Au deposition. The effect of varying metallization thickness is discussed more in section 4.1. A summary of all data can be found in Tables 4 and 5.

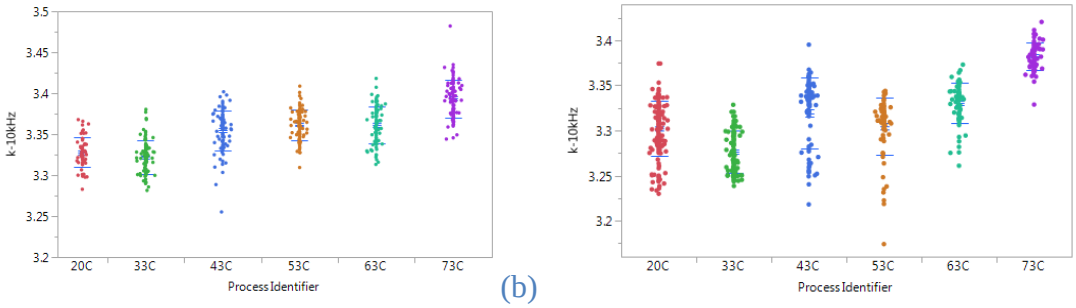

(a) (b)

Figure 12: (a) Mylar elevated temperature permittivity at 10 kHz (b) Modified Mylar elevated temperature permittivity at 10 kHz. There were 2 data point exclusions for Mylar and 4 for modified Mylar.

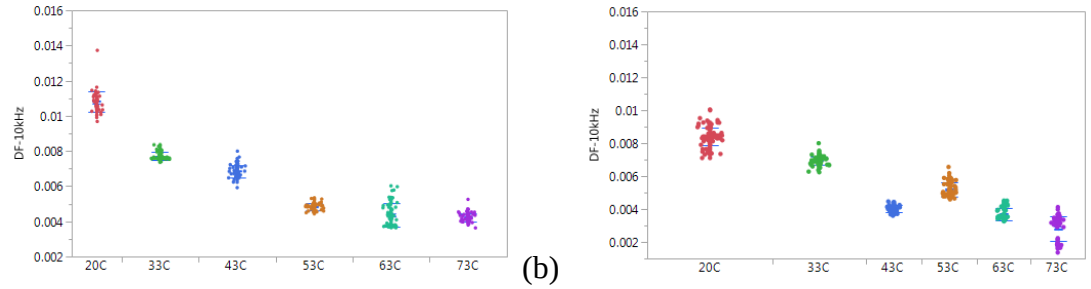

(a) (b)

Figure 13: (a) Mylar elevated temperature dielectric loss at 10 kHz (b) Modified Mylar elevated temperature dielectric loss at 10 kHz. There were 2 data point exclusions for Mylar and 4 for modified Mylar.

Table 4: 200nm Au Mylar permittivity and dielectric loss summary at 10kHz for variable temperature

Temperature	Permittivity, κ	Dielectric Loss
20°C	3.24±0.02	0.011±0.001
33°C	3.24±0.02	0.008±0.001
43°C	3.26±0.02	0.007±0.001
53°C	3.27±0.02	0.005±0.001
63°C	3.27±0.02	0.004±0.001
73°C	3.30±0.02	0.004±0.001

Table 5: 200nm Au Modified Mylar permittivity and dielectric loss summary at 10 kHz for variable temperature

Temperature	Permittivity, κ	Dielectric Loss
20°C	3.30±0.03	0.0085±0.0010
33°C	3.28±0.02	0.0069±0.0002
43°C	3.32±0.04	0.0040±0.0002
53°C	3.30±0.03	0.0052±0.0004
63°C	3.33±0.02	0.0036±0.0004
73°C	3.38±0.02	0.0028±0.0007

50nm Au Metallized Samples

As temperature is increased from room temperature up to 100°C, there is a corresponding increase in the permittivity of Mylar at 10kHz, shown in Figure 14,

however the increase is not consistent with temperature as it was in the 200nm metallized samples. Although the room temperature samples' permittivities are significantly different from all other elevated temperature samples, there is no significant difference between the measured permittivity values of the four elevated temperature samples. The increase in measured permittivity from room temperature to elevated temperature is attributed to the increase in dipole mobility within the material; as the temperature is increased the dipoles are able to move more freely and align with the applied field, giving rise to an increase in the measured permittivity. This increase in permittivity with increasing temperature holds true for Mylar across a range of frequencies from 1kHz to 1MHz, Figure 15, suggesting that temperature does not affect the frequency dependence of permittivity. [14, 16]

In contrast to virgin Mylar, the modified material permittivity data shows that there is no significant difference in the permittivity values as temperature is increased. There is a significant decrease in permittivity for modified Mylar at 43°C. It is not clear at this time why there is a decrease in permittivity at this temperature, but there appear to be two different distributions within the data set that are creating the lower permittivity value. The films have been retested and the values found in the original test set did not change. This result could also potentially be contributed by factors such as film-to-film variability due to doping or damage of the 43°C samples during sample preparation. Further testing of modified Mylar films at 43°C is recommended to obtain accurate results and address this data discrepancy. Nonetheless, despite this discrepancy, there is no consistent change in in the permittivity of modified Mylar as temperature increases.

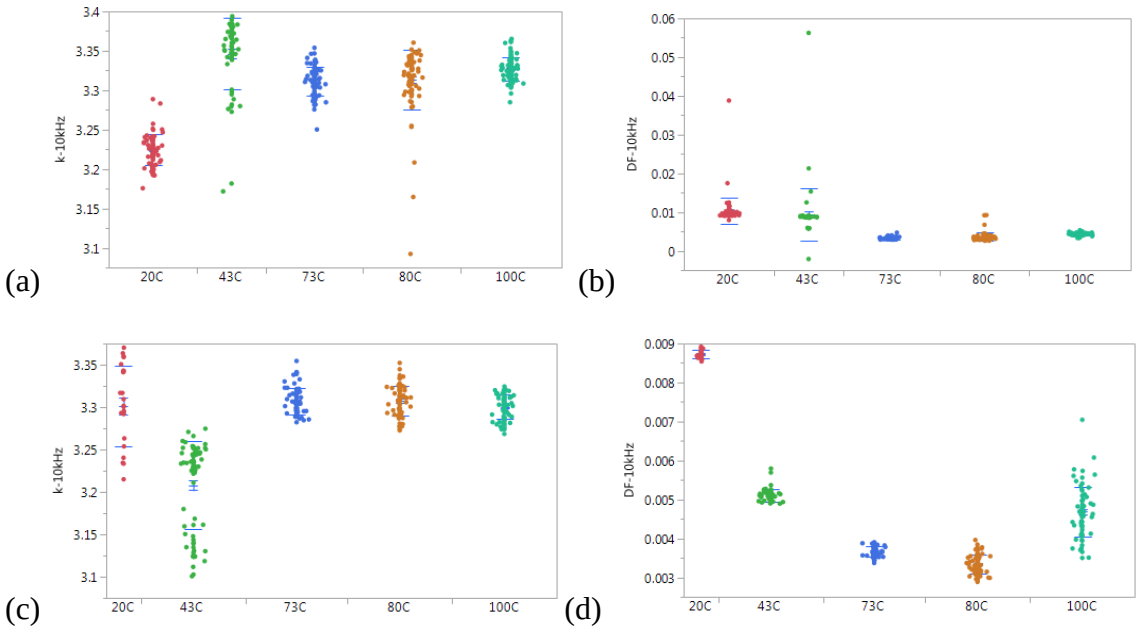

Figure 14: Mylar 50 nm Au metallized samples (a) permittivity at 10 kHz (b) dielectric loss at 10 kHz and modified Mylar samples (c) permittivity at 10 kHz (d) dielectric loss at 10 kHz. There were 7 excluded points for Mylar data set and 1 exclusion from the modified Mylar plots.

Dielectric loss values decrease for both materials from room temperature to T_g, 80°C, Figure 14. A material that readily aligns with an applied field will reduce the phase lag, thus decreasing the dielectric loss of the material. However, as the temperature approaches and exceeds the T_g the dielectric losses begin to increase at 100°C. As temperature is increased above the T_g there is more energy dissipation occurring due to the increased molecular mobility within the sample, resulting in increased loss.

Table 6: 50nm Au Mylar permittivity and loss summary for variable temperature at 10kHz

Temperature	Permittivity, κ	Dielectric Loss
20°C	3.22±0.02	0.0102±0.0034
43°C	3.35±0.04	0.0094±0.0066
73°C	3.31±0.02	0.0032±0.0003
80°C	3.31±0.04	0.0035±0.0010
100°C	3.33±0.02	0.0042±0.0003

Table 7: 50nm Au Modified Mylar permittivity and loss summary for variable temperature at 10kHz

Temperature	Permittivity, κ	Dielectric Loss
20°C	3.30±0.04	0.0087±0.0001
43°C	3.20±0.05	0.0051±0.0002
73°C	3.31±0.02	0.0037±0.0001
80°C	3.31±0.02	0.0033±0.0003
100°C	3.31±0.01	0.0047±0.0006

Figure 15 shows dielectric loss trends across a frequency range of 1kHz to 1MHz. Frequencies of 1kHz to 100kHz are not significantly different from each other, however, the 1MHz samples have much higher losses than the lower frequencies. Examining the dielectric loss of Mylar across this range of frequencies shows a decrease in loss up to 80°C, and at 100°C the losses begin to increase again. The loss also increases with increasing frequency; as the frequency is increased it becomes more difficult for the

dipoles to align with the rapidly changing field leading to larger phase lags and increased loss. Table 6 and Table 7 show the data summaries for both Mylar and modified Mylar.

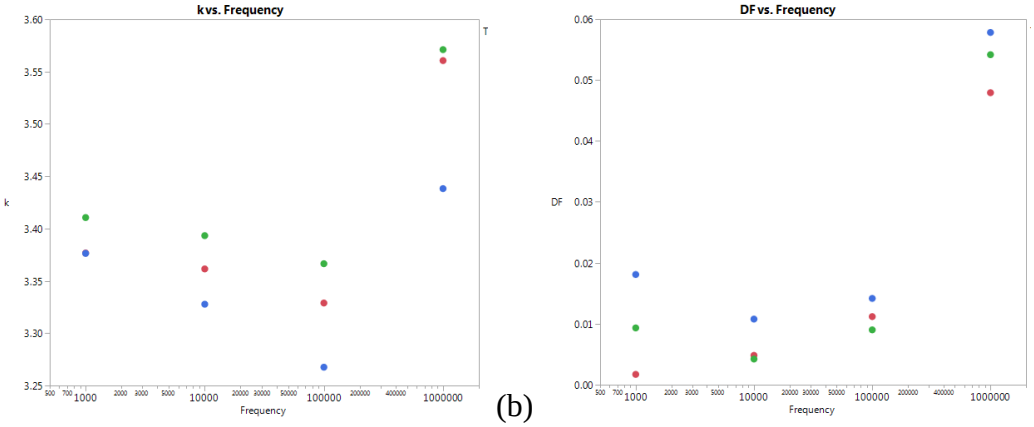

(a) (b)

Figure 15: Frequency log plots for Mylar at room temperature for (a) permittivity versus frequency (b) dielectric loss versus frequency. These plots reveal the frequency dependent behavior of permittivity and loss, 1kHz, 10kHz and 100kHz values are not significantly different from each other, however the 1MHz values are significantly different from the rest of the groups. Behavior of the modified material is similar.

Dielectric Breakdown Strength

200nm Au Metallized Samples

The 200nm Au metallized samples, which were only tested below the T_g, show that as temperature increases the breakdown strength decreases: see Figure 16 and Figure 17 below. Tables 8 and 9 show Weibull parameters for each temperature as well as ΔE_b from room temperature control samples. From room temperature to 73°C there is a decrease in breakdown strength of approximately 1000kV/cm for both Mylar and modified Mylar. As temperature is increased, there is a decrease in the breakdown strength. The decrease in dielectric breakdown strength is likely due to the activation of thermal breakdown pathways not active at room temperature, which results in a greater probability of failure at lower fields. Increasing the temperature increases the mobility of

free electrons and charge carriers that may be present in the polymer; this can result in an increase of conductivity within the polymer. [15, 16] Increased conduction can lead to higher localized Joule heating which in turn increases carrier mobility and conduction. This cycle continues and can result in thermal runaway, which can also contribute to a higher probability of dielectric failure at lower fields. Electromechanical failure could also be a contributing factor in lower breakdown field strengths. Although, the exact breakdown mechanism cannot be determined from the data gathered in this experiment, it is likely that thermal breakdown was not the only factor that led to failure but also electromechanical failure.

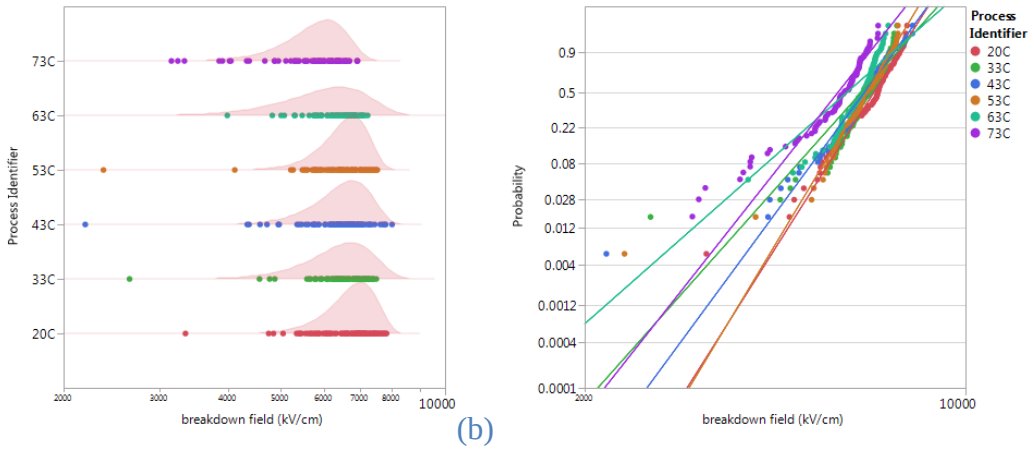

(a) (b)

Figure 16: (a) Scatter plot of dielectric breakdown strength of 200nm Au Mylar at elevated temperatures (b) Weibull analysis of 200nm Au Mylar dielectric breakdown strength at elevated temperatures. A point from the 63C data is cropped out of (b) to visibly show better comparison between the groups. The data point is included in the statistical analysis of the data. For this sample set, 3 data points are excluded from the 63C data set due to failure at fields <250kV/cm.

Table 8: 200nm Au metallized Mylar Weibull Parameters

Temperature	Weibull α (kV/cm^2)	Weibull β	ΔE_b
20°C	7006.3	11.2	0
33°C	6824.1	13.3	-182.2
43°C	6766.1	9.6	-240.2
53°C	6788.9	11.8	-217.4
63°C	6516.3	11.1	-490
73°C	6067.0	9.0	-939.3

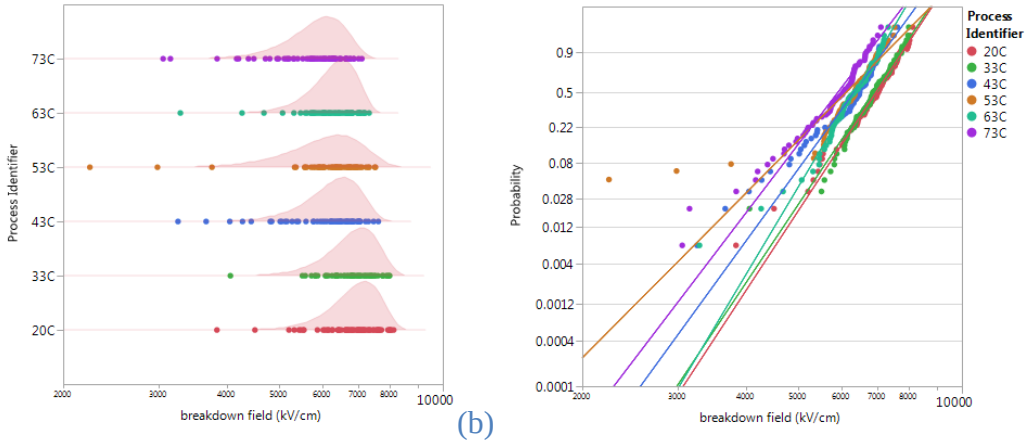

(a) (b)

Figure 17: (a) Scatter plot of dielectric breakdown strength of 200nm Au modified Mylar at elevated temperatures (b) Weibull analysis of 200nm Au modified Mylar dielectric breakdown strength at elevated temperatures. There was 1 data point exclusion from the data set in the 63C samples due to failures at fields <250 kV/cm.

Table 9: 200nm Au metallized Modified Mylar Weibull Parameters

Temperature	Weibull α (kV/cm^2)	Weibull β	ΔE_b
20°C	7179.6	10.8	0
33°C	7098.4	10.6	-81.2
43°C	6563.9	9.7	-615.7
53°C	6432.7	7.1	-746.9
63°C	6542.9	11.9	-636.7
73°C	6140.9	9.3	-1038.7

Ball-plane probe versus wire tip probe

The 50nm Au metallized films were measured from room temperature to 100°C. In order to measure the breakdown strength of the above T_g samples, a ball-plane probe was utilized as discussed in section 2.4 to avoid damage to the softened films by the wire tip probe. A comparison of the two probe types on metallized films is necessary to understand if it is valid to compare samples tested with the two different methods. Figure 18 shows the comparison of the Weibull analysis of the two different probes on Mylar films tested at room temperature. The ball-plane probe produced a greater spread of data, with an overall breakdown strength of only 5028 kV/cm. The wire tip probe produced measurements with lower spread of data, corresponding to a higher Weibull β, and a higher breakdown strength of 6106 kV/cm. The difference in results shows data collected

with these two methods should not be directly compared. Therefore, above T_g data will be considered separately.

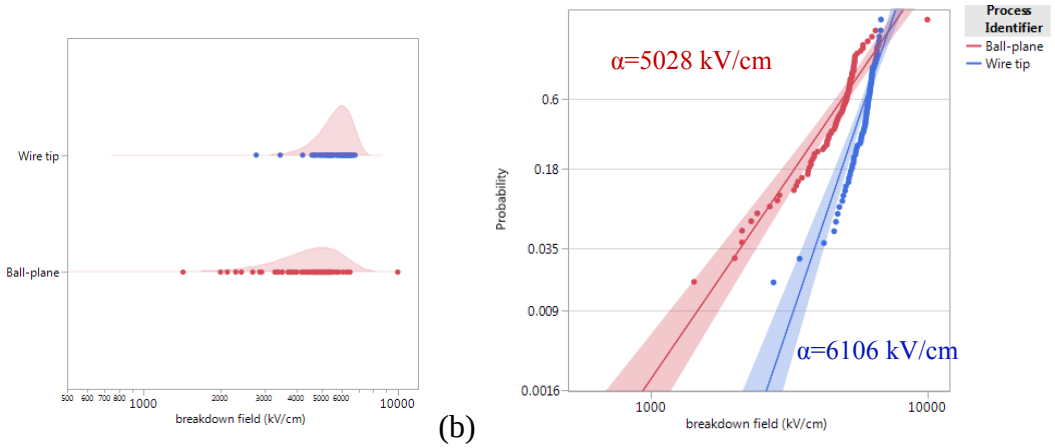

(a) (b)

Figure 18: Weibull distribution function (a) and cumulative probability of failure (b) of wire tip (blue) and ball-plane (red) comparison. The ball-plane probe results in significantly lower breakdown strengths. No data point exclusions.

50nm Au Metallized Samples

Breakdown strength in the 200nm Au metallized films decreased consistently with increasing temperature. The dielectric breakdown strength of 50nm Au metallized films were measured from room temperature to 100°C. This section only compares the below T_g results. Figure 18 (a) and (b) show the cumulative probability of failure plots for Mylar with increasing temperature. Table 10 shows a summary of Mylar Weibull parameters and ΔE_b as temperature increases. As temperature is increased from room temperature to 73° C, there is a significant decrease in the dielectric breakdown strength, by 816 kV/cm. However, the 43°C samples have a breakdown strength lower than the 73° C samples. There could possibly be a different breakdown mechanism active in the 43° C samples, or it could be a result of damage that may have been incurred during film

handling. The 43°C samples were also tested early on in the research of this thesis and test methods may not have been as refined in earlier testing. Further testing at 43° C is recommended to determine what is causing this behavior.

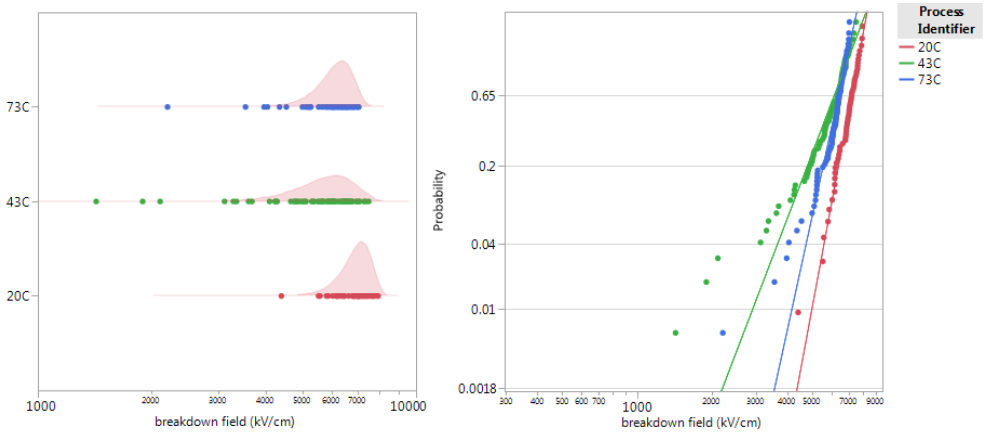

Figure 19: (a) Weibull distribution of dielectric breakdown strength of 50nm Au metallized Mylar at elevated temperatures (b) cumulative probability of 50nm metallized Au Mylar dielectric breakdown strength at elevated temperature. There are 3 data point exclusions from this sample set.

Table 10: 50nm Au Mylar Weibull Statistics at varying test temperature

Temperature	Weibull α (kV/cm)	Weibull β	ΔE_b
20°C	7177.3	12.7	0
43°C	6100.9	6.2	-1076
73°C	6360.6	10.8	-816

Similar to the virgin Mylar, the modified Mylar decreases in breakdown strength by 755 kV/cm from room temperature to 73°C, the 43°C samples also measure lower breakdown strengths in this data set similar to the virgin Mylar study. Figure 21 shows the probability of failure for modified Mylar and Table 11 includes Weibull parameters as well as ΔE_b comparing each temperature to the control. As temperature is increased,

there is a decrease in the breakdown strength. The decrease in dielectric breakdown strength is likely due to the activation of thermal breakdown pathways as discussed in the 200nm Au metallized sample breakdown strength results.

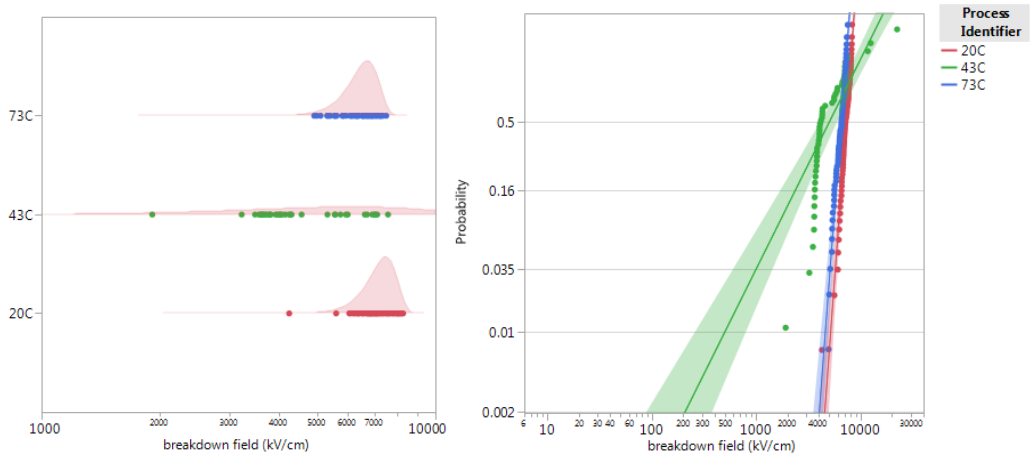

Figure 20: (a) Weibull analysis of dielectric breakdown strength of 50nm Au modified Mylar at elevated temperatures (b) Weibull analysis of 50nm Au modified Mylar dielectric breakdown strength at elevated temperature. There are 2 data point exclusions.

Table 11: 50nm Au Modified Mylar Weibull Analysis

Temperature	Weibull α (kV/cm^2)	Weibull β	ΔE_b
20°C	7467.5	12.4	0
43°C	5233.9	3.8	-2233
73°C	6711.9	12.1	-755

Above T_g 50nm Au Metallized Samples

In above T_g testing, neither material showed a significant difference in breakdown strengths between 80°C and 100°C samples, Figure 21 and Figure 22. However, these breakdown strengths are also not significantly different from the breakdown strength at room temperature for a Mylar sample measured with the same set up (ball-plane probe):

see Figure 18 for the room temperature results. The similarity between the room temperature and elevated temperature results suggests that this method (ball-plane with metallized films) is not ideal for testing of dielectric breakdown strength as currently implemented. The reasons why the ball-plane with metallized film method produces data with higher dispersion and lower breakdown strength are not known at this time. Further studies will include improvement of the ball-plane probe test setup. It may also be insightful to complete tests on above T_g samples with the wire tip probe to determine if there is damage done by the probe contact in comparison to the ball-plane probe.

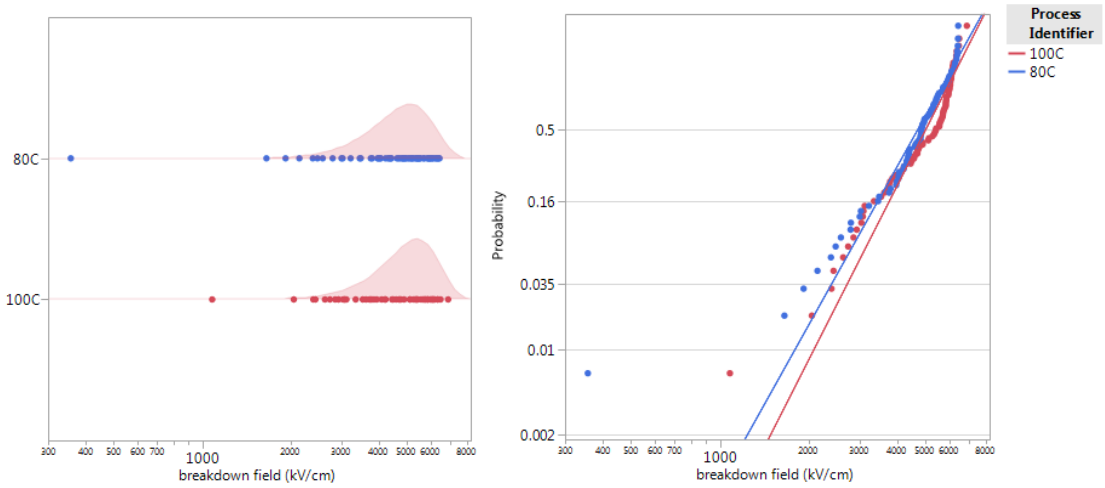

Figure 21: Mylar above T_g Weibull analysis, 80C and 100C. 1 data point excluded.

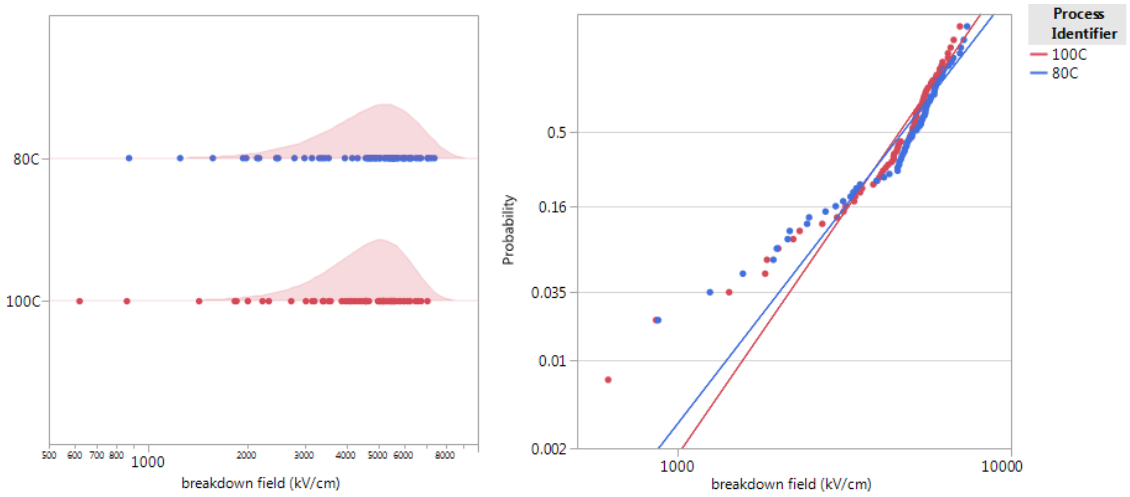

Figure 22: Modified Mylar above T_g Weibull analysis, 80C and 100C. No data exclusions.

Table 12: Weibull parameters for above T_g study for Mylar and modified Mylar

Material Type	Temperature	Weibull α (kV/cm)	Weibull β
Mylar	20°C	5028	3.8
	80°C	5113	4.3
	100°C	5399	4.8
Modified Mylar	80°C	5255	3.8
	100°C	5079	3.9

Conclusions: Variable Temperature

Comparing Mylar and modified Mylar reveals that there is a significant difference for both types of materials in the measured permittivity between room temperature samples and elevated temperature samples. For both materials permittivity exhibited different behavior between the 50nm and 200nm metallized films at elevated testing temperatures. For Mylar in the 50nm films there is a significant increase in permittivity

between the film tested at ambient and those tested at elevated temperatures 20°C versus 43-100 °C, but no significant differences between the films tested at different elevated temperatures (43-100°C). In contrast, for the 200nm metallized films the permittivity increased smoothly with increasing test temperature, up to 73°C. It is not known why the metallization thickness would change the permittivity behavior; however, it is hypothesized that thinner metallized films experience a greater amount of shrinking relative to those with thicker metallization. Lateral shrinking of the films results in an increase in thickness. If the 50nm Au metallized films do shrink more than the films metallized with 200nm Au, this would cause the *calculated* permittivity values to differ due to the difference between the thickness used to calculate permittivity and the true film thickness. The 50nm Au metallized films, if they did shrink more than the 200nm Au metallized films, would show a decreased effect of temperature on permittivity at higher temperatures where more shrinkage occurs. This may be a contributing factor to the differences in temperature dependence. The data obtained from the modified material also shows different behavior between the 50 and 200nm Au metallized samples. The 50nm Au metallized films showed no difference with temperature, whereas the 200nm Au metallized samples showed a significant difference between room temperature and 73°C. However, the similarity between the 200nm Au metallized Mylar and modified Mylar groups suggests that the doping process has no significant effect on the changes in dielectric properties with respect to test temperature, at least over the temperature range studied here.

Similar trends are seen in both Mylar and modified Mylar dielectric breakdown strengths with both 50nm Au and 200nm Au metallization thicknesses. As temperature

increases, breakdown strength decreases, likely due to the activation of thermal breakdown pathways. The modified material tends to have higher breakdown strengths at elevated temperature compared to Mylar, similar to its behavior at room temperature. The Weibull β parameter, also known as the shape parameter, represents the distribution of data within each set. There are no significant trends in the shape parameter with respect to temperature.

It is important to note that some of the films tested at 43°C had unexpected behavior. Specifically, the permittivity of the 50nm Au Mylar films is greater at 43°C compared to any other temperature, whereas the 50nm Au modified Mylar films have the lowest permittivity values at 43°C. The breakdown strengths of the 50nm metallized films tested at 43 °C also did not follow similar trends to the other samples. The exact cause of this behavior in the 43°C samples is unknown, but it could be a result of experimental error or film-to-film variability, which can be high in these films. [31] Further testing at 43°C may determine if there are any mechanisms that are activated at this particular temperature that could be the cause, or if the behavior of these samples is a result of experimental error.

Above T_g breakdown data could not be compared to below T_g data, which was tested with a different experimental setup. The ball-plane probe measured considerably lower breakdown strengths than the wire tip probe used for below T_g testing. The ball-plane probe test setup for this experiment may require refinements of the method to allow comparison to wire tip probe data.

This study also examined the dielectric properties above the T_g with 50nm Au metallized samples. The materials undergo significant physical changes at and above the

T_g, where the material transitions from a hard, glassy form to a soft, rubbery form. It might be assumed that these changes will also lead to changes in the dielectric properties of the materials at these elevated temperatures. The permittivity of the above T_g samples is not significantly different from each other, however, the permittivity values are significantly different from the values of the room temperature samples. As the materials reach 80°C, the dielectric loss begins to increase rather than decrease, compared to the below T_g samples. The above T_g behavior of Mylar and modified Mylar were similar. Dielectric heating increases above the T_g due to the increased dipole rotations and mobility within the sample resulting in greater loss. Measured breakdown strengths of the above T_g samples did not change with temperature; however, these samples were tested with a ball-plane probe with metallized films which room temperature testing showed may not be a reliable method for breakdown strength testing.

3.2: Variable Humidity

As discussed in Chapter 1, it has been shown that dielectric properties can be significantly influenced by the level of relative humidity during storage and testing. To better understand the behavior of Mylar and modified Mylar with varying humidity levels, a study was completed on the effects of humidity on permittivity, dielectric loss and breakdown. Permittivity and loss sample sizes consisted of 1 film for each humidity level that was measured multiple times over the given time period. The dielectric breakdown strength data sets consisted of 2 films for each humidity level.

Permittivity and Loss

Permittivity and dielectric loss values were measured at specific time intervals as dry films were allowed to equilibrate to the target humidity level for both Mylar and modified Mylar. These time intervals vary from 0 minutes to 1 week. However, the 1 week data are not plotted as they are not statistically significantly different from the 24 hour data and inclusion of the 1 week time point made trends in data at shorter time periods difficult to distinguish. Table 13 shows the measured permittivity for each humidity at 24 hours and 1 week, clearly showing that the data are not significantly different and the films are well equilibrated to the humidity level after 24 hours. See Appendix A for more detailed information of the humidity chamber equilibrations. Any exclusions from the data sets are noted below each plot; data for these excluded points can be found in the Appendices.

Table 13: Comparison of Mylar and Modified Mylar measured permittivity at 10 kHz for each humidity level at 24 hours and 1 week

	Mylar		**Modified Mylar**	
Target RH (%)	**24 hour κ (10kHz)**	**1 week κ (10kHz)**	**24 hour κ (10kHz)**	**1 week κ (10kHz)**
0	3.22±0.01	3.23±0.01	3.22±0.01	3.22±0.01
25	3.27±0.01	3.27±0.02	3.26±0.02	3.26±0.02
50	3.29±0.01	3.32±0.02	3.28±0.01	3.29±0.01
75	3.35±0.01	3.34±0.02	3.34±0.01	3.34±0.02

Figure 23 shows the changes in permittivity for each humidity level as a function of time for the Mylar films. As expected the dry control samples do not change significantly over a 24-hour time period. However, as time elapses for each humidity there is an increase in permittivity from 0 minutes to 24 hours. Table 14 presents the overall change in permittivity at each humidity level, relative to the 0% control sample. It is suggested that the water molecules form clusters at the terminal –OH groups of PET, which can sustain an effective dipole within the material, contributing to the existing polarization and increasing permittivity. [43] The overall change in permittivity also increases as humidity increases, showing that permittivity is dependent on the relative humidity.

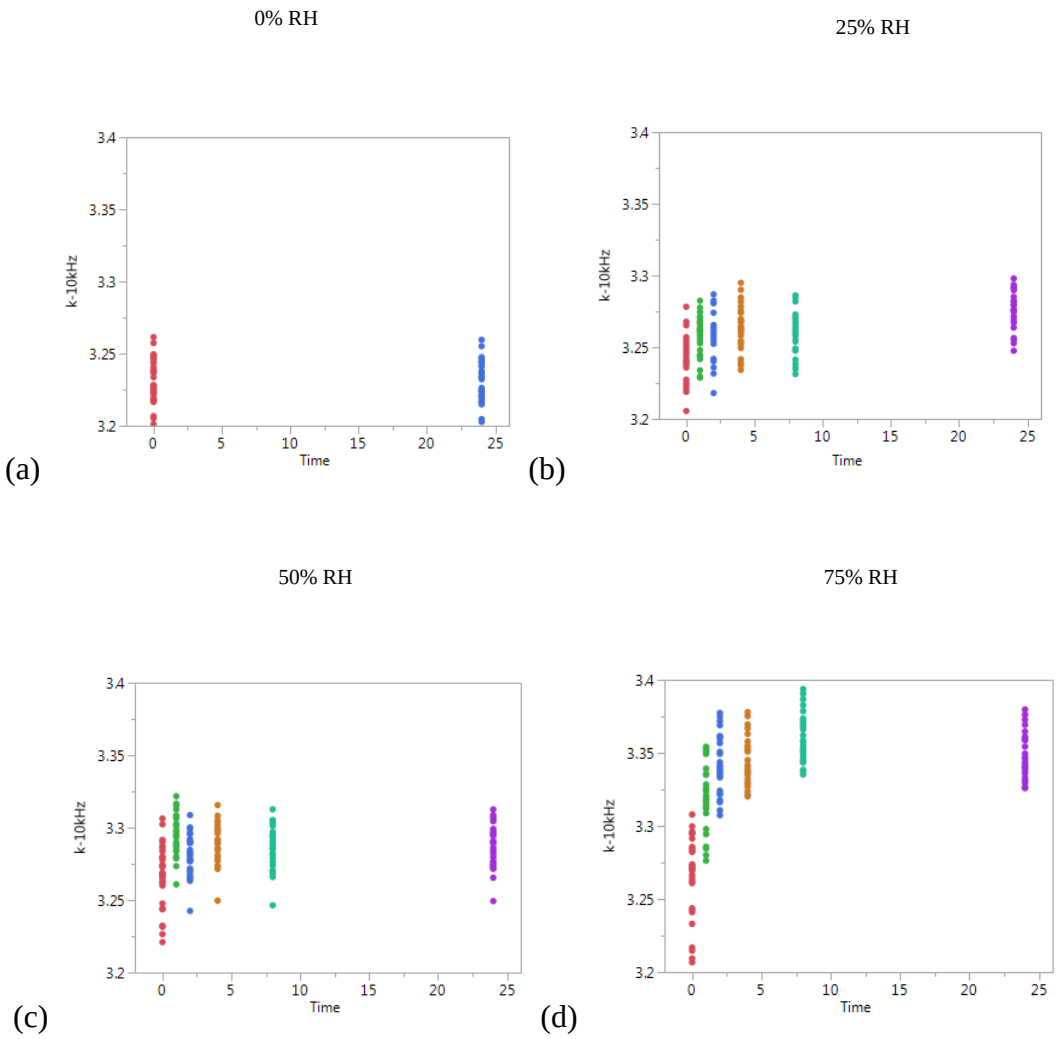

Figure 23: Mylar permittivity measurements versus time at (a) 0%RH (b)25%RH (c) 50%RH (d)75%RH. There were 5 data point exclusions from this data.

Table 14: Mylar Δκ from 0 to 24 hours

% RH	Δκ (24 hrs)
0%	0.01
25%	0.03
50%	0.03
75%	0.08

The overall change in permittivity also increases as humidity increases, suggesting that permittivity is indeed dependent on the relative humidity. This dependence on the relative humidity shows that the water uptake of the samples increases with increasing humidity. In previous work it was found that equilibrium moisture content in PET does increase with increasing relative humidity. [46] Figure 24 shows the changes in permittivity for each humidity level as a function of time for the modified Mylar samples. When comparing modified to virgin Mylar, the changes is permittivity with relative humidity are similar, suggesting that the dopant does not create any additional favorable interactions with water relative to the virgin material;

Table 15 shows the changes in permittivity for the modified Mylar, relative to dry conditions, which are similar to those seen in the virgin material.

0% RH

25% RH

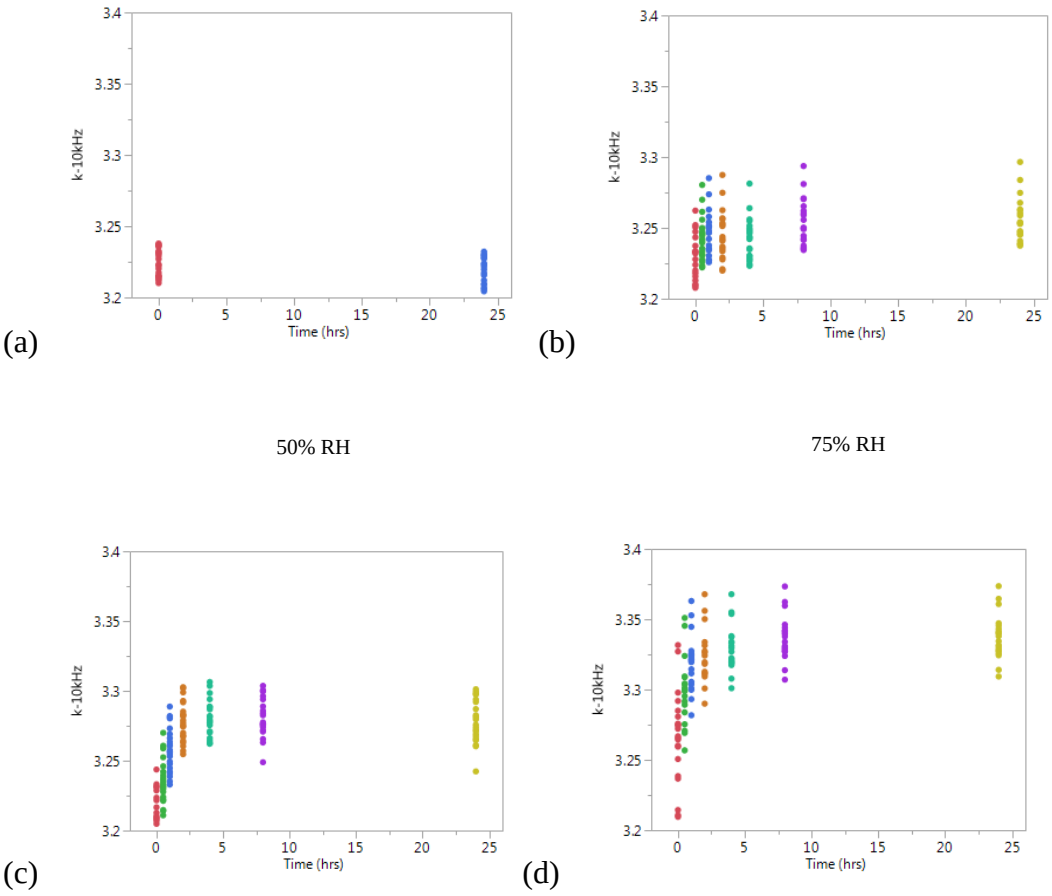

Figure 24: Modified Mylar permittivity measurements versus time at (a) 0%RH (b)25%RH (c) 50%RH (d)75%RH. No data point exclusions.

Table 15: Modified Mylar Δκ from 0 to 24 hours

% RH	Δκ (24 hrs)
0%	0.00
25%	0.04
50%	0.06
75%	0.08

Obtaining reliable dielectric loss data with the newly designed humidity chamber experimental setup proved to be difficult and it was not possible to produce consistent

results, and so it is unlikely that the data obtained are representative of the actual behavior of the films. The roughness of the ground plate may have made contact between the probe and the ground plate imperfect, which could increase the noise in the measurement system. High noise in the circuit makes the open/short correction less reliable especially for the measurement of dielectric loss. Due to the poor contact on the test setup when measuring loss, the data is not discussed. Future work is required to improve the accuracy and reliability of loss measurements using this setup and determine effects of humidity on the dielectric loss.

Dielectric Breakdown Strength

To investigate the effects of humidity on the breakdown strength, the samples were stored in controlled humidity environments for a period of 12 days. After equilibration to target humidity levels, the samples were then tested as discussed in section 2.4. Figure 25 shows the probability distribution function of Mylar breakdown data. As the humidity levels increase, there is a decrease in dielectric breakdown strength. In Mylar, the Weibull α parameter decreases from 6524kV/cm at 0% relative humidity to 5380kV/cm at 75% relative humidity. A similar trend is seen in the modified Mylar samples as well, Figure 26, with a field of 6167 at 0% relative humidity to 5504kV/cm at 75% relative humidity. Table 16 and Table 17 show the Weibull statistics and ΔE_b for each humidity level.

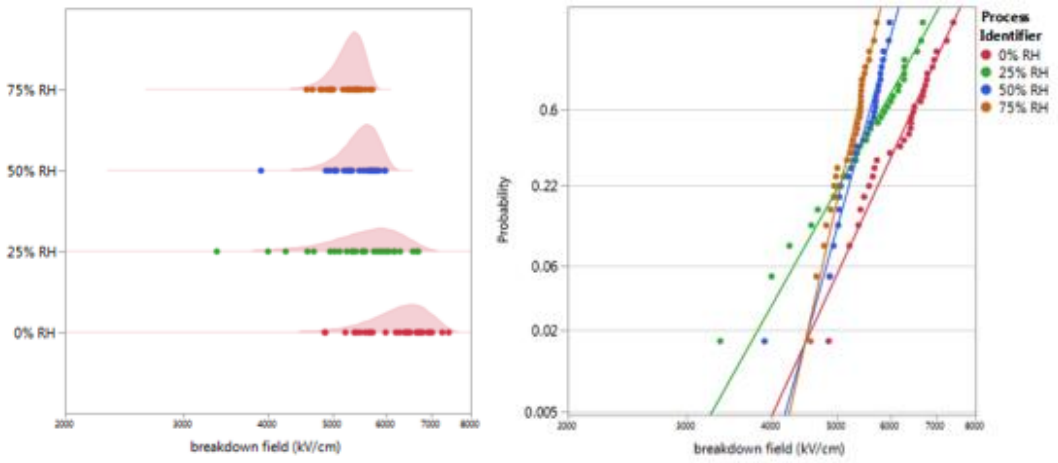

Figure 25: Probability distribution function of Mylar breakdown strength at humidity, no data point exclusions.

Table 16: Summary of Weibull statistics for Mylar variable humidity breakdown strength

% RH	Weibull α	Weibull β	ΔE_b
0	6524.2	11.0	0
27	5878.6	9.0	-645.6
50	5602.7	18.2	-921.5
69	5350.6	22.6	-1173.6

The decrease in breakdown strength in humid conditions may be due to new breakdown pathways that are activated by the presence of water molecules in the films. When sufficient water is present, water can assist in the dissociation of impurities under electrical stress [37], leading to increases in electrical conduction and thermal breakdown of the dielectric via localized Joule heating. The Joule heating increases carrier mobility and conduction, and this cycle continues, resulting in a thermal runaway.[36-37] It is also interesting that the Weibull β parameter increases with increasing humidity in both

materials, signifying a reduction in the variability of failures within a sample as the film absorbs more moisture. As samples are exposed to humidity, there may be new breakdown pathways that are active at lower fields that the materials will prefer to follow instead of sustaining additional field. The likelihood for these materials to follow this low failure pathway increases with increasing humidity; the dispersion of data lessens yielding a higher β parameter. Humidity exposure is highly important to the integrity of the dielectric; highly humid environments could compromise the electrical properties of the material.

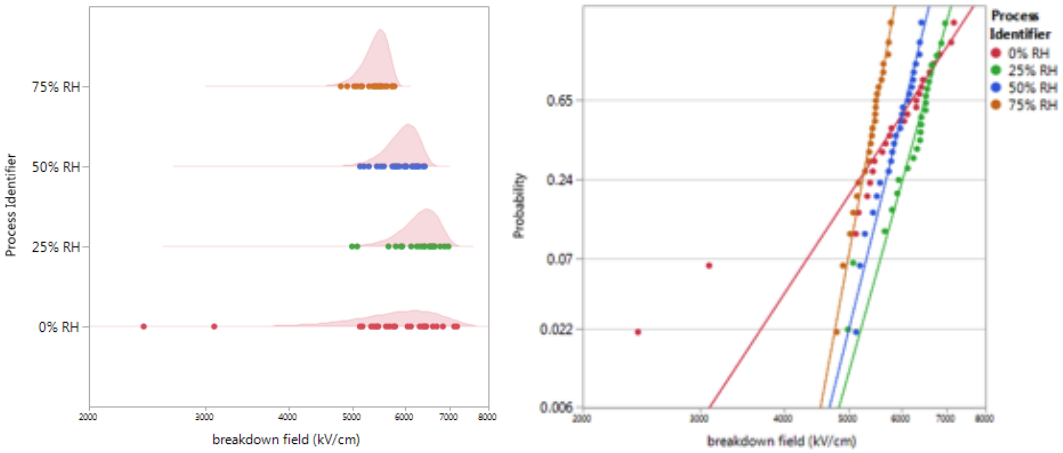

Figure 26: Weibull analysis of modified Mylar at humidity, no data point exclusions.

Table 17: Summary of Weibull statistics for modified Mylar variable humidity breakdown strength

% RH	Weibull α	Weibull β	ΔE_b
0	6167.3	7.4	0
25	6474.9	17.5	307.6
50	6066.8	19.7	-100.5
75	5504.6	26.5	-662.7

Conclusions: Variable Humidity

As humidity increases the permittivity of both materials increases as the films equilibrate to target humidity levels and the permittivity also increases as the final RH level increases. It is suggested that water molecules form clusters at the terminal –OH groups of PET, which can sustain an effective dipole within the material, contributing to the existing polarization and increasing permittivity. [17]

As humidity levels are increased from 0% to 75%, the breakdown strength of both Mylar and modified Mylar decrease. This decrease in breakdown strength is attributed to new breakdown pathways that are created by the presence of water. When sufficient amounts of water are present in the film, they can assist in the dissociation of impurities under electrical stress leading to an increase in electrical conduction and a higher probability of thermal breakdown of the dielectric. Increased conduction can lead to higher localized Joule heating which increases carrier mobility and conduction. This cycle continues and can result in a thermal runaway, contributing to failure at a lower field. [47]

3.3 Short-term Aging Study

Previous work, which examined long-term, accelerated thermal aging of the materials, was discussed in Chapter 1. From these earlier studies it had been determined that a short-term accelerated aging study would be beneficial to understanding the aging processes of Mylar and modified Mylar, as time periods less than 30 days were not examined in the previous studies. Four unmetallized samples of each material were placed into ovens at the specified temperatures. These samples were then removed from the ovens at specific time periods and tested to determine aging effects on the dielectric

properties. Each sample underwent permittivity, dielectric loss and breakdown strength testing as discussed in sections 2.3 and 2.4. Table 3 in section 2.5 shows the accelerated aging time points for this study. Any data exclusions are noted below each plot and results for these data points can be found in the Appendices.

Permittivity and Loss

Figure 27 shows permittivity and loss data after 1-day thermal aging for both Mylar and modified Mylar samples, and

Figure 28 shows data for the 29-day thermal aging. At the 1-day time point, although there is variation between the temperature groups, there are no statistically significant differences relative to the control for Mylar. For modified Mylar, there are no significant differences between the samples aged at different temperatures, although they are all statistically significantly lower than the control sample. Only one film was tested for each time/temperature point in this study, including the control. Therefore the higher permittivity of the room temperature control relative to the aged samples in the modified Mylar group may be due to film-to-film variability, rather than an aging effect. The loss values of Mylar increase as the aging temperature increases. However, there is no overall trend for modified Mylar, although the 40°C sample is significantly lower.

For virgin Mylar, after 29 days of aging permittivity values of the aged samples are significantly higher than the control, except for the 80°C sample. In addition, the 124C sample has a significantly higher permittivity than the other aged samples. Again, for modified Mylar there are no permittivity differences between the samples aged at different temperatures, although they are lower than the control. The loss generally increases with temperature for Mylar group, although there is some variability within the

temperature groups. For modified Mylar, there is significant variability and no trend with temperature.

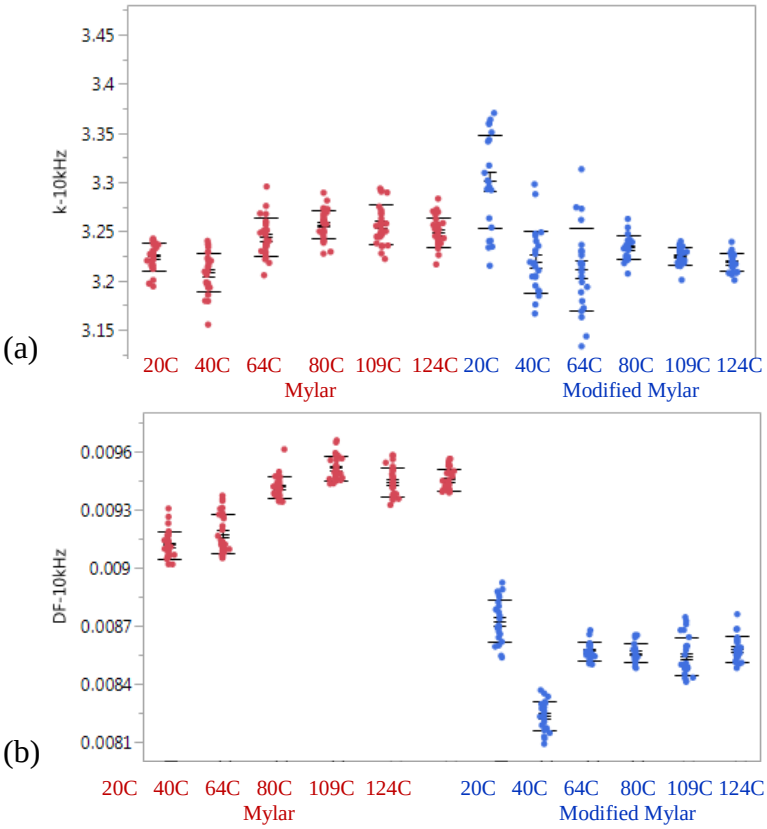

Figure 27: (a) Permittivity and (b) loss at time point T1(1 day) for Mylar (red) and modified Mylar (blue). There are 6 data point exclusions over the entire range of temperatures and test dates for Mylar and no exclusions for the modified Mylar samples.

For virgin Mylar, after 29 days of aging permittivity values of the aged samples are significantly higher than the control, except for the 80°C sample. In addition, the 124C sample has a significantly higher permittivity than the other aged samples. Again, for modified Mylar there are no permittivity differences between the samples aged at different temperatures, although they are lower than the control. The loss generally increases with temperature for Mylar group, although there is some variability within the

temperature groups. For modified Mylar, there is significant variability and no trend with temperature.

The variability within the data makes evaluation of the detailed behavior over time infeasible with the available data set. For example, for the 7-day time point in Modified Mylar the permittivity at 124°C, 7 days is much higher than both previous and subsequent time points at 124°C. This variability in results could be due to the small sample sizes, as there was only one film tested for each temperature/time point. The full sets of data can be found in Appendix B for Mylar and Appendix C for modified Mylar.

While the data does show that short-term thermal aging has some effects on permittivity and loss, the small sample size results in high variability, which makes the identification of detailed trends with the existing data set impossible. Further studies may include aging with larger sample sizes.

(a)

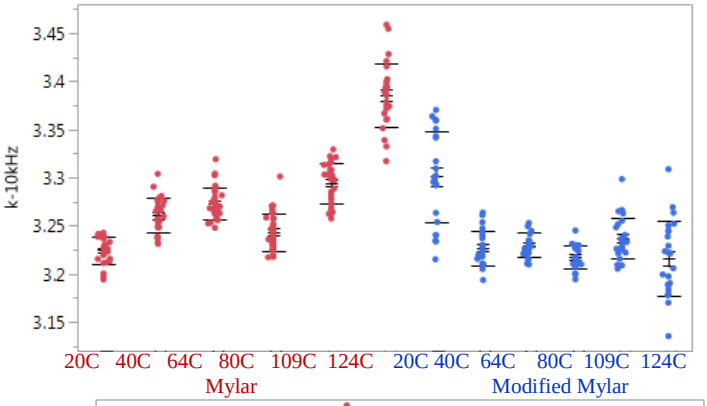

(b)

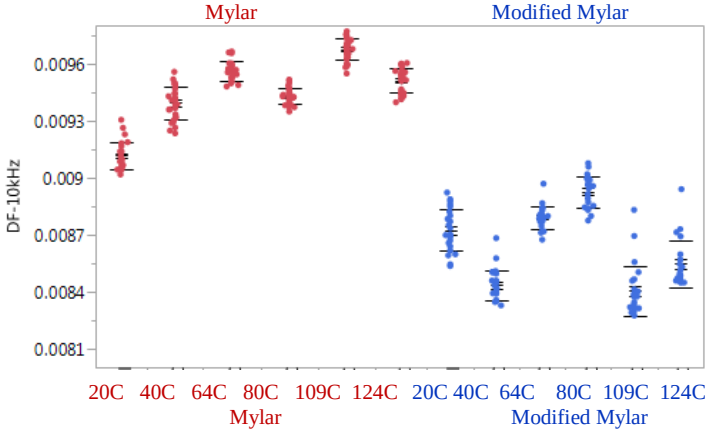

Figure 28: (a)Permittivity and (b) loss for Mylar and modified Mylar at T4 (29 days). There are 6 data point exclusions over the entire range of temperatures and test dates for Mylar and no exclusions for the modified Mylar samples.

Table 18: Mylar permittivity and loss values for each temperature over the aging time period

Mylar	**T1 = 24 hrs**		**T2 = 3 days**		**T3 = 7days**		**T4 = 29 days**	
Temperature	**κ**	**DF**	**κ**	**DF**	**κ**	**DF**	**κ**	**DF**
20°C	3.22± 0.02	0.0091 ±0.0001	-	-	-	-	-	-
40°C	3.21± 0.02	0.0092 ±0.0001	3.27± 0.03	0.0093 ±0.0001	3.18± 0.03	0.0090 ±0.0001	3.26± 0.01	0.0094± 0.0001
64°C	3.24± 0.02	0.0094 ±0.0001	3.29± 0.03	0.0096 ±0.0001	3.23± 0.01	0.0093 ±0.0001	3.27± 0.02	0.0096± 0.0001
80°C	3.26± 0.01	0.0095 ±0.0001	3.25± 0.02	0.0093 ±0.0001	3.27± 0.02	0.0093 ±0.0001	3.24± 0.02	0.0094± 0.0001
109°C	3.26± 0.02	0.0094 ±0.0001	3.25± 0.01	0.0094 ±0.0001	3.29± 0.02	0.0093 ±0.0001	3.29± 0.02	0.0097± 0.0001
124°C	3.25± 0.02	0.0095 ±0.0001	3.33± 0.03	0.0094 ±0.0001	3.31± 0.02	0.0096 ±0.0001	3.38± 0.03	0.0095± 0.0001

Table 19: Modified Mylar permittivity and loss values for each temperature over the aging time period

Modified Mylar	T1 = 24 hrs		T2 = 3 days		T3 = 7days		T4 = 29 days	
Temperature	**κ**	**DF**	**κ**	**DF**	**κ**	**DF**	**κ**	**DF**
20°C	3.30±0.05	0.009 ±0.0001	-	-	-	-	-	-
40°C	3.22±0.03	0.0082 ±0.0001	3.21± 0.02	0.0080 ±0.0001	3.21± 0.01	0.0080 ±0.0001	3.23±0.02	0.0084± 0.0001
64°C	3.21±0.04	0.0086 ±0.0001	3.21± 0.01	0.0086 ±0.0001	3.24± 0.02	0.0087 ±0.0001	3.23±0.01	0.0088± 0.0001
80°C	3.23±0.01	0.0086 ±0.0001	3.21± 0.01	0.0086 ±0.0001	3.29± 0.01	0.0086 ±0.0001	3.22±0.01	0.0089± 0.0001
109°C	3.22±0.01	0.0085 ±0.0001	3.23± 0.01	0.0085 ±0.0001	3.29± 0.02	0.0085 ±0.0001	3.24±0.02	0.0084± 0.0001
124°C	3.22±0.01	0.0086 ±0.0001	3.25± 0.01	0.0086 ±0.0001	3.37± 0.03	0.0089 ±0.0001	3.22±0.04	0.0085± 0.0001

Dielectric Breakdown Strength

Breakdown measurements were performed on aged samples to determine if the aging process changes the dielectric breakdown strength. Previous, long-term aging studies showed that there was no effect on the breakdown strength that could be correlated to thermal aging of the materials. This conclusion also holds true for the short-term aging experiments performed in this thesis. Figure 29 shows plots of the cumulative

distribution function for each aging temperature at time points 1 day, 3 days, 7 days and 29 days, for the Mylar samples. The Weibull α parameter fluctuates between about 6200kV/cm and 6500kV/cm over all temperatures and aging time periods. Below (Table 20) are listed Weibull α and Weibull β parameters for each temperature and time period for Mylar. The β parameters also follow no distinct trend, but rather confirm the stochastic nature of dielectric breakdown strength in polymeric materials.

Table 20: Mylar short-term aging Weibull parameter summary by temperature

Mylar	**T1 = 24 hrs**		**T2 = 3 days**		**T3 = 7days**		**T4 = 29 days**	
Temperature	**α (kV/cm)**	**β**	**α (kV/cm)**	**β**	**α (kV/cm)**	**β**	**α (kV/cm)**	**β**
40°C	6548.4	11.0	6316.8	7.1	6580.2	8.0	6205.8	8.1
64°C	6546.2	10.3	6656.6	13.2	6510.1	10.6	6493.1	17.3
80°C	6391.9	10.5	6464.2	8.9	6751.1	10.9	6544.2	14.7
109°C	6363.9	12.2	6606.5	11.8	5852.9	2.6	6437.1	12.3
124°C	6636.5	8.8	6590.5	9.5	6646.7	24.9	6122.6	18.4

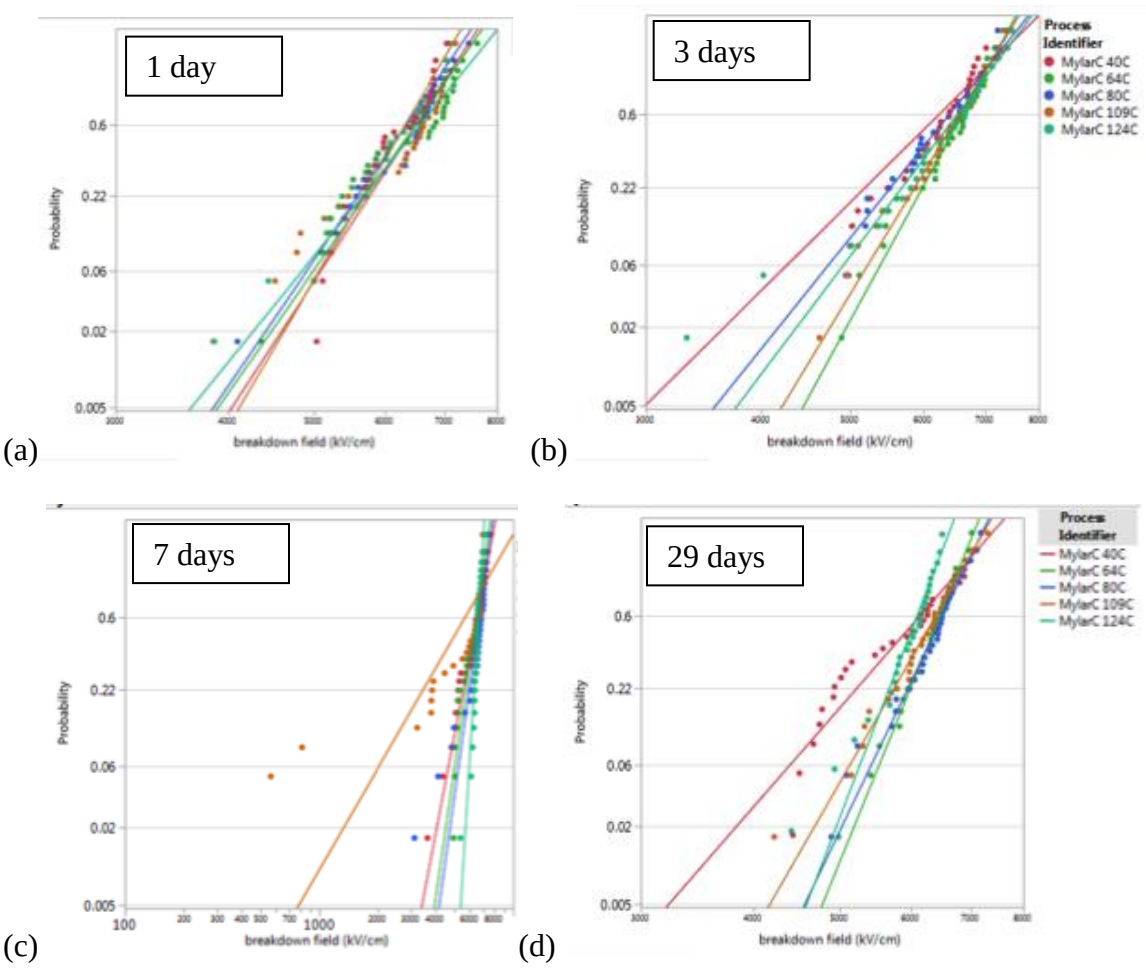

Figure 29: Mylar short-term aging breakdown strength (a) Weibull Analysis of T1 for all temperatures (b) Weibull Analysis of T2 for all temperatures (c) Weibull Analysis of T3 for all temperatures (d) Weibull Analysis of T4 for all temperatures. There are 2 data point exclusions over the course of the aging time periods.

Figure 30 shows the probability distribution functions for modified Mylar for each aging temperature at time intervals of 1 day, 3 days, 7 days and 29 days. The Weibull α parameter in the modified material varies from about 6600kV/cm to 7300kV/cm but does not follow a trend with time for any of the individual temperatures suggesting that aging does not have an effect on the breakdown strength. The variations in data could be a consequence of small sample sizes (single film for each

time/temperature) and film variability. The modified material has proven to be much variable, this is possibly due to the doping process, leading to a greater spread of data values. Table 21 lists the Weibull α and Weibull β parameters for each temperature. Short-term aging appears to have no significant effects on the breakdown strength of modified Mylar.

Table 21: Modified Mylar short-term aging Weibull parameter summary by temperature

Modified Mylar	**T1 = 24 hrs**		**T2 = 3 days**		**T3 = 7days**		**T4 = 29 days**	
Temperature	**α (kV/cm)**	**β**	**α (kV/cm)**	**β**	**α (kV/cm)**	**β**	**α (kV/cm)**	**β**
40°C	6747.7	5.3	6678.8	8.8	6978.7	9.1	6508.9	7.1
64°C	6702.6	9.4	7148.2	8.6	6890.2	6.3	6719.2	12.6
80°C	6402.2	7.2	7190.6	11.3	7646.3	14.4	6648.0	6.1
109°C	6712.2	8.9	7160.1	10.0	7234.1	11.3	6100.2	6.2
124°C	6547.5	7.8	7337.1	9.9	6748.1	8.2	7285.3	13.2

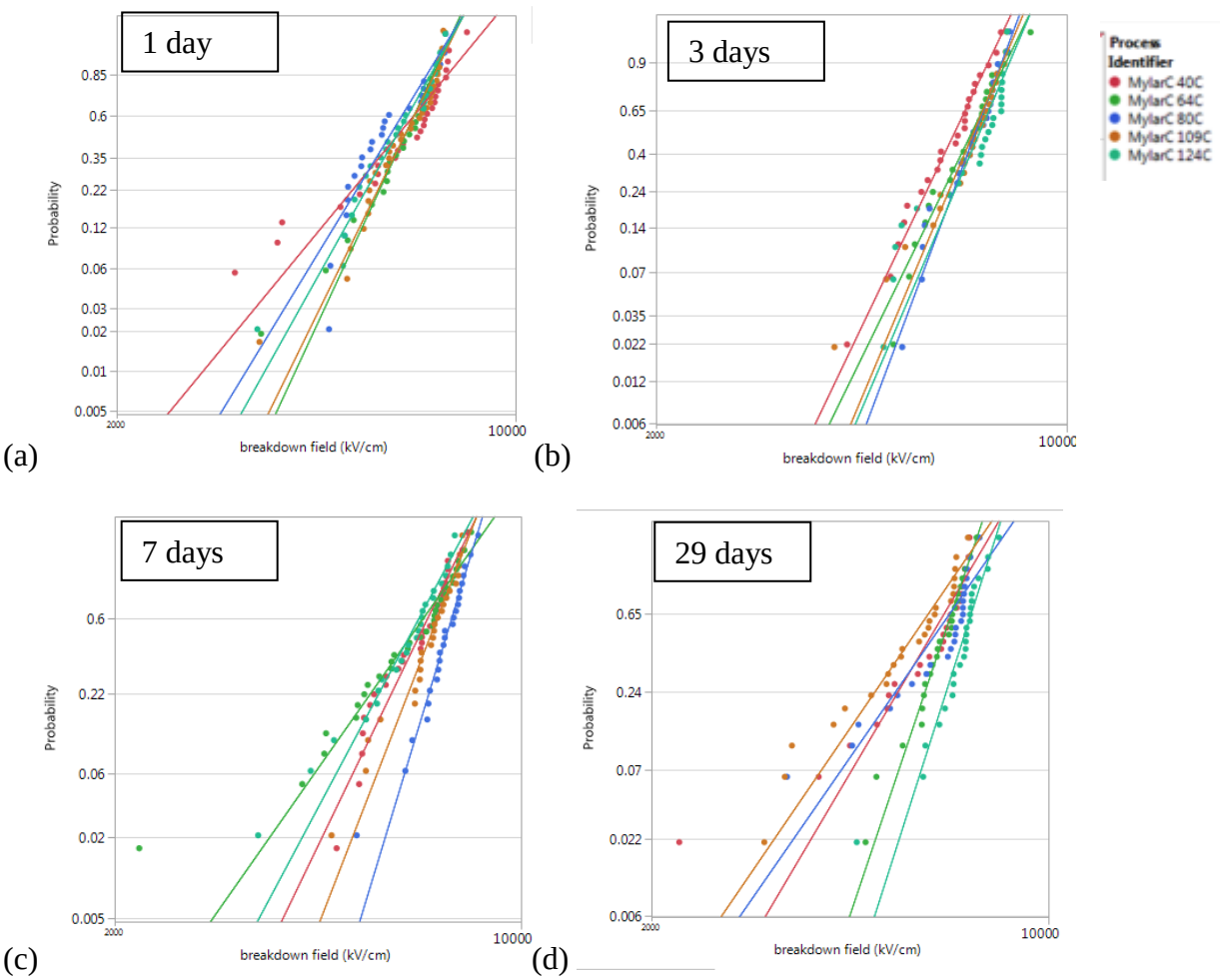

Figure 30: Modified Mylar short-term aging breakdown strength (a) Weibull Analysis of T1 for all temperatures (b) Weibull Analysis of T2 for all temperatures (c) Weibull Analysis of T3 for all temperatures (d) Weibull Analysis of T4 for all temperatures. There are 7 data point exclusions over the course of the aging study.

Conclusions: Short-term Aging

While the data does show that short-term thermal aging has some effects on permittivity and loss, the analysis of permittivity and loss data for this aging study is complicated due to variability in results. Only one film was tested for each time/temperature point, resulting in a high impact on the results of film-to-film variation. In order to draw strong conclusions about the time dependence of short-term aging,

studies with larger sample sizes will be necessary. Dielectric breakdown strengths of Mylar or modified Mylar are not affected by aging from 0 to 29 days. For dielectric breakdown strength, the modified material consistently measured higher breakdown strengths compared to the virgin material; this trend has been noted throughout the course of this thesis and also in literature. [38-41]

Chapter 4: Effect of varying test setup parameters

4.1 Metallization Thickness and Self-clearing

In Chapter 1, the effects of metallization on dielectric properties were discussed in terms of self-clearing properties of metallized polymer dielectric materials. Self-clearing events happened more readily in thinner metallized films than in films with thicker metallization. [34] To determine if self-clearing happens in these samples, films that have been coated with both 50nm Au deposition and 200nm Au deposition were tested. The metallization thickness comparisons presented are the same samples from the variable temperature study with the same sample size and exclusions for the 20°C data sets for both 50nm Au and 200nm Au metallization. In addition to different metallization thicknesses on multi-electrode films, metallization thickness effects were also studied on single electrode films and compared to multi-electrode samples. Metallization thickness samples for the multi-electrode study consists of the standard 3 x 30 electrode sample films. However, all of the tests for the single electrode study were performed on one 30 electrode film for Mylar and one 24 electrode film for modified Mylar. The sample sizes are smaller than for most of the other studies in this work which tested 3 films each. Any data exclusions are noted below each plot and results for those excluded data points can be found in the Appendices.

4.1.1 Metallization thickness

Permittivity and Loss

Au thickness corrections are made during calculation and analysis of data for both 50 and 200nm Au metallized samples for the comparison of metallization thickness studies. After measuring permittivity and loss, it is apparent that there are not statistically

significant differences between the different metallization thicknesses at each temperature. However, the trend with temperature did vary with metallization thickness, possibly due to differences in shrinkage of the polymer at elevated temperatures as discussed in section 3.1. Permittivity and loss are intrinsic to the material itself, and should be dependent only on the material itself not the metallization thickness. Figure 31 shows a comparison of 50nm Au metallized films and 200nm Au metallized films for both permittivity and loss. There is no statistically significant difference between the 200nm and 50nm data. Table 22 and Table 23 show permittivity and loss data for each metallization thicknesses at 20°C, 43°C and 73°C.

(a)

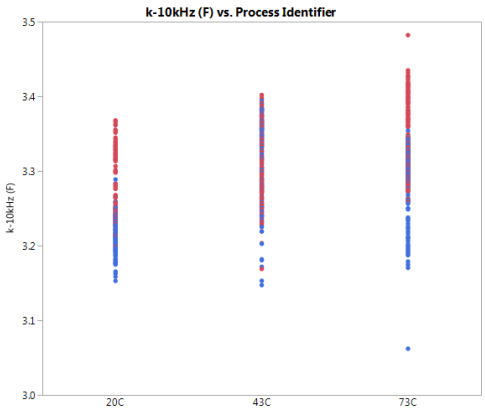

(b)

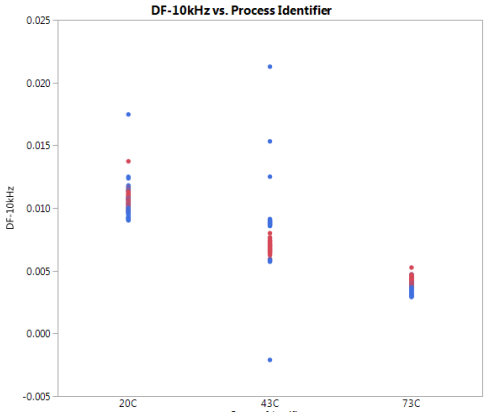

Figure 31: (a) Permittivity comparison between 50nm Au metallized samples (blue) and 200nm metallized samples (red) (b) Dielectric loss comparison of 50nm Au metallized samples (blue) and 200nm Au metallized samples (red)

Table 22: Mylar permittivity for 50nm Au vs. 200nm Au metallization

Permittivity, κ (10kHz)		
Parameter	50nm	200nm
20°C	3.22±0.02	3.27±0.04
43°C	3.31±0.05	3.31±0.04
73°C	3.29±0.02	3.32±0.05

Table 23: Mylar dielectric loss for 50nm Au vs. 200nm Au metallization

Dielectric Loss, κ (10kHz)		
Parameter	50nm	200nm
20°C	0.0099±0.0007	0.0108±0.0006
43°C	0.0061±0.0001	0.0069±0.0003
73°C	0.0036±0.0001	0.0042±0.0002

Dielectric Breakdown Strength

Although there were no differences in dielectric loss and permittivity between the two metallization thicknesses, it was hypothesized that there would be differences in the breakdown strengths. Permittivity and loss are properties that are intrinsic to the material itself, and should not be affected by metallization thickness, which is taken into account during calculations of permittivity. It is hypothesized that self-clearing, which was discussed in Chapter 1, may occur more extensively in samples with thinner metallization. Self-clearing may remove defects from surrounding electrodes during the breakdown event of the electrode under test, leading to higher measured

breakdown strengths for electrodes tested later in the test order. However, Figure 32 shows that there are not significant differences in the breakdown strengths for the two different metallization for either Mylar or modified Mylar, suggesting that self-clearing either does not occur, or occurs to the same extent in the 50 and 200nm Au metallized films. The next section will discuss results of single versus multi-electrode breakdown studies, which attempt to confirm the existence of self-clearing in these metallized films.

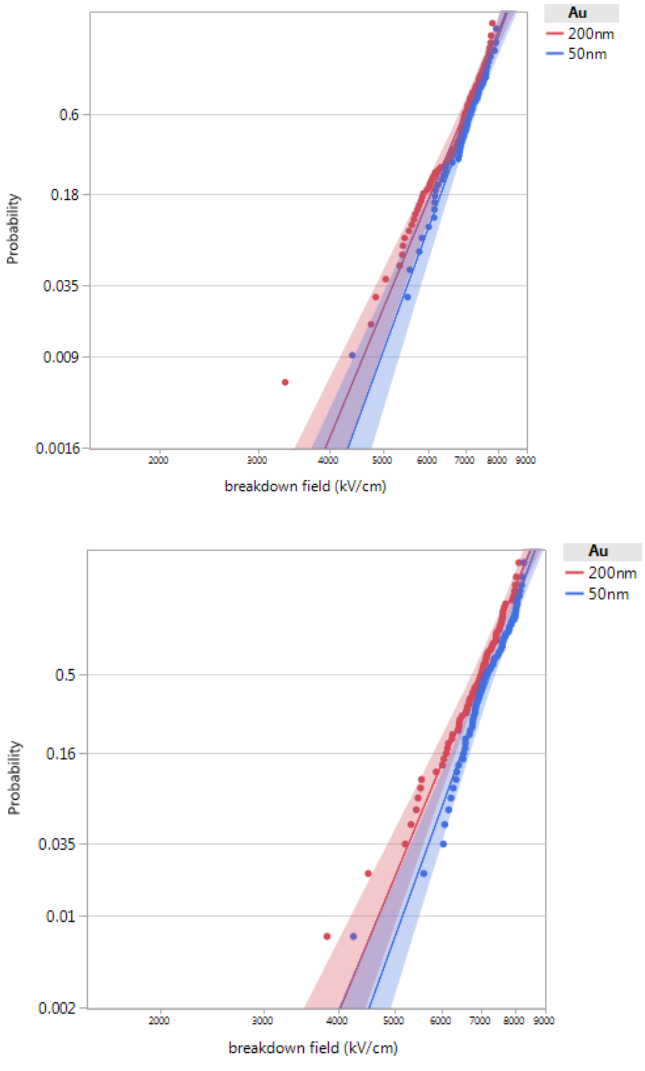

Figure 32: Comparison of Weibull parameters between 50nm Au and 200nm Au metallization thicknesses for multi-electrode samples of (a) Mylar and (b) modified Mylar

4.1.2: Single Electrode Samples

Single electrode vs. Multi-electrode film breakdown

As mentioned in the previous section, there is concern that self-healing may occur in metallized multi-electrode films due to the small electrode-to-electrode distance, yielding higher measured breakdown strengths due to the removal of defects during breakdown of adjacent electrodes. Figure 33 shows the cumulative distribution plots of the single electrode breakdown study of both Mylar and modified Mylar with 50nm Au and 200nm Au metallization. There are significant differences in the breakdown strengths of the 50nm Au and 200nm Au metallized single electrode samples. The 200nm Au metallized samples consistently measure lower breakdown strengths than the 50nm Au metallized samples. Table 24 shows Weibull parameters for Mylar and modified Mylar single electrode samples at each metallization thickness. The 200nm Au metallized samples also have a consistently lower β parameter than the 50nm Au metallized samples; this is a result of greater spread of measured breakdown strengths. This variability in data could also be a result of a sample size that consisted of one standard film that was cut into individual electrodes.

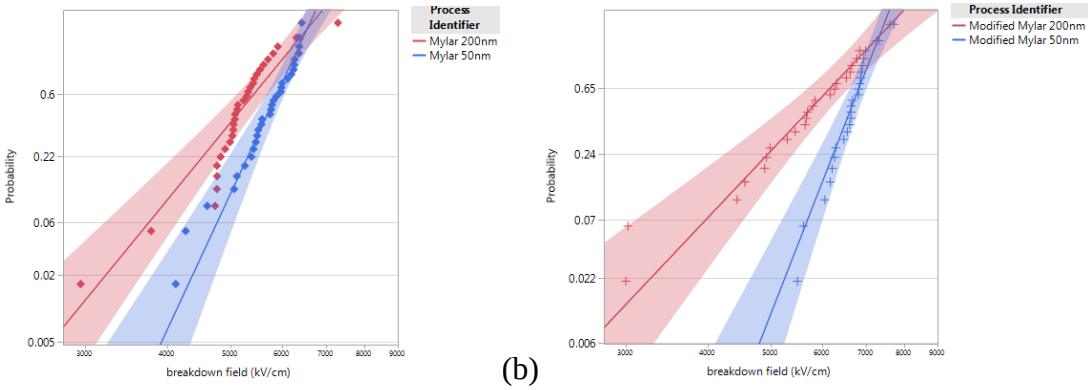

Figure 33: Weibull analysis of single electrode breakdown with different metallization thickness for (a) Mylar and (b) modified Mylar, no exclusions.

Table 24: Weibull parameters for Mylar and modified Mylar single and multi-electrode films at 50nm and 200nm Au metallization thickness

Sample	Weibull α (kV/cm)	Weibull β
Mylar 50nm Au single electrode	5926	12.8
Mylar 50nm Au multi-electrode	7177	12.7
Mylar 200nm Au single electrode	5497	7.3
Mylar 200nm Au multi-electrode	7006	11.2
Modified Mylar 50nm Au single electrode	6801	14.7
Modified Mylar 50nm Au multi-electrode	7468	12.4
Modified Mylar 200nm Au single electrode	6117	6.1
Modified Mylar 200nm Au multi-electrode	7180	10.8

Figure 34 shows the cumulative probability distribution plots for Mylar, comparing single and multi-electrode samples at each metallization thickness. It is evident from these plots that the breakdown strengths of the single electrode samples are significantly lower than in the multi-electrode samples, suggesting that self-clearing is occurring in the multi-electrode samples, causing them to measure higher breakdown strengths than the single electrode samples. This trend is also seen in the modified material, Figure 35.

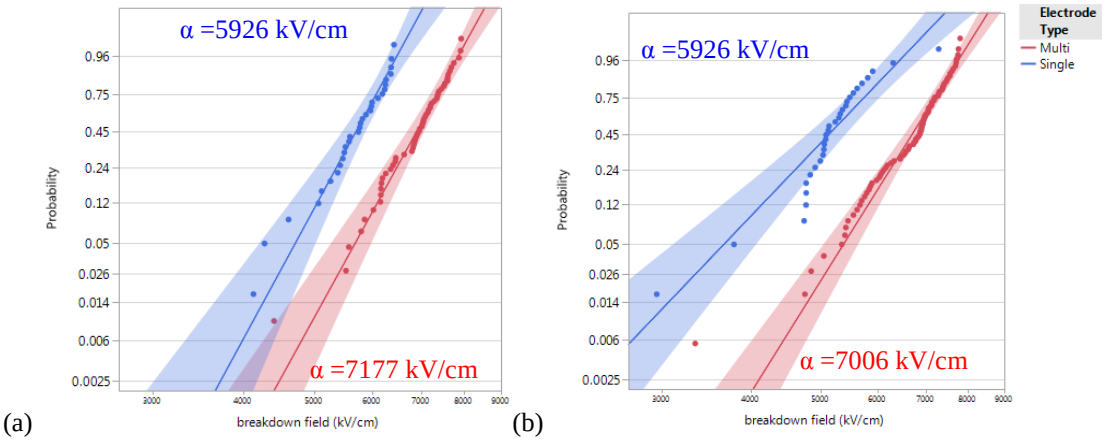

Figure 34: Mylar cumulative probability distribution plots comparing multi and single electrode samples at (a) 50nm Au metallization and (b) 200nm Au metallization

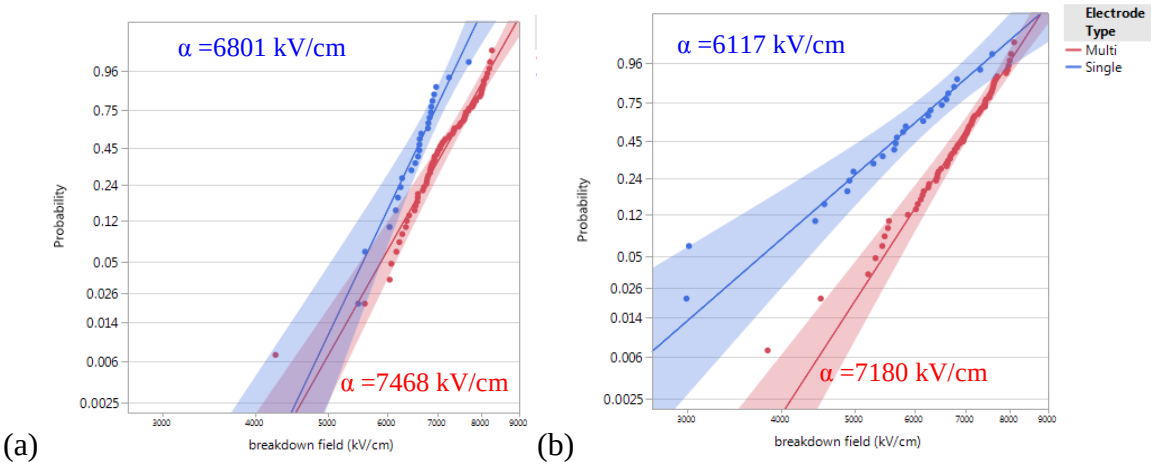

Figure 35: Modified Mylar cumulative probability distribution plots comparing multi and single electrode samples at (a) 50nm Au metallization and (b) 200nm Au metallization

A set of experiments was also completed on films that were masked with the 30-electrode mask on both sides of the film during deposition rather than a single mask with a full blanket metallization on the back. The electrodes in the case of the double masked films are the exact same size on both sides of the dielectric. It was hypothesized that these samples would experience reduced self-clearing effects due to the lack of a common back electrode. Figure 36 shows the Weibull analysis of the 50nm Au double masked sample compared to the 50nm Au multi-electrode sample. Although the

distributions of these samples are not the same, the Weibull α parameters, which are taken at 63.2% probability show no significant difference between the double masked sample and single masked sample. The double masked samples may experience reduced self-clearing. Self-clearing within a sample should yield tighter distributions and decreased dispersions due to the elimination of low breakdown pathways by self-clearing.

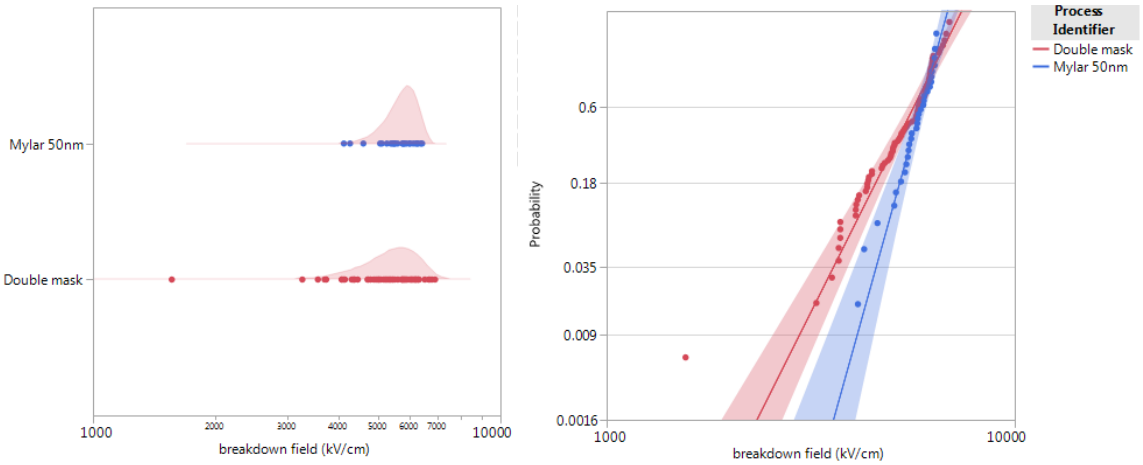

Figure 36: Weibull analysis of 50nm Au single mask, 200nm Au single mask and 50nm Au double mask samples, no exclusions

Conclusions: Metallization and Self-Clearing

The data presented revealed no significant differences in permittivity and loss of Mylar and modified Mylar multi-electrode samples at 50nm Au metallization and 200nm Au metallization. There were also no differences in dielectric breakdown strength for multi-electrode samples with different metallization thicknesses. There are two possible explanations that the breakdown strength would be the same for multi-electrode samples with different metallization thicknesses. One explanation would be that there is no self-clearing occurring within the samples, while the second explanation would be that the extent of self-clearing is not affected by the metallization thickness up to 200nm. Comparison of single and multi-electrode samples revealed that multi-electrode samples

consistently measured higher breakdown strengths than the single electrode samples. These results support the hypothesis that self-clearing is occurring in multi-electrode samples. However, there was a significant difference in the breakdown strengths of the 50 and 200nm Au metallized electrode samples when tested individually (single electrode). It is unclear why metallization thickness has an effect in single electrode samples but not multi-electrode samples. To minimize the effects of self-clearing, previous studies have suggested optimal electrode geometries and spacing. [50] Further studies could enable better understanding of how metallization thickness contributes to decreased breakdown strengths, but only in single electrode samples.

4.2: Electrode Area

In Chapter 1, it was discussed that test volume can have a significant impact on measured breakdown strength of a material. For a material with a constant defect density, as the test volume increases, the number of defects present within the test volume also increases, leading to an increased probability of failure. There are two ways to change the test volume; by increasing film thickness or by increasing electrode diameter. In this work an electrode diameter of 6.3mm is utilized, to allow for comparison of results to previous studies. However, it is important to understand the effect of electrode area on breakdown strength for large-scale applications. Laboratory studies of these dielectric materials are performed on electrode areas much smaller than the active area of a capacitor. It is important to understand how electrode area affects dielectric performance so that data obtained in the laboratory setting can be extended to capacitor application. The next portion of this thesis examines the area effects by changing electrode diameter. Diameters of 9mm, 12.65mm, and 18.9mm have been investigated and electrode

diameters and spacing configurations are shown in Figure 37. Sample sizes varied based on the electrode diameters; Table 27 shows the sample sizes for each electrode diameter for both Mylar and modified Mylar. Any exclusions from the data analysis are noted below each plot and results for those points can be found in the Appendices.

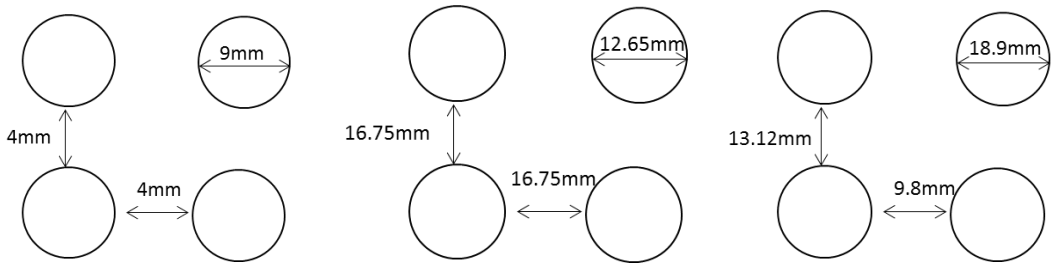

Figure 37: 9mm, 12.65mm and 18.9mm electrode configurations

Permittivity and Loss

It was expected that there would be no changes to permittivity and loss over the diameter range, as area is taken into consideration during the calculation of permittivity from measured capacitance. As shown in Figure 38 and Table 25, there are no significant changes in permittivity or loss values over the range of electrode areas. This holds true for modified Mylar as well (Figure 39), and a summary of permittivity and loss values for modified Mylar is found in Table 26. Although there were no significant changes in permittivity or loss, it is expected that there will be significant effects on the breakdown strength as area is increased.

It is important to note that, these permittivity and loss measurements were measured on an uncalibrated LCR meter, which resulted in higher measured permittivity values than films measured with the calibrated LCR meter. This issue was not found until after breakdown strength testing had been completed, making retesting these films

impossible. Therefore these permittivity and loss values are compared only to each other and not to the 6.3mm diameter samples utilized throughout the rest of the thesis.

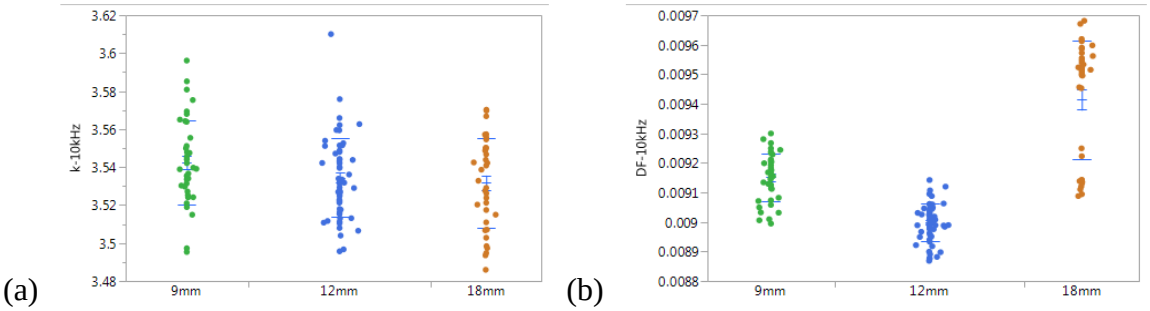

Figure 38: Mylar (a) permittivity and (b) loss plots for variable electrode diameters

Table 25: Mylar Permittivity and Los values for variable electrode area

Electrode Diameter	Electrode Area	Permittivity (10kHz)	Loss (10kHz)
9mm	44.4 mm^2	3.57±0.02	0.0091±0.0001
12.65mm	62.4 mm^2	3.56±0.02	0.0092±0.0001
18.9mm	101.3 mm^2	3.56±0.02	0.0094±0.0002

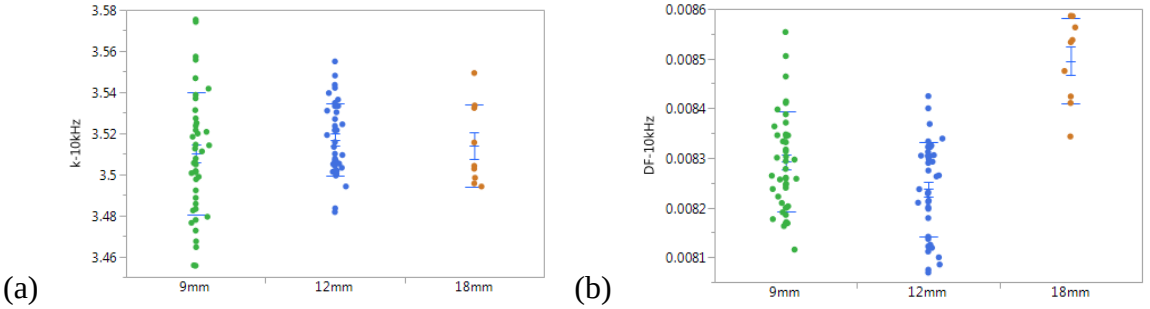

Figure 39: Permittivity and loss for modified Mylar varying electrode area, no data exclusions.

Table 26: Modified Mylar permittivity and loss values for variable electrode area

Electrode Diameter	Electrode Area	Permittivity (10kHz)	Loss (10kHz)
9mm	44.4 mm^2	3.57±0.02	0.0091±0.0001
12.65mm	62.4 mm^2	3.56±0.02	0.0092±0.0001
18.9mm	101.3 mm^2	3.56±0.02	0.0094±0.0002

Dielectric Breakdown Strength

Breakdown testing was completed on sets of samples at 500V/s ramp-to-fail breakdown: see Table 27 for sample sizes for each electrode area. It was hypothesized in previous sections that the dielectric breakdown strength for larger electrode areas would decrease, and the number of defects present in the test area should increase as the area increases. Figure 40 shows the Weibull analysis of Mylar at 6.3mm, 9mm, 12.65mm, and 18.9mm electrode diameters, and Figure 41 is the Weibull analysis of the modified Mylar for the same electrode diameters. The data obtained from this experiment show that as electrode area increases, the breakdown strength decreases. Comparing the Mylar and modified Mylar to each other (Table 28 and Table 29), there is a significant difference between the two materials in the change in breakdown strength as electrode area increases. The decrease in breakdown strength is much greater in the modified material compared to the virgin Mylar. This suggests that the doping processes may increase the defect density or change the type of defect present in the material, resulting in greater sensitivity to the test volume in the modified Mylar. It is important to note the differences in sample sizes, show in Table 27, as the larger test area samples had much smaller sample sizes, this should be taken into consideration in evaluating differences between

these groups. Future studies with larger sample sizes would allow for confirmation of the results seen in this study.

Table 27: Mylar and modified Mylar electrode area sample sizes

Electrode Area Sample Sizes	**Mylar**		**Modified Mylar**	
Electrode Diameter	N (films)	N (electrodes)	N (films)	N (electrodes)
6.3mm	3	30	3	24
9mm	2	20	2	15
12.65mm	5	12	5	8
18.9mm	4	6	4	2

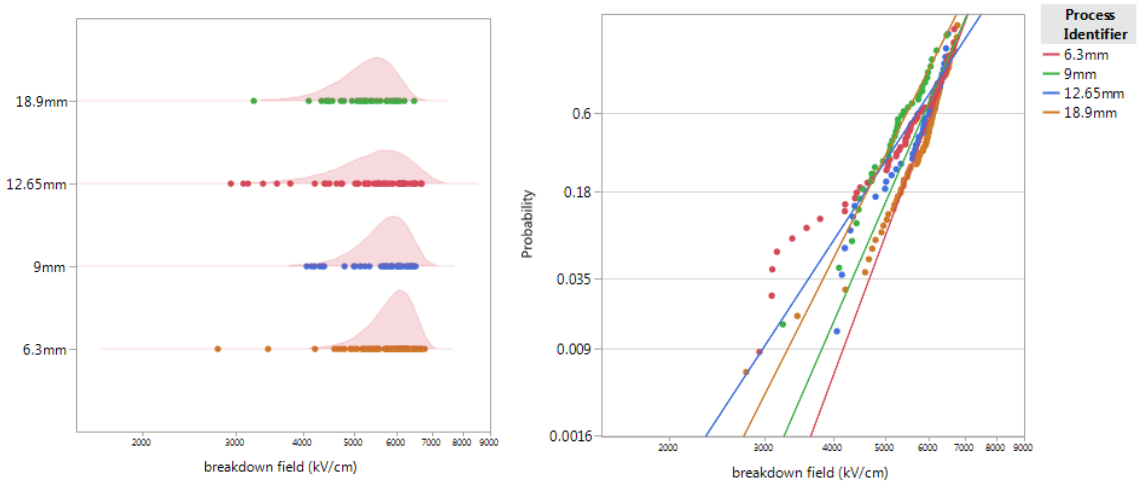

Figure 40: Mylar Weibull analysis for varying electrode area, 2 data points are excluded.

Table 28: Comparison of Mylar Weibull parameters for varying electrode area

Electrode Diameter	Weibull α (kV/cm)	Weibull β	ΔE_b (kV/cm)
6.3mm	6106.5	12.5	0
9mm	5941.9	10.7	-164.6
12.65mm	5775.9	7.1	-330.6
18.9mm	5522.0	9.2	-584.5

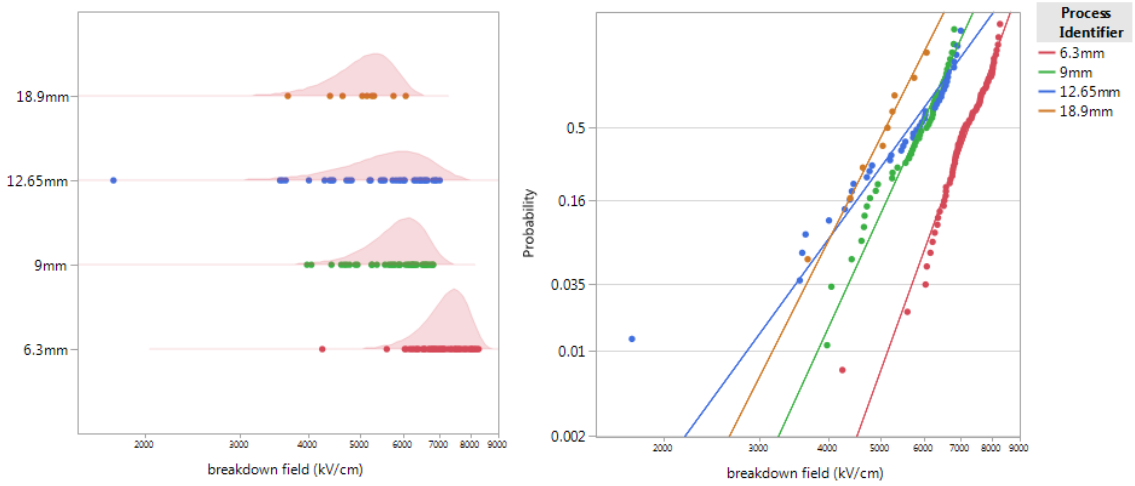

Figure 41: Modified Mylar Weibull analysis for varing electrode area, no exclusions.

Table 29: Comparison of modified Mylar Weibull parameters for varying electrode area

Electrode Diameter	Weibull α (kV/cm)	Weibull β	ΔE_b (kV/cm)
6.3mm	7467.5	12.4	0
9mm	6132.1	9.7	-1335.4
12.65mm	5991.4	6.1	-1476.1
18.9mm	5319.9	8.9	-2147.6

Conclusions: Electrode Area

As expected, increasing electrode area by increasing the diameter of the electrodes deposited onto the films did not affect the permittivity or loss in the 9mm, 12.65mm and 18.9mm diameter electrodes. The electrode area is taken into consideration during the calculation of permittivity from capacitance, as discussed in Chapter 1.

However, there was a significant effect on the breakdown strengths of the materials. As electrode diameter increased the measured dielectric breakdown strength decreased. The increase in area also increases the number of defects present in the test area. The greater number of defects present in the test area increases the possible pathways by which failure can occur, resulting in lower measured breakdown strength. Both virgin and modified Mylar showed decreases in measured breakdown strength with increasing electrode area. However, the modified Mylar shows a greater decrease compared to Mylar. The modified material may a different defect population than the virgin material, possibly due to the doping process.

4.3: DC Voltage Ramp Rate

Another important parameter in establishing a reliable and accurate measurement of dielectric breakdown strength is voltage ramp rate. All other breakdown experiments in this thesis were completed at a ramp rate of 500 V/s with a stepped voltage increase of 50V per 100 milliseconds. However, applied voltages can be ramped in two ways, as a stepped voltage ramp or as a continuous voltage ramp. Stepped ramps apply the voltage increase in incremented time periods, the amount voltage applied in the specified period step changes as ramp rates increase and the voltage increase for each step is ‘instantaneous’. Continuous ramp rates apply the voltage increase steadily rather than in a

stepwise fashion. This study examined the effects of varying ramp rate, as well as stepped versus continuous ramp rates on Mylar and modified Mylar with samples sets of 2 x 15 electrode films. Since the DC voltage sources and data acquisition hardware and programs in the stepped and continuous ramp rates were different, it is important to note the differences in the program outputs of each setup and the true voltage that is being provided. The instruments are calibrated by use of a multimeter, and Table 30 and Table 31 show the calibration data for each instrument at two different ramp rates, as well as the voltage difference between the two ramp methods. The method for calibrations is described in detail in the Appendix, which also contains the calibration plots. The difference in the two instruments at the 500V/s ramp increases over the course of the ramp. The stepped ramp actually leads the true voltage output over the course of the ramp, whereas the continuous ramp lags behind the true voltage. At 3000V/s ramp rate both stepped and continuous ramps lag behind the true voltage. The lag in the stepped voltage increases over the course of the voltage ramp. The continuous voltage lags by about 100 V consistently throughout the course of the ramp. The variance between the program output and the true voltage makes it necessary to correct the collected data prior to comparing different the different ramp types and different ramp rates, as the variance is not the same for every ramp rate.

Table 30: Stepped and continuous ramp rate calibration data, 500V/s

True Voltage	Stepped Output	Continuous Output	ΔV Stepped	ΔV Continuous	ΔV (Stepped vs. Continuous)
3000	3126.833	2728.08	-126.833	271.92	398.753
6000	6229.133	5249.58	-229.133	750.42	979.553
9000	9331.433	7771.08	-331.433	1228.92	1560.353
12000	12433.733	10292.58	-433.733	1707.42	2141.153
15000	15536.033	12814.08	-536.033	2185.92	2721.953

Table 31: Stepped and continuous ramp rate calibration data, 3000V/s

True Voltage	Stepped Output	Continuous Output	ΔV Stepped	ΔV Continuous	ΔV (Stepped vs. Continuous)
3000	2811.041	2879.36	188.959	120.64	309.599
6000	5704.241	5891.96	295.759	108.04	403.799
9000	8597.441	8904.56	402.559	95.44	497.999
12000	11490.641	11917.16	509.359	82.84	592.199
15000	14383.841	14929.76	616.159	70.24	686.399

In order to compare the two ramp methods to one another, correction of data by calibration is required as there may be differences in the program output voltage for each

ramp method. Corrections to the 500V/s and 3000 V/s ramp rates were conducted based off the calibration data presented in Table 30 and Table 31. Figure 42 and Figure 43 compare ramp rates of 500V/s and 3000V/s for each ramp method. For Mylar and modified Mylar, the breakdown strengths of the stepped ramp method at 500V/s and 3000V/s ramp rates are not statistically different from one another. However, the breakdown strengths of the 500V/s and 300V/s continuous ramp method are significantly different for both materials. As the continuous ramp rate increases, the breakdown strength increases as well. This could be due to the time period in which the material is placed under electrical stress, as slower ramp rates are exposed to applied voltage much longer to reach the same voltage levels as the faster ramp rates. This electrical stress can degrade the film, causing failure at lower fields before the ramp rate can ever reach equivalent voltages as the faster rates.

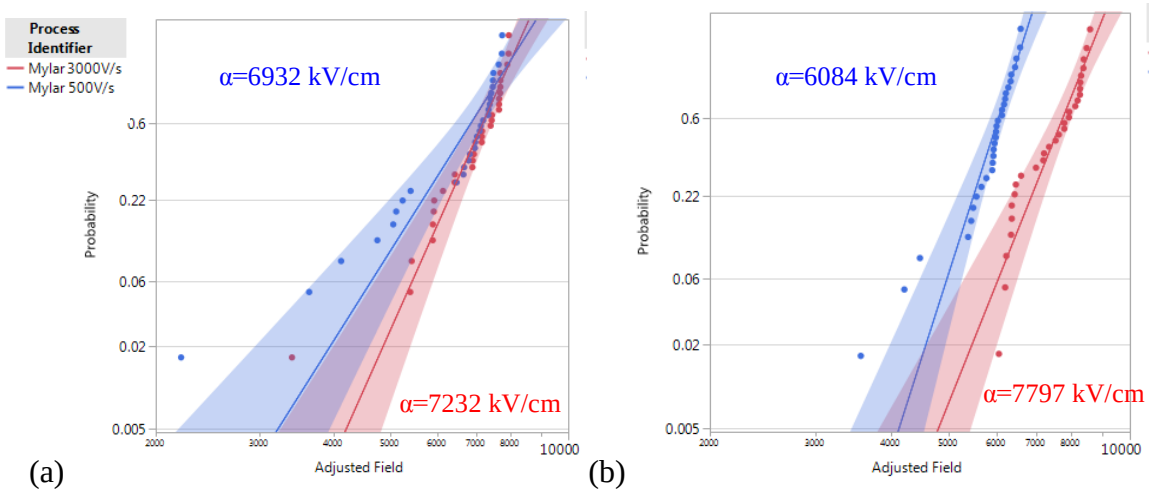

Figure 42: Comparison of ramp rates for (a) stepped and (b) continuous ramp rate at 500V/s and 3000V/s for modified Mylar

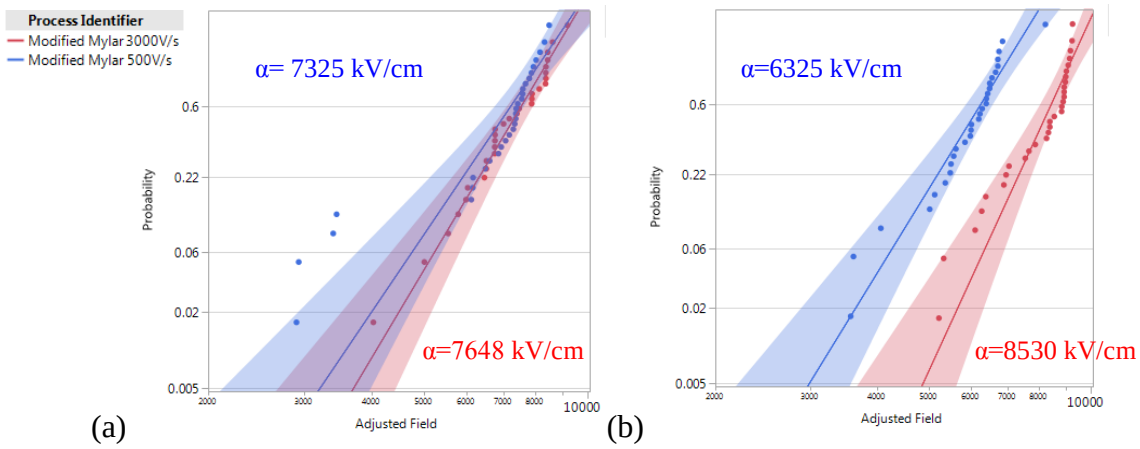

Figure 43: Comparison of ramp rates for (a) stepped and (b) continuous ramp rates at 500V/s and 3000V/s for modified Mylar

After comparing ramp rates to one another for each ramp methods, it became apparent that the ramp methods have a significant effect on the breakdown strength as well. Figure 44 compares corrected stepped and continuous ramp rates for Mylar at 500V/s and 3000V/s. These data show that the stepped and continuous ramp rates are indeed significantly different from one another. Another interesting result is that at the slower ramp rates, the stepped ramp measures higher breakdown strengths than the continuous ramp rates. However, at faster ramp rates, this trend is reversed and continuous ramp rates measure higher breakdown strengths than the stepped ramp. These same trends are seen in the modified material as well, Figure 45. In the stepped ramp a discrete amount of voltage is applied 'instantaneously'; as the ramp rates increase, the instantaneous step size increases as well. For example, in the 500V/s stepped ramp the voltage is increased by 50V every 100 milliseconds, whereas in the 3000V/s ramp the voltage is increased by 300V every 100 milliseconds. This increase in step size may result in the differences seen between stepped and continuous voltage ramps at different ramp rates because a greater amount of voltage is being instantaneously applied to the

sample within the same time period which imposes a greater amount of electrical stress on the sample that could activate breakdown mechanisms.

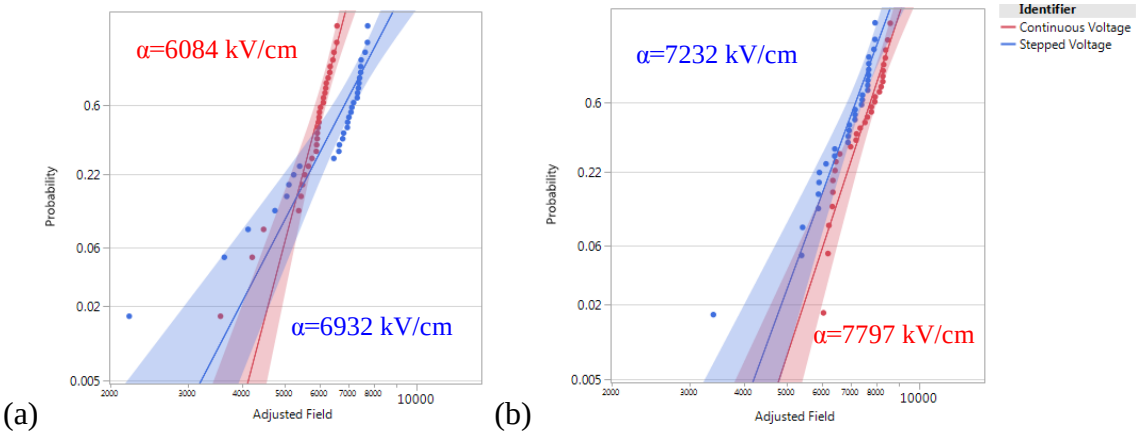

Figure 44: Comparison of stepped and continuous ramp rates for Mylar breakdown strengths at (a)500V/s and (b) 3000V/s. There is one excluded data point from the Mylar 300 V/s data set.

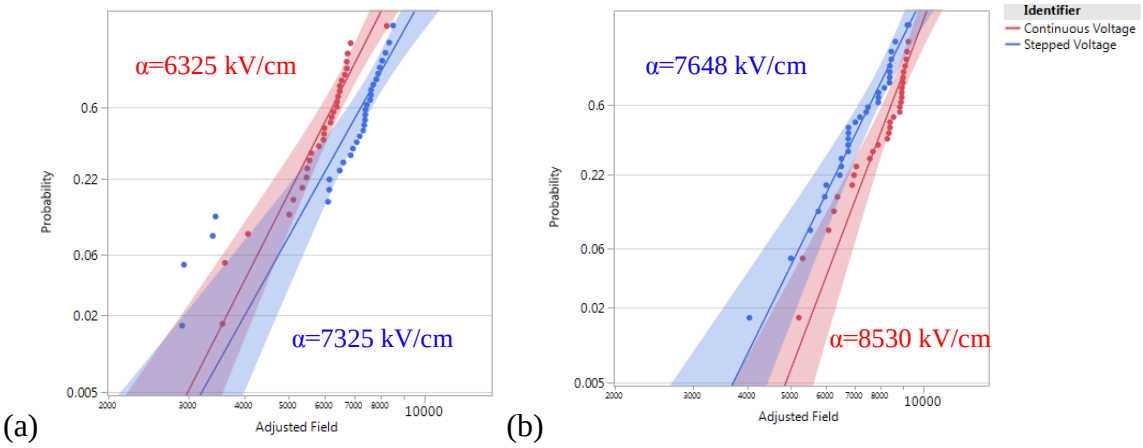

Figure 45: Comparison of stepped and continuous ramp rates for modified Mylar breakdown strengths at (a) 500V/s and (b) 3000V/s

Conclusions: DC Voltage Ramp Rate

As DC voltage ramp rate is increased the measured breakdown strengths of both the virgin and modified materials increase as well. The continuous ramp method resulted in a significant increase of breakdown strength from 500v/s to 3000V/s compared to the stepped ramp method.

The voltage ramp can be applied in two different ways. Voltage applied by a stepped method adds the voltage at incremented time periods, and the amount of voltage applied in the step changes as ramp rates increase. Continuous voltage ramp rates are applied continuously. Calibrations comparing the output voltages of each method to true voltage measured by a multi-meter show that the test setups and programs both have significant deviations between program output and the true voltage applied to the film. Therefore to compare methods the data must be corrected for each test setup before comparison of the two methods can be done accurately. After correcting the data for the 500V/s and 3000V/s ramp rates stepped and continuous ramp rates were compared. The comparison showed that at slower ramp rates the stepped voltage yields higher breakdown strengths. However, at faster ramp rates the continuous voltage yielded higher breakdown strengths. The increase in step size may result in the differences seen between stepped and continuous voltage ramps at different ramp rates; a greater amount of voltage is being instantaneously applied to the sample within the same time period. This may impose a greater amount of electrical stress on the sample that could activate breakdown mechanisms that result in lower measured breakdown strengths.

Chapter 5: Conclusions and Future Work

Although dielectric properties of Mylar have been well-studied and documented, until now there has been very little work completed to understand the effects of dopants and doping processes on Mylar films used as dielectric materials. The materials studied in this thesis were Mylar and modified Mylar, in which a chemical dopant was introduced into the material to enhance performance characteristics of the material. Understanding the effects of the dopant and doping process, if any, on the dielectric properties of the modified material is vital for application of the material as a dielectric medium in capacitors. This thesis examined the effects of varying test setup, environmental changes, and short-term accelerated thermal aging on the dielectric properties of Mylar and modified Mylar.

The data presented show that test setup parameters are important to consider when comparing data from multiple studies and experiments. Aspects such as electrode area, metallization thickness, and DC voltage ramp rate can have great effects on the measured dielectric properties, which may also be affected by the doping processes. Variable temperature studies revealed that the 50nm Au metallized films showed no difference with temperature, whereas the 200nm Au metallized samples showed a significant difference between room temperature and 73°C. However, the similarity between the 200nm Au metallized Mylar and modified Mylar groups suggests that the doping process has no significant effect on the changes in permittivity and loss with respect to test temperature, at least over the temperature range studied here. This increase in temperature also resulted in decreased loss values below the T_g. However, above the T_g the loss increased dipole rotations and mobility within the sample resulting in greater

loss. Dielectric breakdown strength decreased with increasing temperature in both virgin and modified Mylar, likely due to the activation of thermal breakdown pathways at elevated temperature.

Variable humidity studies found that the presence of water can also influence the permittivity and dielectric breakdowns strength of both materials. The permittivities increased as the samples equilibrated to target humidity and increased more at higher humidity levels. Dielectric breakdown strength decreased with increasing humidity, likely due to the dissociation of water molecules which increases conduction leading to localized Joule heating that results in a thermal runaway.[47] The presence of water due to varying humidity levels can significantly change the measured permittivity and breakdown strength. The results of the variable humidity and temperature studies suggest that temperature and humidity can significantly change the dielectric properties of both materials. However, the changes in each material are similar suggesting that the doping process has no effect on the relationship between temperature/humidity and dielectric properties. After determining the effects of temperature and humidity, short-term aging studies were conducted indicating that although significant changes in dielectric properties were seen, there are no consistent trends over the entire time period to suggest that these changes are aging-induced. Aging had no effect on the breakdown strengths of either material over the course of the time period.

The effects of metallization thickness were studied as well. The data showed that metallization in the multi-electrode samples does not affect the dielectric properties of either material. This result suggests that either self-clearing does not occur in these films, or that the extent of self-clearing is similar in both metallization thicknesses. To

determine if self-clearing is occurring a study comparing single and multi-electrode samples for both Mylar and modified Mylar was completed, revealing that multi-electrode samples consistently measured higher breakdown strengths than the single electrode samples in both materials. These results support the hypothesis that self-clearing is occurring in multi-electrode samples of Mylar and modified Mylar films. However, there was also a significant difference in the breakdown strengths of the 50 and 200nm Au metallized electrode samples when tested individually (single electrode). It is unclear why metallization thickness has an effect in single electrode samples but not multi-electrode samples.

As electrode area increased, the breakdown strengths decreased, suggesting that a higher number of defects are present in the larger electrode areas. Electrode area had a greater effect on the breakdown strength of the modified material; as electrode area increased there was a much greater decrease in the breakdown strength compared to the virgin material. These results suggest that the doping process could have an effect on the number of defects within the material due to the process itself and film handling during the process. However, this possible increase in defect density did not result in poor performance in any of the other experiments, which were tested on 6.3mm electrode samples, compared to the virgin material.

DC voltage ramp rate studies showed that there is a significant difference in the measured dielectric breakdown strength depending on the ramp method, stepped versus continuous, as well as ramp rate. Calibration data reveals that the data output from the different ramp methods must be corrected to compare stepped and continuous data to one another. Comparison of corrected data for 500V/s and 3000 V/s show that as voltage

ramp rate is increased the measured breakdown strengths of both the virgin and modified materials increase as well. At slower ramp rates the samples are exposed to electrical stresses by the applied field for a longer amount of time than the faster ramp rates. This increased exposure time for slower rates could stress and degrade the polymers, resulting in the lower measured breakdown strengths. The continuous ramp method resulted in a significant increase of breakdown strength from 500V/s to 3000V/s compared to the stepped ramp method. The comparison of stepped and continuous ramp methods showed that at slower ramp rates the stepped voltage yields higher breakdown strengths. However, at faster ramp rates the continuous voltage yielded higher breakdown strengths. The increase in step size may result in the differences seen between stepped and continuous voltage ramps at different ramp rates; a greater amount of voltage is being instantaneously applied to the sample within the same time period. This may impose a greater amount of electrical stress on the sample that could activate breakdown mechanisms that result in lower measured breakdown strengths.

This thesis encompassed a large range of various studies, and a few studies performed raised more questions that would be interesting to answer. For example, technical issues with the loss measurement setup made obtaining usable data for the analysis of the effects of humidity on dielectric loss problematic. After refinement of the test setup, further studies are required to accurately define a correlation between humidity and loss. It is expected that as humidity increases the dielectric loss would increase as well due to the dielectric heating of water.

The method to measure breakdown strength above the T_g needs improvement, and studies on above T_g samples with the wire tip probe could determine if the wire tip probe

will damage the samples, resulting in lower breakdown strengths similar to the ball-plane probe. Another study that left unanswered questions what the effects of metallization thickness on dielectric properties, specifically breakdown strength. Although it was hypothesized that self-clearing could be the cause of differences of measured dielectric properties in samples with different metallization thicknesses, changes were found between 50nm Au and 200nm Au single electrode films as well. This suggests that self-clearing may not be the only influence, but rather there is a significant effect due to the metallization thickness itself. Studies examining a range of metallization thicknesses and types would allow for better understanding of the effects of metallization thickness on dielectric properties and if there is a relationship between increasing metallization thickness and measured dielectric properties.

The results presented in this thesis suggest that there are very few differences between the changes in dielectric properties of Mylar and modified Mylar due to aging, environmental and test setup factors. Mylar has proven itself to be a successful dielectric material for capacitor applications due to its cost effectiveness, low losses and high efficiency. The ability to improve the material by creating other desirable properties through doping processes makes Mylar an even more attractive candidate for future enhanced capacitor designs and applications.

Appendix A: Calibration Data (Voltage Ramp Rate and Humidity)

Calibration of the applied and breakdown voltage output of the stepped and continuous ramp rate methods is performed by use of a calibrated Agilent model 34401A digital multimeter with a calibrated 1000:1 resistive divider that contains three resistors in a series-parallel combination. The divider is then placed in parallel with the test circuit. The test sample used to hold off voltage during the calibration run is a ¼" thick piece of Teflon placed in the Fluorinert bath. The programs are then ramped to 15000V at the desired rate and the reading from the mulimeter is recorded using the Intuilink software package from Agilent. The LabVIEW program simultaneously records the voltage value output from the amplifier monitor. The program output (the value recorded by LabVIEW) can then be corrected to the 'true voltage' (the value recorded at the test circuit by the calibrated multimeter). The correction to the program voltage value can be calculated by performing a linear regression of the program value vs. true value.. The plots below show the calibration data for each ramp rate method and the linear regressions that were used to calculate the corrected data sets.

Stepped Ramp Calibrations

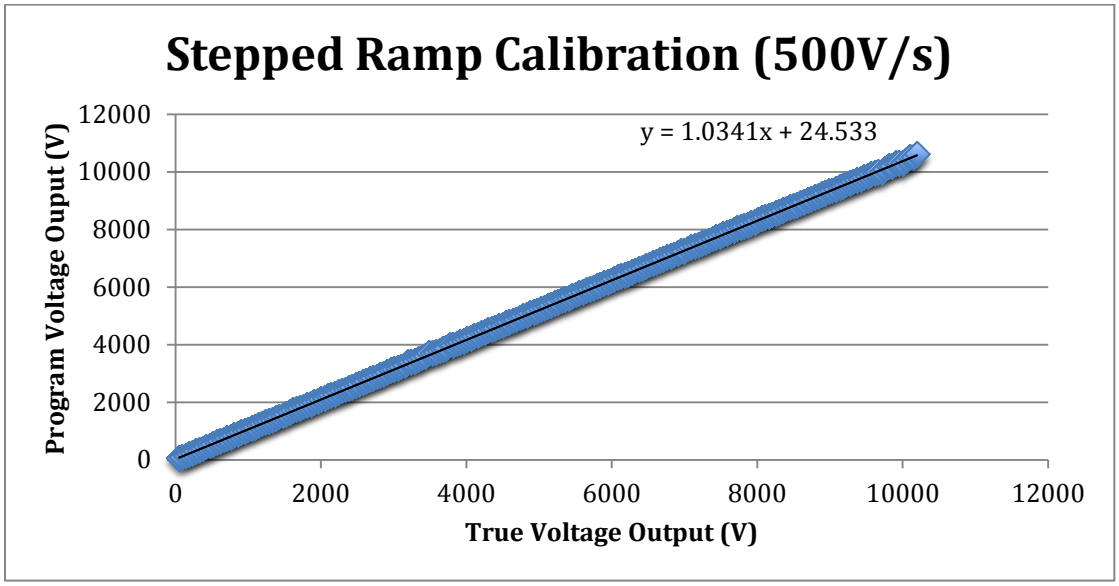

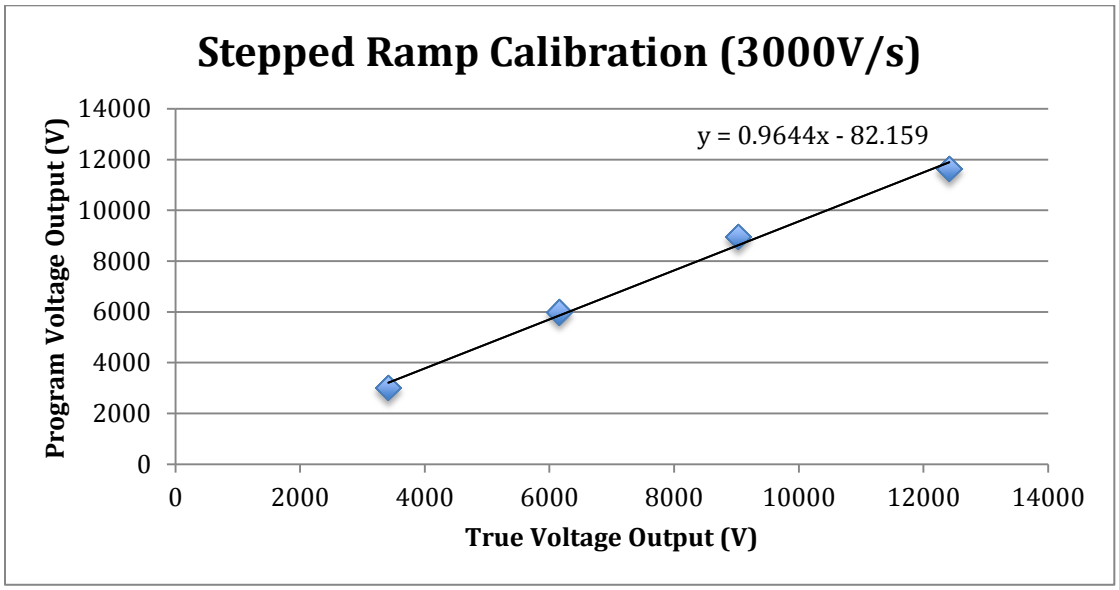

Continuous Ramp Calibrations

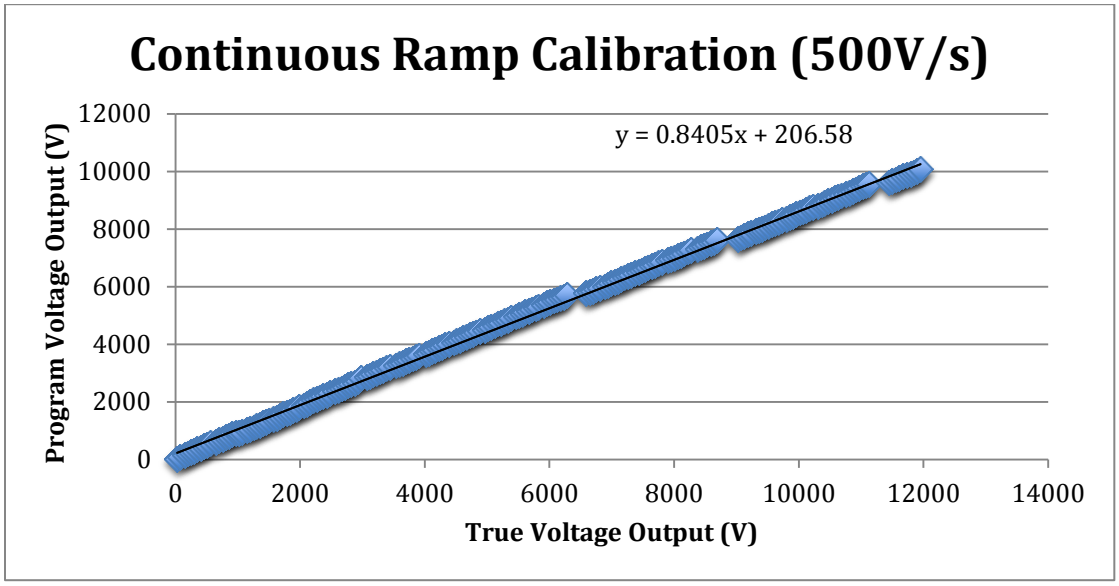

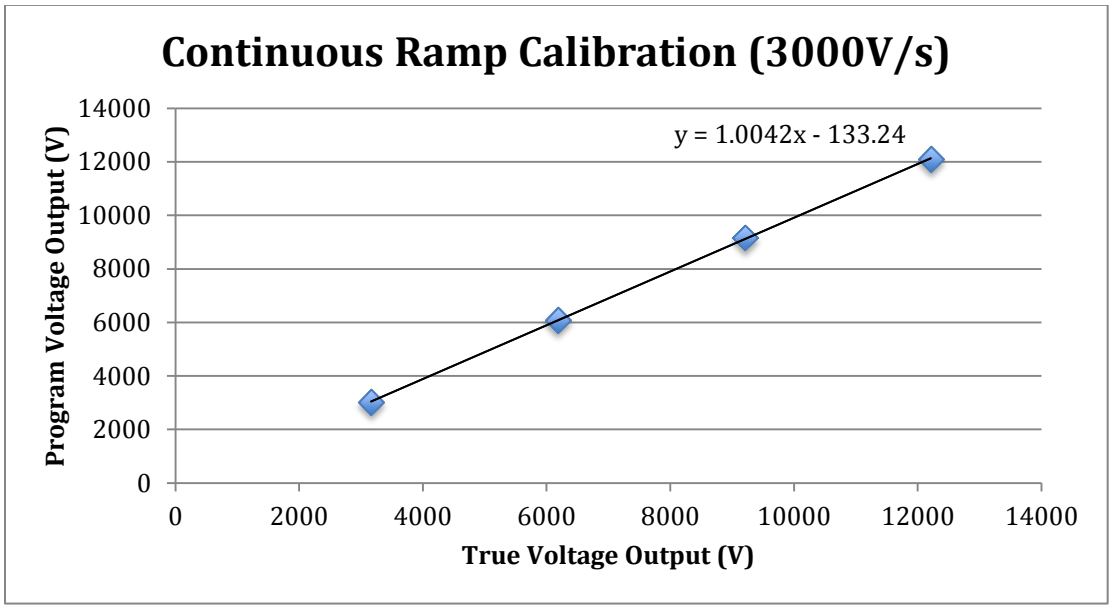

Humidity Storage Chamber Equilibration Data

The plots shown below are the equilibration rates for the saturated salt bath humidity chambers.

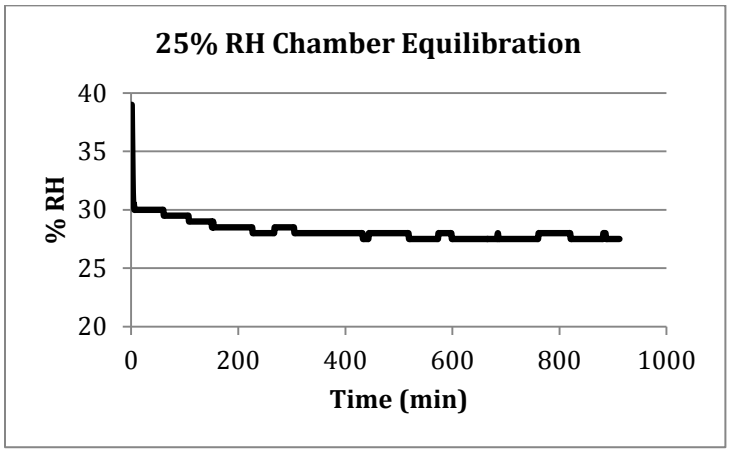

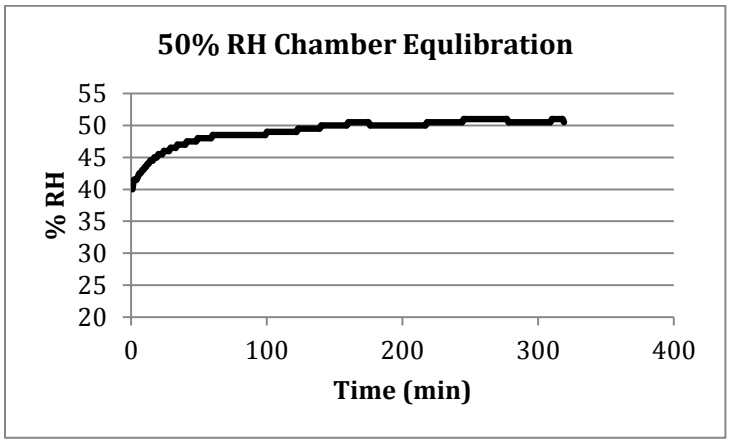

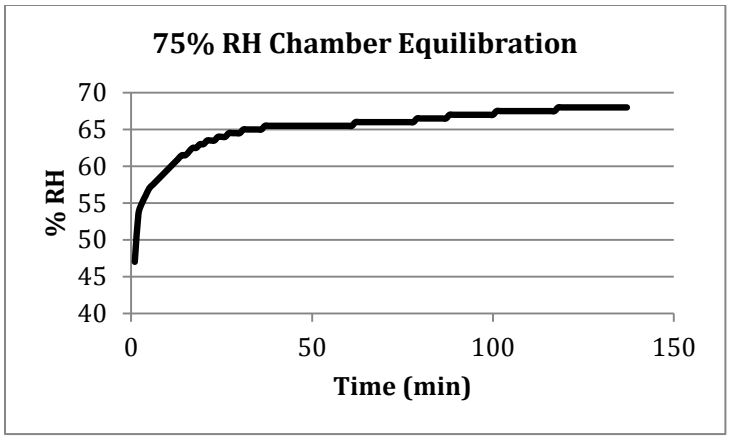
75% RH Chamber Equilibration
% RH
70
65
60
55
50
45
40
0
50
100
150
Time (min)

Appendix B: Virgin Mylar dielectric properties and breakdown data

This appendix contains sample sizes per study and any data points that may have been excluded from data analysis that was discussed in the body of this work for Mylar samples. N (exclusions from results) are the total number of data points excluded, the results of these excluded points (if any) are included in a separate table.

B.1: Variable Temperature

50nm Au metallization	N (films per temperature)	N (electrodes)	N(exclusions from results)
Permittivity and Loss	3	90	7
Dielectric Breakdown	3	90	0

Permittivity and Loss exclusions

Temperature	Electrode #	Thickness	DF (10kHz)	K(10kHz)
20C	12	11.67	0.004847488	2.873984364
73C	2	11.83	-0.006573462	2.844283277
73C	16	11.73	-0.001010066	2.933854653
80C	1	11.73	0.6614934	1.577441181
80C	10	11.81	1.081529	0.351504774
80C	12	11.78	1.204878	0.258194491

100C	15	1.81	0.03403736	0.5203216

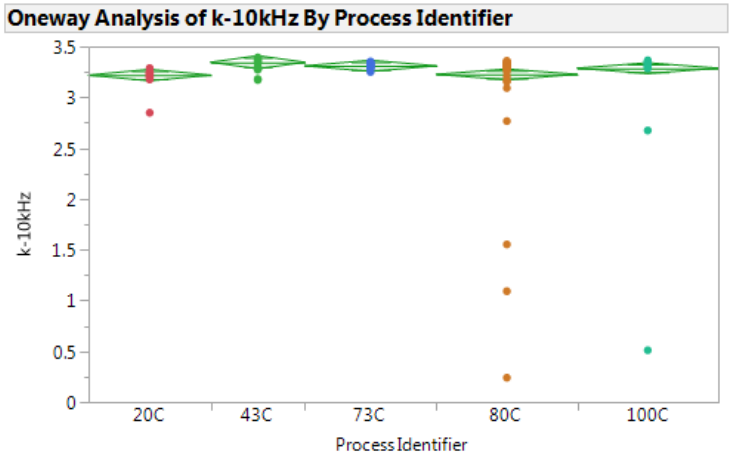

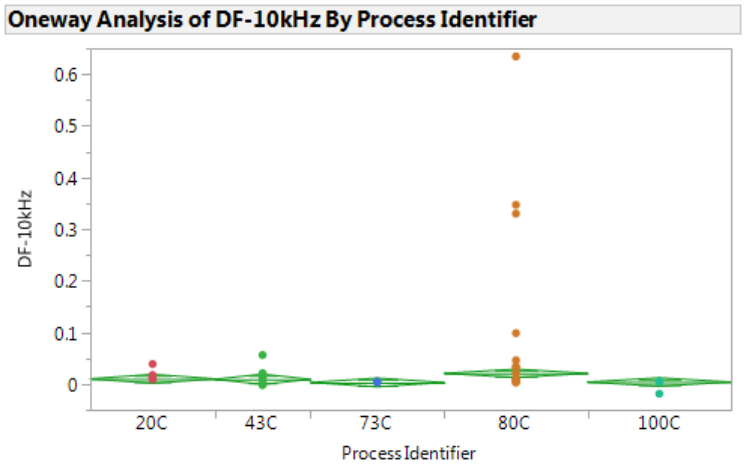

200nm Au metallization	N (films per temperature)	N (electrodes)	N(exclusions from results)
Permittivity and Loss	3	90	2
Dielectric	3	90	3

Breakdown			

Permittivity and Loss exclusions

Temperature	Electrode #	Thickness	DF (10kHz)	K(10kHz)
20C	21	12.07	328.4106	7314.691186
20C	26	11.85	4047.452	791.0485357

Breakdown Strength exclusions

Temperature	Electrode #	Thickness	Breakdown Field (kV/cm)
33C	27	12.17	14.60059162
63C	3	11.88	50.34159091
73C	5	11.99	0

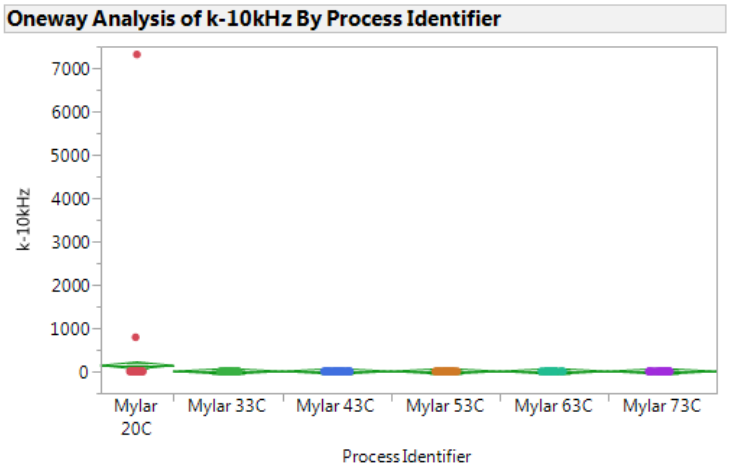
Oneway Analysis of k-10kHz By Process Identifier
k-10kHz
7000
6000
5000
4000
3000
2000
1000
0
Mylar 20C
Mylar 33C
Mylar 43C
Mylar 53C
Mylar 63C
Mylar 73C
Process Identifier

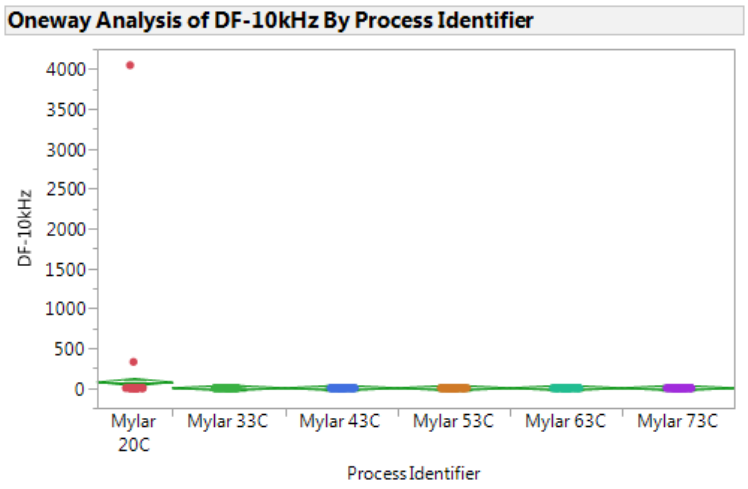
Oneway Analysis of DF-10kHz By Process Identifier
DF-10kHz
4000
3500
3000
2500
2000
1500
1000
500
0
Mylar 20C
Mylar 33C
Mylar 43C
Mylar 53C
Mylar 63C
Mylar 73C
Process Identifier

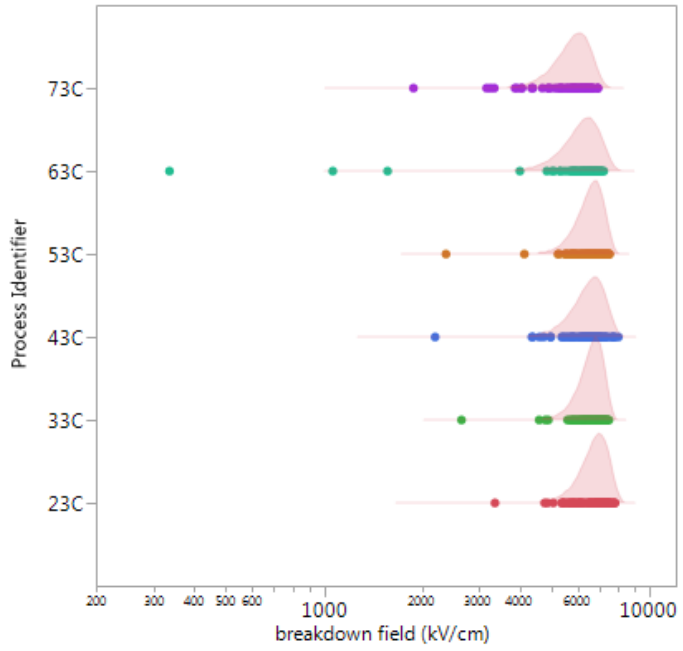
Process Identifier
73C
63C
53C
43C
33C
23C
200
300
400
500
600
1000
2000
3000
4000
6000
10000
breakdown field (kV/cm)

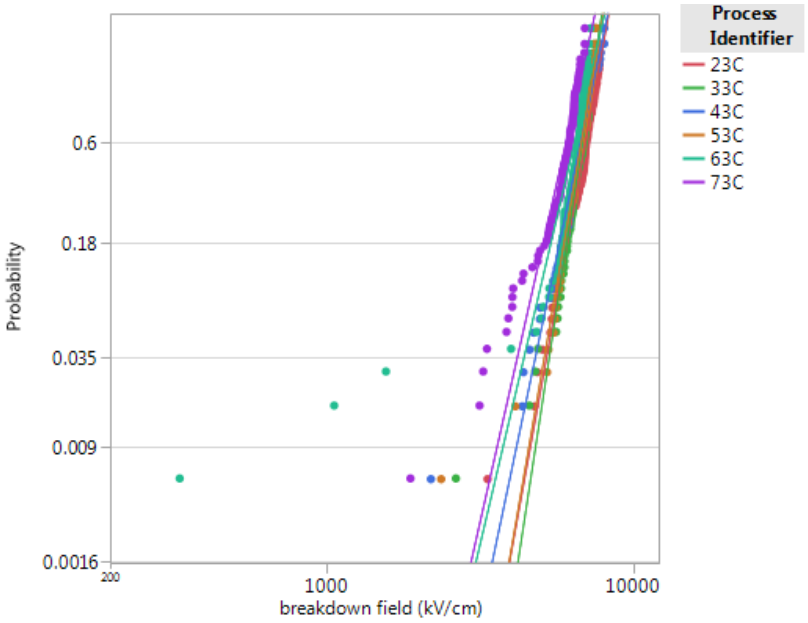
Process Identifier
23C
33C
43C
53C
63C
73C
Probability
0.6
0.18
0.035
0.009
0.0016
200
1000
10000
breakdown field (kV/cm)

Weibull α 0	7006.2989
Weibull β 0	11.2106
Weibull α 1	6824.0778
Weibull β 1	13.2742
Weibull α 2	6766.0777
Weibull β 2	9.6328
Weibull α 3	6788.8502
Weibull β 3	11.7865
Weibull α 4	6471.0244
Weibull β 4	8.6409
Weibull α 5	6066.9817
Weibull β 5	8.9737

B.2: Variable Humidity

	N (films per humidity)	N (electrodes)	N(exclusions from results)
Permittivity and Loss	1 (tested 7 times over 1 wk)	30	5
Dielectric Breakdown	2	60	0

Permittivity and Loss exclusions

Humidity/Time point	Electrode	Thickness	DF (10kHz)	K (10kHz)

25%RH t5	20	11.65	0.0746291	0.024887751
25%RH t5	25	11.76	0.0544623	0.023400494
25%RH t5	29	11.59	0.03388947	0.020725411
50%RH t1	7	11.74	-0.08524045	0.02253909
75%RH t2	16	11.54	-0.004751648	0.019666552

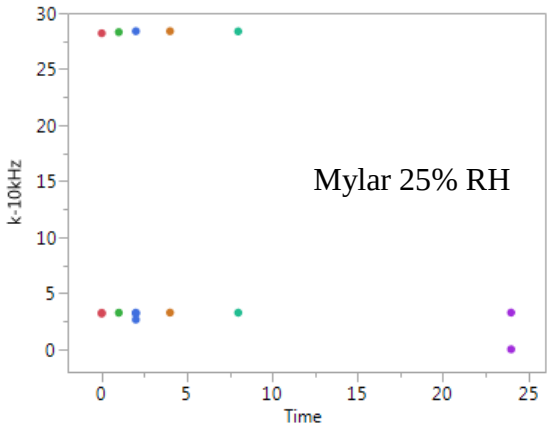

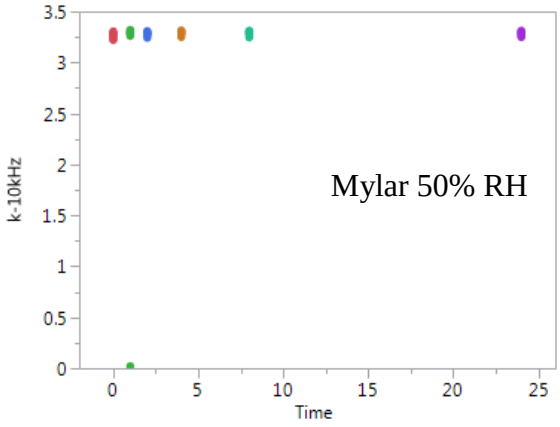

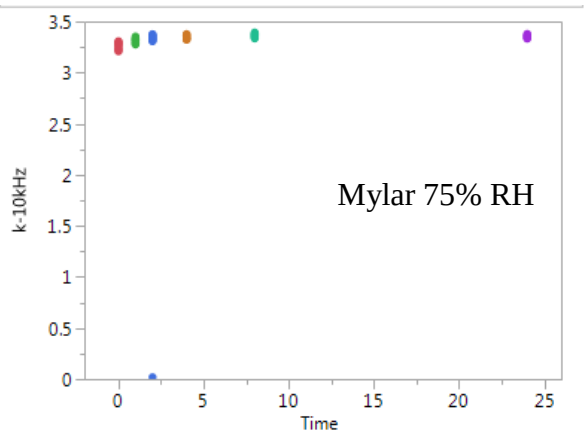

Permittivity Values for Mylar at 10kHz			
Time Point	25% RH	50% RH	75% RH
0 hours	3.24±0.02	3.27±0.02	3.27±0.03
1 hour	3.26±0.01	3.29±0.01	3.32±0.02
2 hours	3.26±0.02	3.28±0.01	3.34±0.02
4 hours	3.26±0.02	3.29±0.01	3.34±0.02
8 hours	3.26±0.01	3.28±0.01	3.36±0.02
24 hours	3.28±0.01	3.29±0.01	3.35±0.01

B.3: Metallization Thickness

Sample sizes match those in B.1 for 20C, 43C, and 73C.

B.4: Electrode Area

Permittivity and Loss	N (films)	N (total electrodes)	N(exclusions from results)
6.3mm	3	90	0
9mm	2	40	0
13mm	5	60	0
18mm	4	24	0

Dielectric Breakdown	N (films)	N (electrodes)	N(exclusions from results)
6.3mm	3	90	1
9mm	2	40	0
13mm	5	60	0
18mm	4	24	1

Breakdown Strength exclusions

Electrode Diameter	Electrode #	Thickness	Breakdown Field (kV/cm)
18mm	6	11.98	388.0538397
6.3mm	20	11.85	14.9948692

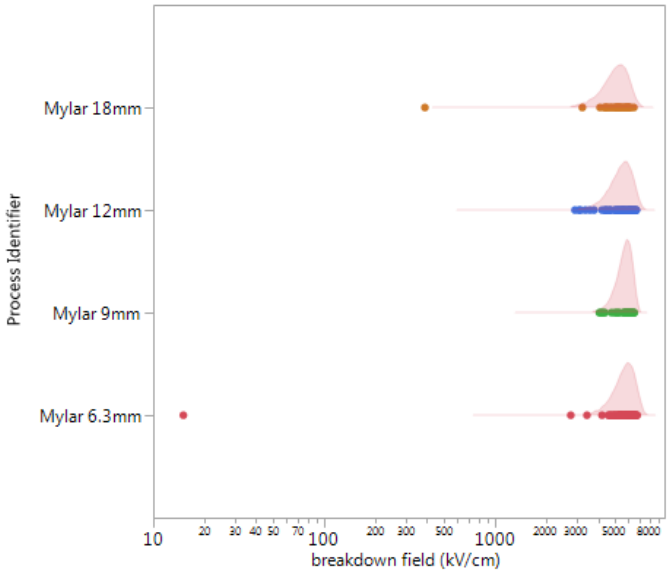

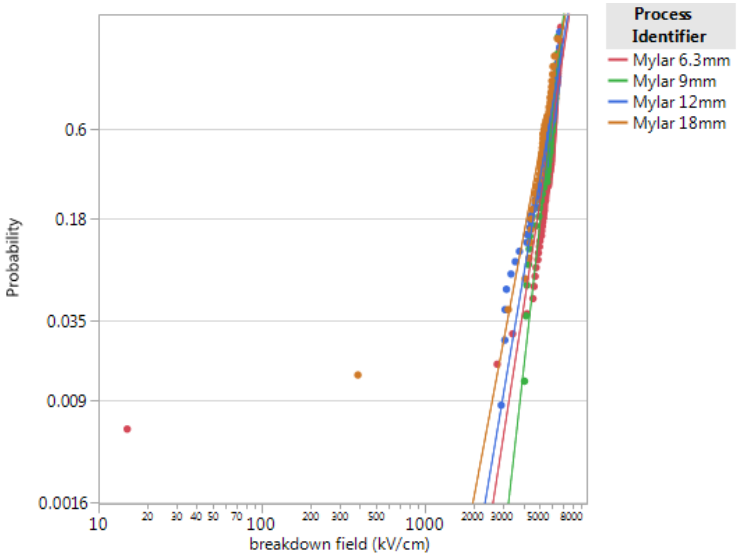

B.5: DC Voltage Ramp Rate

Dielectric Breakdown	N (films)	N (electrodes)	N(exclusions from results)
Stepped Ramp Rate	2	30	0
Continuous Ramp Rate	2	30	1

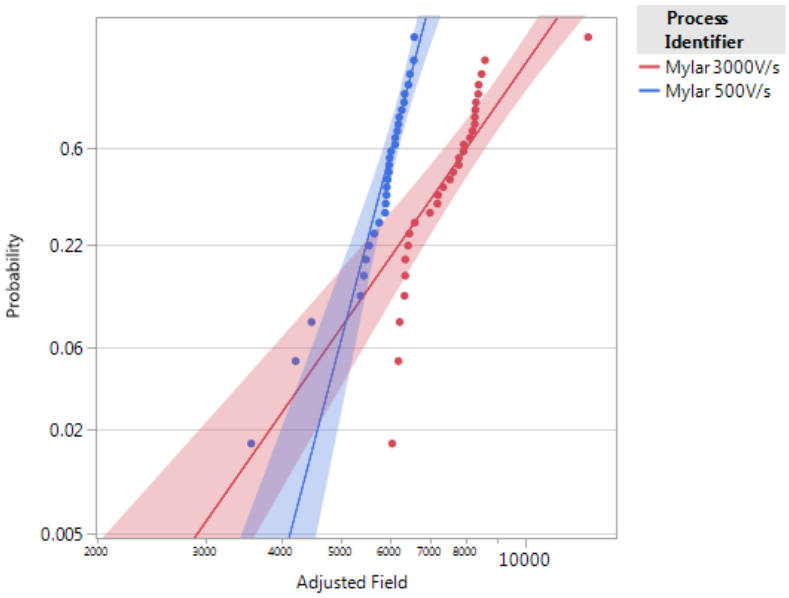

B.6: Short-term Aging

	N (films per aging temp)	N (electrodes)	N(exclusions from results)
Permittivity and Loss	1	30	6
Dielectric Breakdown	1	30	2

Permittivity and Loss Exclusions

Temperature	Electrode #	Thickness	DF (10kHz)	K (10kHz)
40C_t2	21	11.96	0.004536514	30.99288048
40C_t4	25	11.25	176.4264	6125.477669
109C_t3	7	101.9	0.004679904	28.5086606
124C_t4	20	12.31	660.916	2628.075351
124C_t4	25	12.38	12481.1	203.1754955
124C_t4	30	12.39	11519.1	246.3669294

Breakdown Strength Exclusions

Temperature	Electrode #	Thickness	Breakdown Field (kV/cm)
40C_t4	25	11.25	19.19152
109C_t3	4	12.03	97.36392352

Permittivity and Loss

T1: 1 day

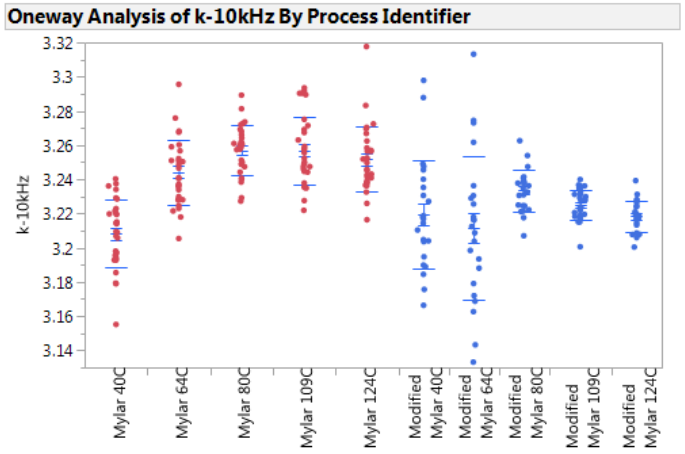

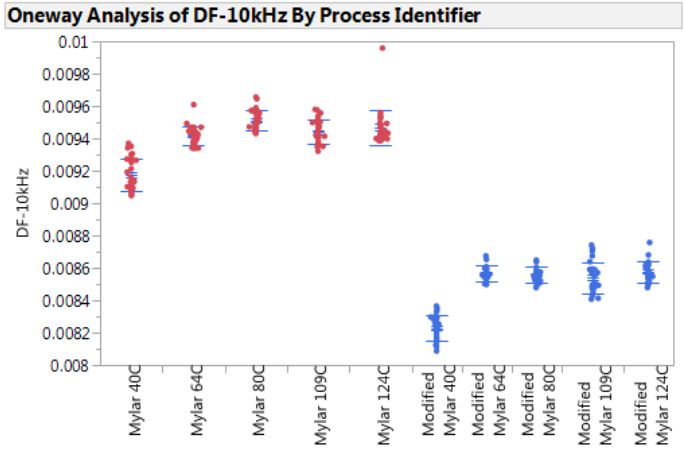

T2: 3 days

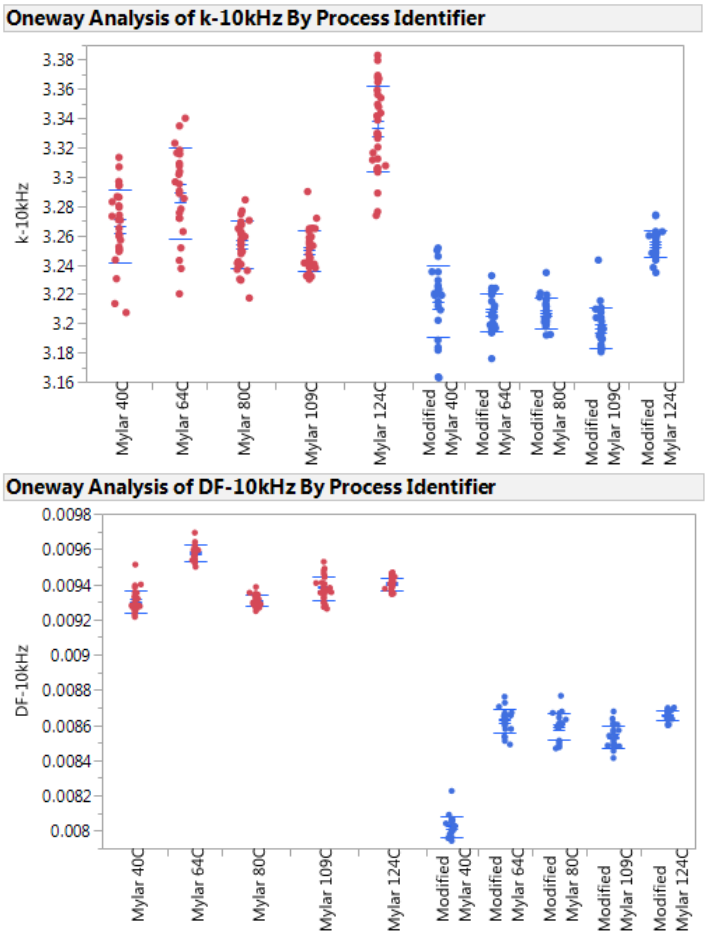
Oneway Analysis of k-10kHz By Process Identifier
k-10kHz
3.38
3.36
3.34
3.32
3.3
3.28
3.26
3.24
3.22
3.2
3.18
3.16
Mylar 40C
Mylar 64C
Mylar 80C
Mylar 109C
Mylar 124C
Modified Mylar 40C
Modified Mylar 64C
Modified Mylar 80C
Modified Mylar 109C
Modified Mylar 124C
Oneway Analysis of DF-10kHz By Process Identifier
DF-10kHz
0.0098
0.0096
0.0094
0.0092
0.009
0.0088
0.0086
0.0084
0.0082
0.008
Mylar 40C
Mylar 64C
Mylar 80C
Mylar 109C
Mylar 124C
Modified Mylar 40C
Modified Mylar 64C
Modified Mylar 80C
Modified Mylar 109C
Modified Mylar 124C

T3: 7 days

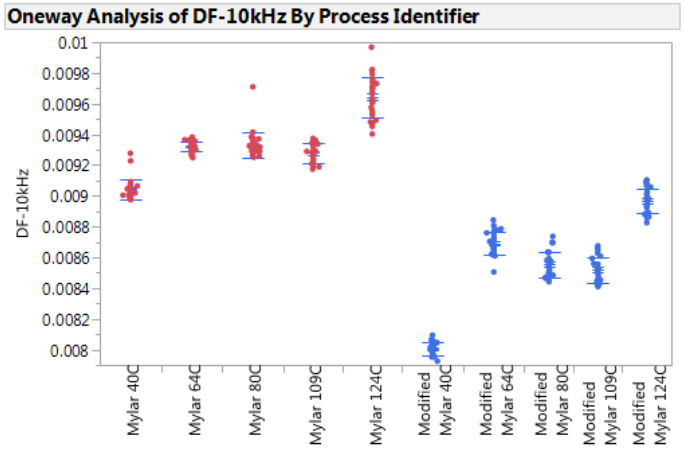
Oneway Analysis of DF-10kHz By Process Identifier
DF-10kHz
0.01
0.0098
0.0096
0.0094
0.0092
0.009
0.0088
0.0086
0.0084
0.0082
0.008
Mylar 40C
Mylar 64C
Mylar 80C
Mylar 109C
Mylar 124C
Modified Mylar 40C
Modified Mylar 64C
Modified Mylar 80C
Modified Mylar 109C
Modified Mylar 124C

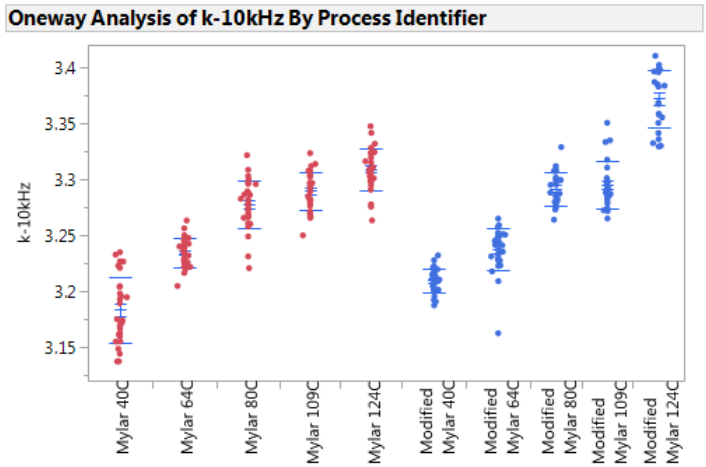
Oneway Analysis of k-10kHz By Process Identifier
k-10kHz
3.4
3.35
3.3
3.25
3.2
3.15
Mylar 40C
Mylar 64C
Mylar 80C
Mylar 109C
Mylar 124C
Modified Mylar 40C
Modified Mylar 64C
Modified Mylar 80C
Modified Mylar 109C
Modified Mylar 124C

T4: 29 days

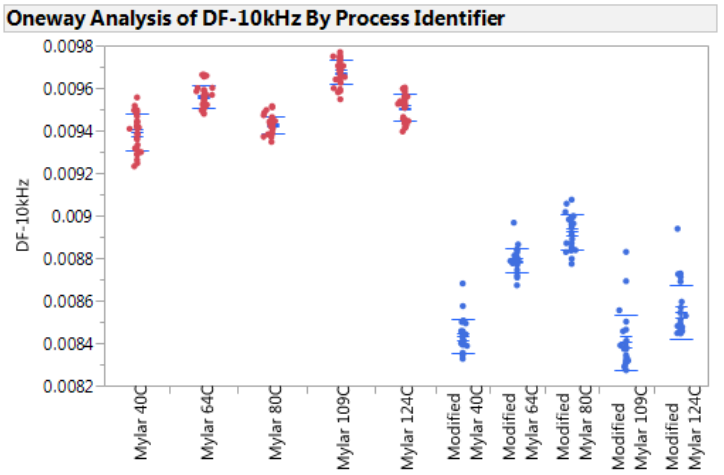

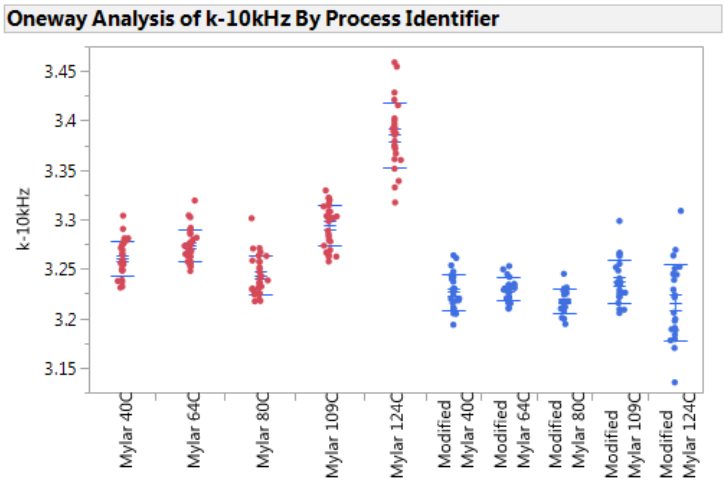

Breakdown Strength

T1: 1 day

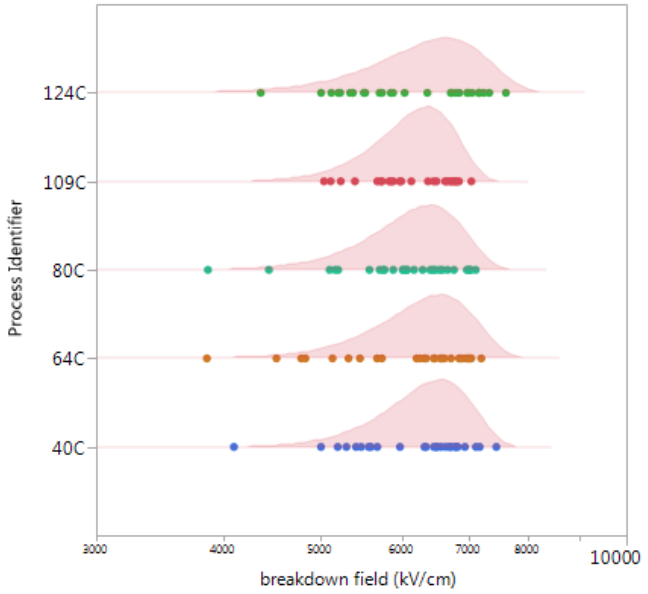

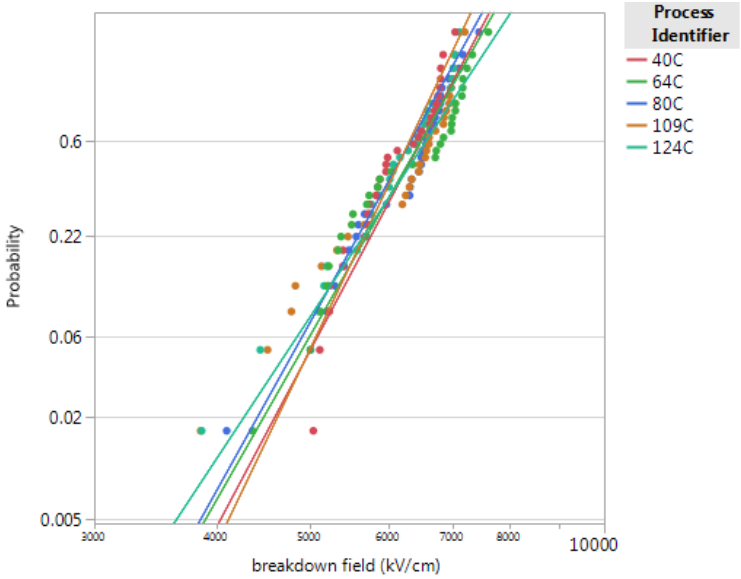

Weibull α 0	6548.4350
Weibull β 0	11.0053
Weibull α 1	6546.1718
Weibull β 1	10.2548
Weibull α 2	6391.9419
Weibull β 2	10.5052
Weibull α 3	6363.9847
Weibull β 3	12.2064
Weibull α 4	6636.5169
Weibull β 4	8.8525

T2: 3 days

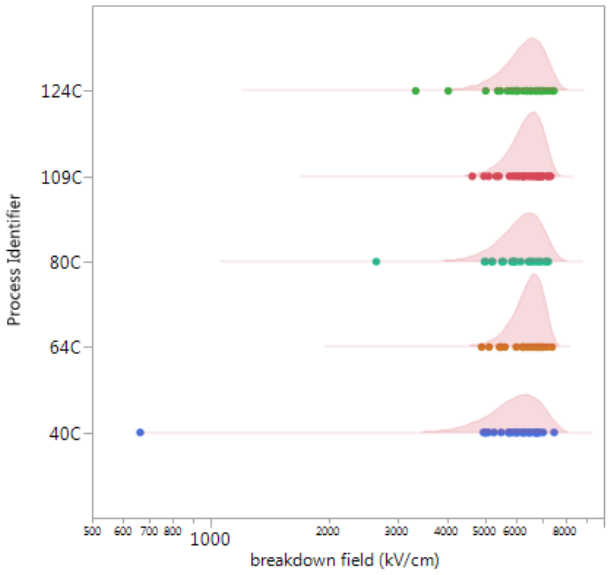

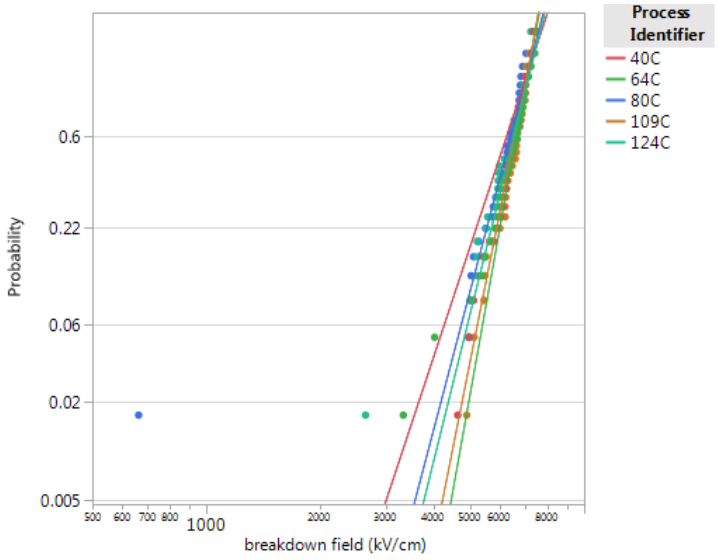

Weibull α 0	6316.8185
Weibull β 0	7.1066
Weibull α 1	6656.6461
Weibull β 1	13.1637
Weibull α 2	6464.2028
Weibull β 2	8.9355
Weibull α 3	6606.4853
Weibull β 3	11.8341
Weibull α 4	6590.4905
Weibull β 4	9.4919

T3: 7 days

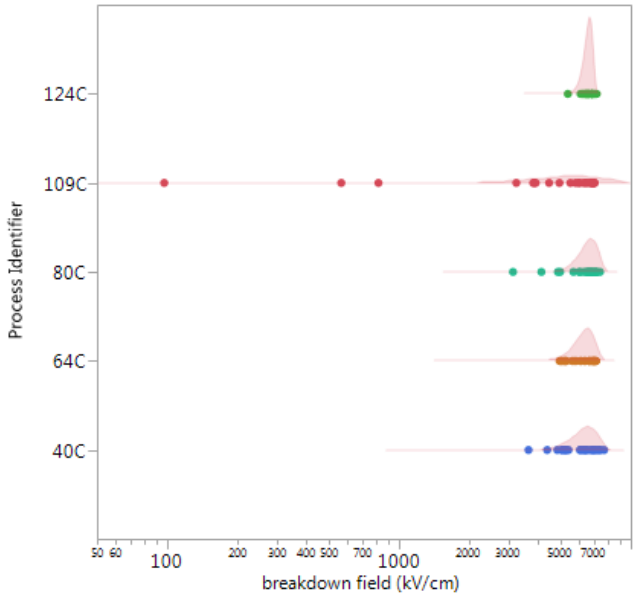

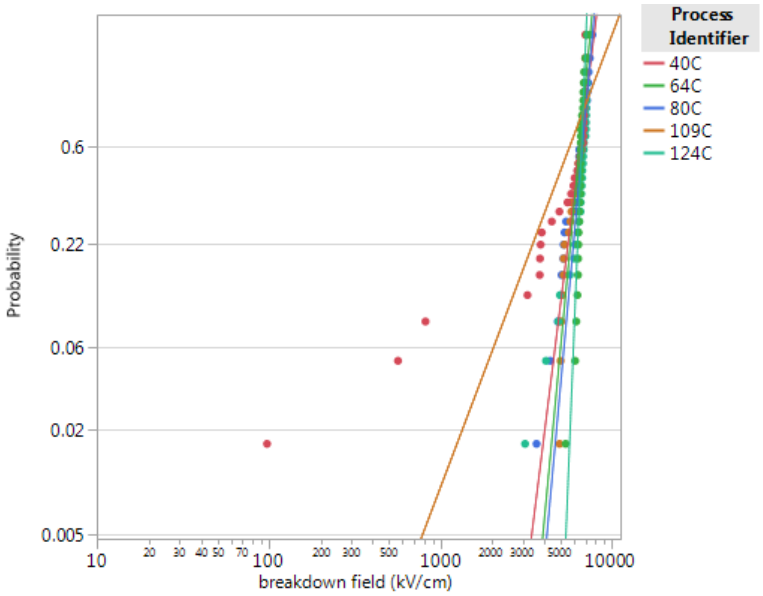

Weibull α 0	6580.2126
Weibull β 0	8.0200
Weibull α 1	6510.0660
Weibull β 1	10.5958
Weibull α 2	6751.1393
Weibull β 2	10.9845
Weibull α 3	5852.9942
Weibull β 3	2.6402
Weibull α 4	6646.7314
Weibull β 4	24.9577

T4: 29 days

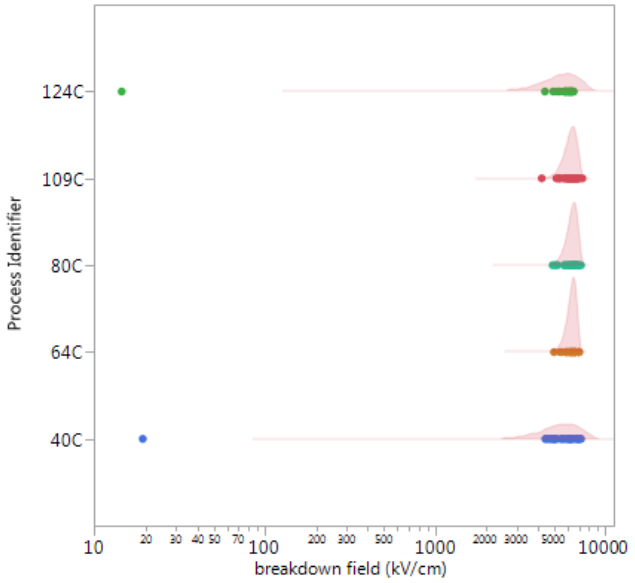

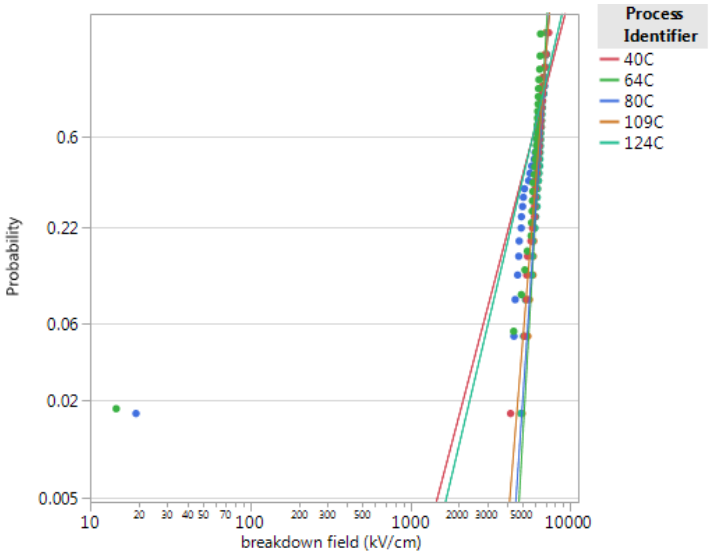

Weibull α 0	5950.3366
Weibull β 0	3.7964
Weibull α 1	6493.0535
Weibull β 1	17.3156
Weibull α 2	6544.2070
Weibull β 2	14.7482
Weibull α 3	6437.1287
Weibull β 3	12.2598
Weibull α 4	5934.9824
Weibull β 4	4.1961

Appendix C: Modified Mylar dielectric properties and breakdown data

This appendix contains sample sizes per study and any data points that may have been excluded from data analysis that was discussed in the body of this work for modified Mylar samples. N (exclusions from results) are the total number of data points excluded, the results of these excluded points (if any) are included in a separate table.

C.1: Variable Temperature

50nm Au metallization	N (films per temperature)	N (electrodes)	N(exclusions from results)
Permittivity and Loss	3	72	1
Dielectric Breakdown	3	72	2

Permittivity and Loss Exclusions

Temperature	Electrode #	Thickness	DF (10kHz)	K (10kHz)
73C	23	12.06	2219.634	975.5758438

Breakdown Strength Exclusions

Temperature	Electrode #	Thickness	Breakdown Field (kV/cm)
80C	23	11.68	-7.689916096
100C	1	11.57	18.66072602

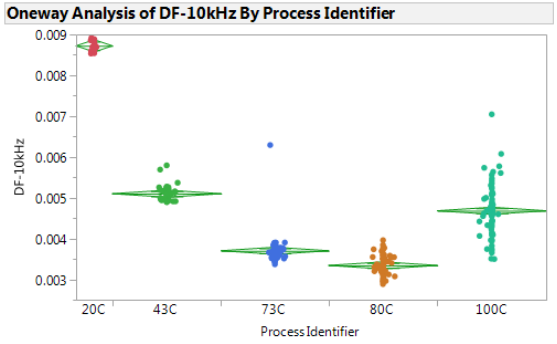

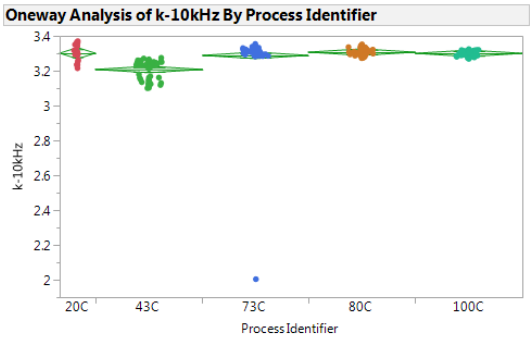

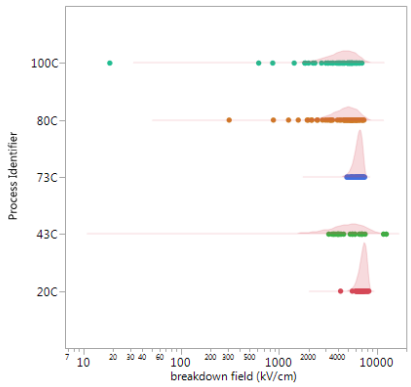

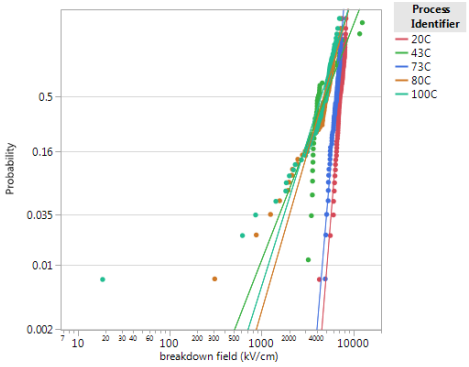

Weibull α 0	7467.5067
Weibull β 0	12.4133
Weibull α 1	5699.9712
Weibull β 1	2.5780
Weibull α 2	6711.8684
Weibull β 2	12.0498
Weibull α 3	5254.6889
Weibull β 3	3.4777
Weibull α 4	4975.2372
Weibull β 4	3.2056

200nm Au metallization	N (films per temperature)	N (electrodes)	N(exclusions from results)
Permittivity and Loss	3	72	4
Dielectric Breakdown	3	72	1

Permittivity and Loss Exclusions

Temperature	Electrode #	Thickness	DF (10kHz)	K (10kHz)
20C	11	11.75	0.007410472	40.13914455
20C	23	11.84	121.6268	4448.240639
73C	1	11.9	1.98E+37	8.54E+47
73C	13	11.84	-6028.412	97.58605366

Breakdown Strength Exclusions

Temperature	Electrode #	Thickness	Breakdown Field (kV/cm)
53C	2	12.21	14.55276003

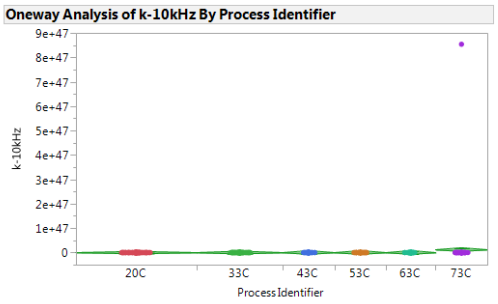

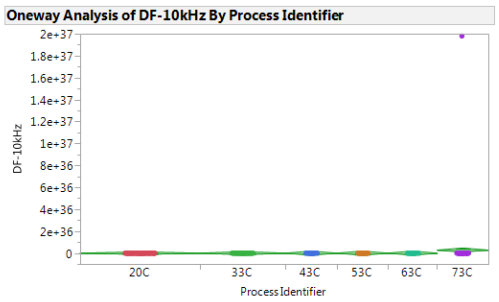

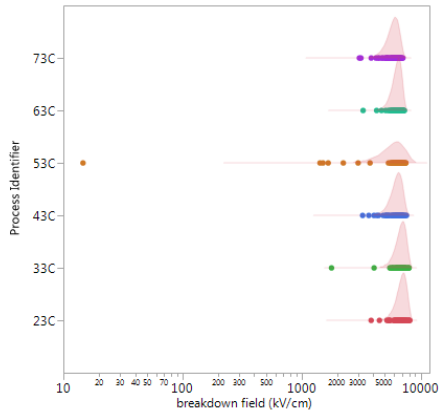

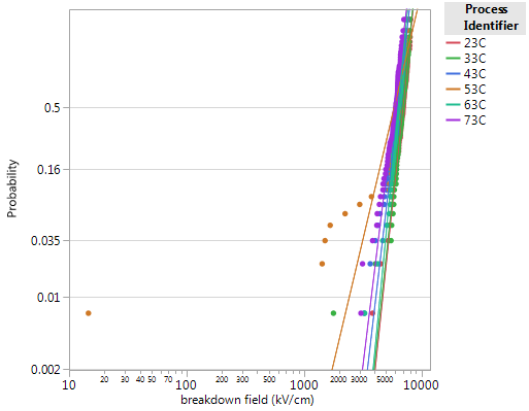

Weibull α 0	7179.6486
Weibull β 0	10.8283
Weibull α 1	7098.4126
Weibull β 1	10.6346
Weibull α 2	6563.9779
Weibull β 2	9.7740
Weibull α 3	6328.8852
Weibull β 3	4.8122
Weibull α 4	6542.5237
Weibull β 4	11.8913
Weibull α 5	6140.9540
Weibull β 5	9.3159

C.2: Variable Humidity

	N (films per	N (electrodes)	N(exclusions from

	humidity)		results)
Permittivity and Loss	1 (tested 7 times over 1 wk)	24	0
Dielectric Breakdown	2	48	0

Permittivity Values for Mylar at 10kHz			
Time Point	25% RH	50% RH	75% RH
0 hours	3.23±0.01	3.21±0.02	3.26±0.03
0.5 hours	3.24±0.02	3.23±0.02	3.30±0.02
1 hour	3.25±0.02	3.26±0.02	3.32±0.02
2 hours	3.24±0.02	3.28±0.01	3.32±0.02
4 hours	3.24±0.02	3.28±0.01	3.33±0.01
8 hours	3.25±0.02	3.28±0.01	3.34±0.01
24 hours	3.26±0.02	3.28±0.01	3.34±0.01

C.3: Metallization Thickness

Sample sizes are the same as those in C.1 for 20C, 43C, and 73C.

C.4: Electrode Area

Permittivity and	N (films)	N (electrodes)	N(exclusions from

Loss			results)
6.3mm	3	72	0
9mm	2	30	0
13mm	5	40	0
18mm	4	8	0

Dielectric Breakdown	N (films)	N (electrodes)	N(exclusions from results)
6.3mm	3	72	0
9mm	2	30	0
13mm	5	4	0
18mm	4	8	0

C.5: DC Voltage Ramp Rate

Dielectric Breakdown	N (films)	N (electrodes)	N(exclusions from results)
Stepped Ramp Rate	2	30	0
Continuous Ramp Rate	2	30	0

C.6: Short-term Aging

	N (films per aging temp)	N (electrodes)	N(exclusions from results)
Permittivity and Loss	1	24	0
Dielectric Breakdown	1	24	7

Breakdown Strength Exclusions

Temperature/time point	Electrode #	Thickness	Breakdown Field (kV/cm)
40C_t1	10	11.8	-7.611713559
40C_t1	15	11.91	8.501973132
40C_t2	1	1108	61.24284296
64C_t1	15	11.7	2.122036752

64C_t1	20	11.79	15.07117897
64C_t1	25	11.72	18.4218942
64C_t1	30	11.78	15.08397284

Permittivity and Loss

T1: 1 day

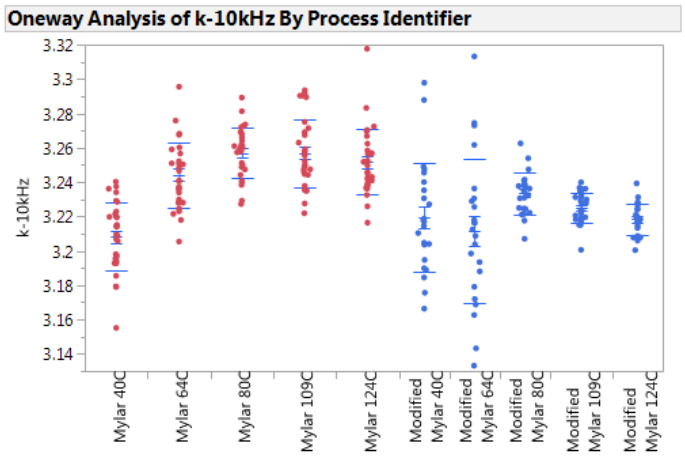

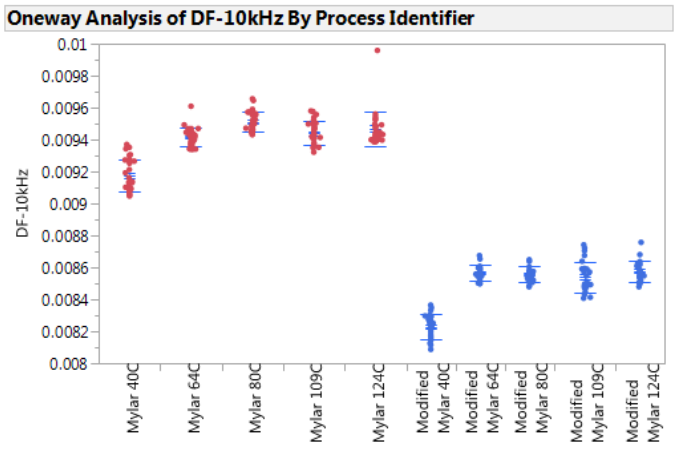

T2: 3 days

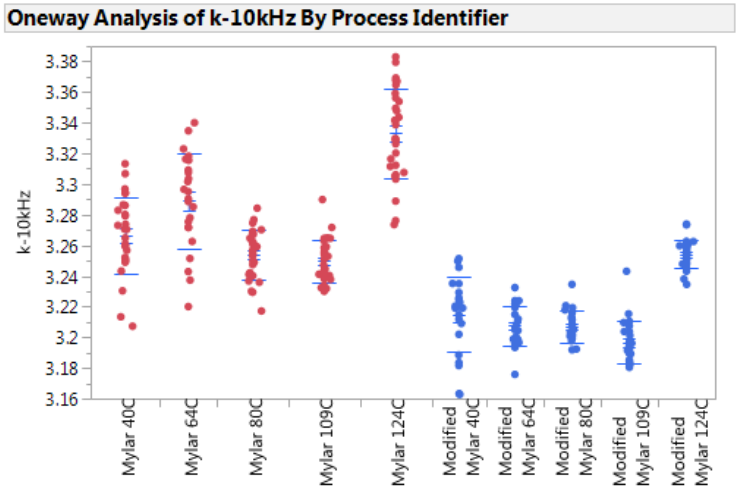
Oneway Analysis of k-10kHz By Process Identifier
k-10kHz
3.38
3.36
3.34
3.32
3.3
3.28
3.26
3.24
3.22
3.2
3.18
3.16
Mylar 40C
Mylar 64C
Mylar 80C
Mylar 109C
Mylar 124C
Modified Mylar 40C
Modified Mylar 64C
Modified Mylar 80C
Modified Mylar 109C
Modified Mylar 124C

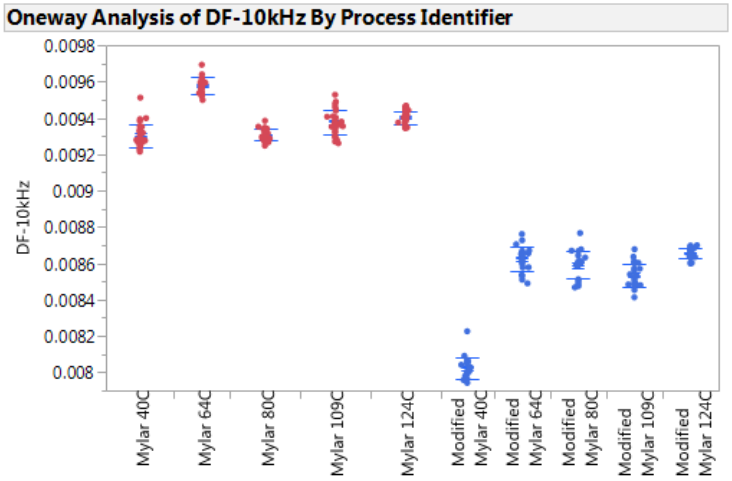
Oneway Analysis of DF-10kHz By Process Identifier
DF-10kHz
0.0098
0.0096
0.0094
0.0092
0.009
0.0088
0.0086
0.0084
0.0082
0.008
Mylar 40C
Mylar 64C
Mylar 80C
Mylar 109C
Mylar 124C
Modified Mylar 40C
Modified Mylar 64C
Modified Mylar 80C
Modified Mylar 109C
Modified Mylar 124C

T3: 7 days

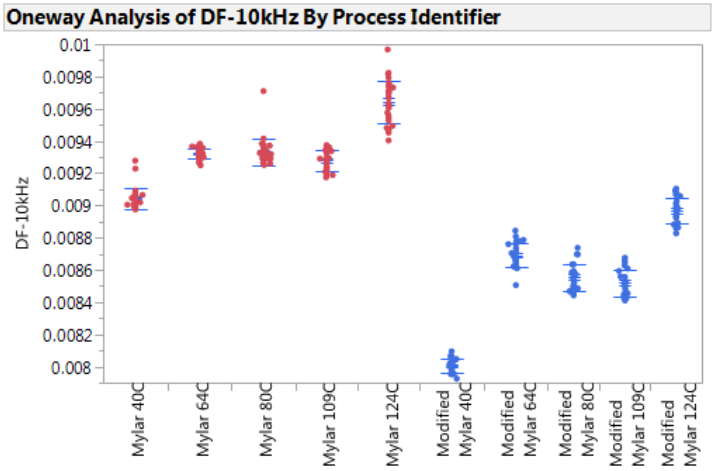
Oneway Analysis of DF-10kHz By Process Identifier
DF-10kHz
0.01
0.0098
0.0096
0.0094
0.0092
0.009
0.0088
0.0086
0.0084
0.0082
0.008
Mylar 40C
Mylar 64C
Mylar 80C
Mylar 109C
Mylar 124C
Modified Mylar 40C
Modified Mylar 64C
Modified Mylar 80C
Modified Mylar 109C
Modified Mylar 124C

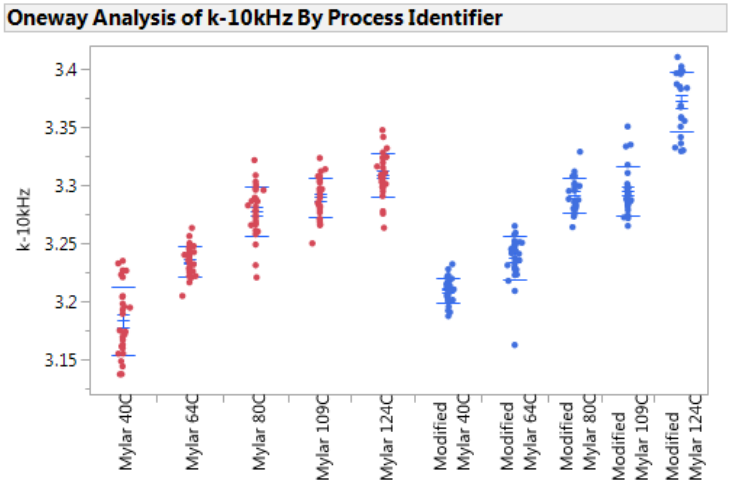
Oneway Analysis of k-10kHz By Process Identifier
k-10kHz
3.4
3.35
3.3
3.25
3.2
3.15
Mylar 40C
Mylar 64C
Mylar 80C
Mylar 109C
Mylar 124C
Modified Mylar 40C
Modified Mylar 64C
Modified Mylar 80C
Modified Mylar 109C
Modified Mylar 124C

T4: 29 days

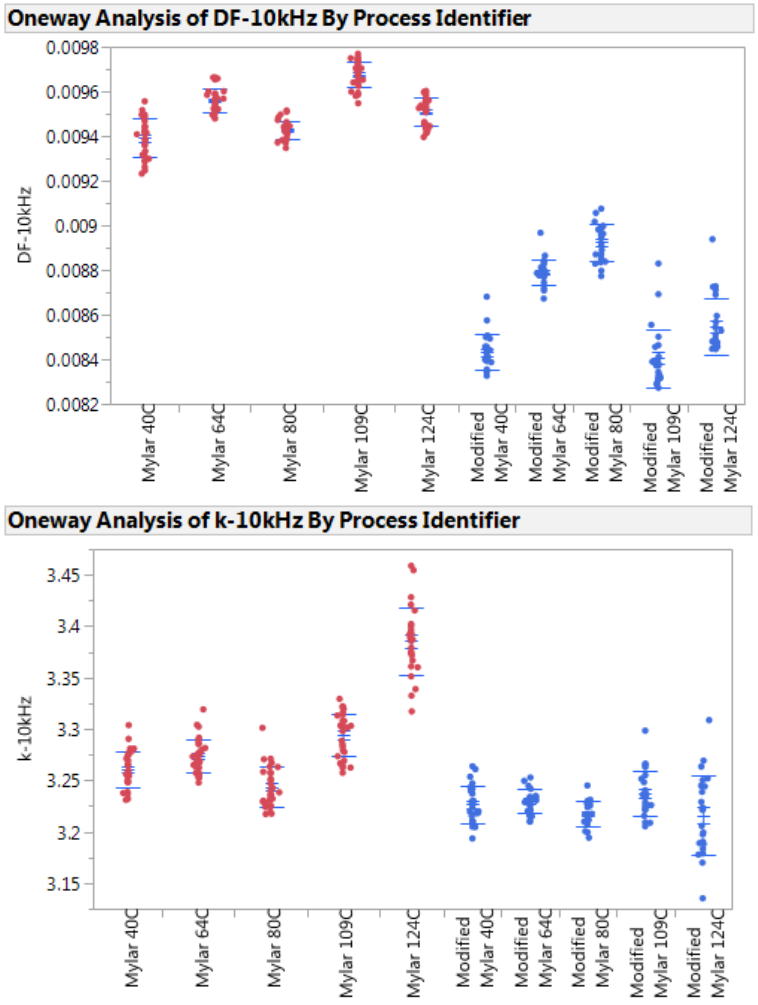
Oneway Analysis of DF-10kHz By Process Identifier
DF-10kHz
0.0098
0.0096
0.0094
0.0092
0.009
0.0088
0.0086
0.0084
0.0082
Mylar 40C
Mylar 64C
Mylar 80C
Mylar 109C
Mylar 124C
Modified Mylar 40C
Modified Mylar 64C
Modified Mylar 80C
Modified Mylar 109C
Modified Mylar 124C
Oneway Analysis of k-10kHz By Process Identifier
k-10kHz
3.45
3.4
3.35
3.3
3.25
3.2
3.15
Mylar 40C
Mylar 64C
Mylar 80C
Mylar 109C
Mylar 124C
Modified Mylar 40C
Modified Mylar 64C
Modified Mylar 80C
Modified Mylar 109C
Modified Mylar 124C

Dielectric Breakdown

T1: 1 day

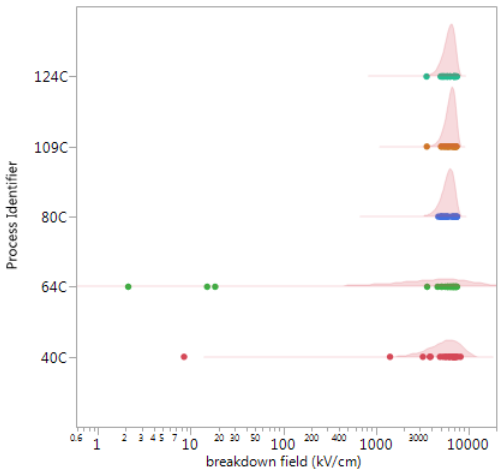

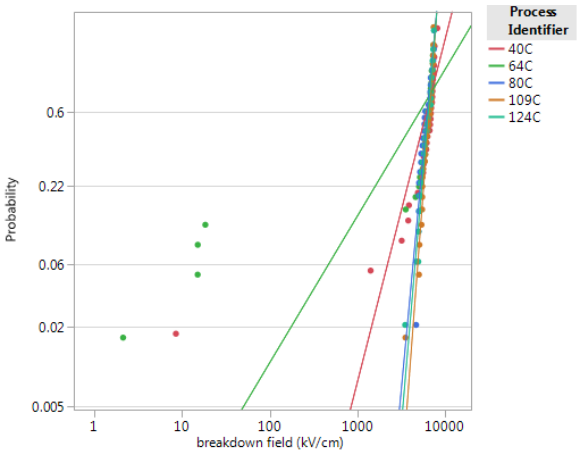

Estimates

Parameter	Estimate	Std Error	Lower 95%	Upper 95%
μ0	8.7647	0.07275	8.6222	8.9073
σ0	0.3800	0.06660	0.2495	0.5106
μ1	8.6291	0.16399	8.3077	8.9505
σ1	0.8878	0.15956	0.5750	1.2005
μ2	8.7644	0.03012	8.7054	8.8234
σ2	0.1392	0.02201	0.0961	0.1823
μ3	8.8117	0.02143	8.7697	8.8537
σ3	0.1119	0.01689	0.0788	0.1450
μ4	8.7868	0.02740	8.7331	8.8406
σ4	0.1277	0.02122	0.0862	0.1693
Weibull α 0	6404.3826	465.91079	5553.3293	7385.8607
Weibull β 0	2.6315	0.46119	1.9587	4.0083
Weibull α 1	5591.8892	916.99149	4054.8373	7711.5856
Weibull β 1	1.1264	0.20245	0.8330	1.7390
Weibull α 2	6402.1788	192.82558	6035.1863	6791.4877
Weibull β 2	7.1842	1.13592	5.4846	10.4104
Weibull α 3	6712.2610	143.85039	6436.1587	7000.2077
Weibull β 3	8.9348	1.34812	6.8956	12.6866
Weibull α 4	6547.5486	179.43042	6205.1491	6908.8416
Weibull β 4	7.8284	1.30042	5.9056	11.6076

T2: 3 days

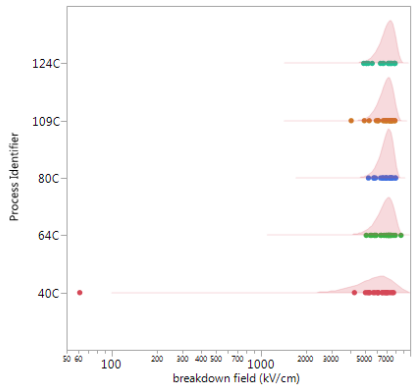

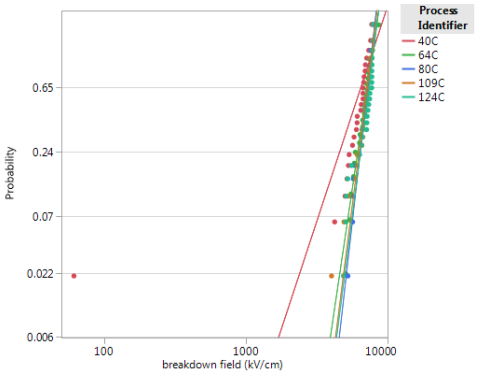

Estimates

Parameter	Estimate	Std Error	Lower 95%	Upper 95%
μ0	8.7642	0.05320	8.6599	8.8684
σ0	0.2579	0.04817	0.1635	0.3523
μ1	8.8746	0.02553	8.8246	8.9247
σ1	0.1158	0.01812	0.0803	0.1514
μ2	8.8805	0.01904	8.8432	8.9179
σ2	0.0887	0.01476	0.0598	0.1177
μ3	8.8763	0.02122	8.8347	8.9179
σ3	0.0998	0.01723	0.0660	0.1336
μ4	8.9007	0.02147	8.8586	8.9428
σ4	0.1010	0.01824	0.0653	0.1368
Weibull α 0	6400.7390	340.50661	5766.9725	7104.1537
Weibull β 0	3.8772	0.72408	2.8383	6.1157
Weibull α 1	7148.2049	182.48369	6799.3439	7514.9653
Weibull β 1	8.6330	1.35070	6.6070	12.4512
Weibull α 2	7190.6291	136.94066	6927.1778	7464.0999
Weibull β 2	11.2692	1.87406	8.4990	16.7184
Weibull α 3	7160.1261	151.97287	6868.3753	7464.2698
Weibull β 3	10.0191	1.72989	7.4858	15.1438
Weibull α 4	7337.1218	157.49543	7034.8398	7652.3927
Weibull β 4	9.8964	1.78610	7.3104	15.3132

References:

1. Whinfield, J. R. Chemistry of 'Terylene'. *Nature,* 1946, 930-931.
2. Whinfield, J. The Development of Terylene. *Textile Research Journal,* 1953, 289-293.
3. Reddish, W. The dielectric properties of polyethylene terephthalate (Terylene). *Transactions of the Faraday Society,* 1950, 459.
4. Amborski, L. E., & Flierl, D. W., Physical Properties of Polyethylene Terephthalate Films. *Industrial & Engineering Chemistry,* 1953, 2290-2295.
5. How Mylar Is Made, DuPont Product Information Sheet, DuPont Teijin Films, 2003.
6. A. R. Blythe, Electrical Properties of Polymers, Cambridge University Press, Cambridge, 1979.
7. Johnson, G., *Solid State Tesla Coil*, Tesla Museum and Science Center International Conference on Nikola Tesla, Farmingville, New York, 2006.
8. "Introduction to Capacitor Technologies", Kemet Corporation, 2013.
9. Dissado, L. A., & Fothergill, J. C., *Electrical degradation and breakdown in polymers*. London: P. Peregrinus, 1992.
10. Nelson,J.K., Breakdown Strength of Solids, in "Engineering Dielectrics Volume IIA Electrical Properties of Solid Insulating Materials: Molecular Structure and Behaviour," pp 445 - 520, R. Bartnikas and R.M. Eichorn, (eds)., ASTM Special Technical Publication 783, ASTM, 1983.

11. R. Bartnikas and R.M. Eichorn, Engineering Dielectrics Volume IIA Electrical Properties of Solid Insulating Materials: Molecular Structure and Behaviour, ASTM, Baltimore, 1983.
12. R. Stratton, "The Theory of Dielectric Breakdown in Solids," Progress in Dielectrics 3, 1961, 233-292.
13. Odwyer, J. *J. Advances in Physics*, 1958, 7, 349.
14. Mylar Polyester Film: Electrical Properties, DuPont Teijin Films. 2003.
15. Coburn, J. C., & Boyd, R. H., Dielectric relaxation in poly(ethylene terephthalate). *Macromolecules*, 1986, 2238-2245.
16. Reddish, W., The dielectric properties of polyethylene terephthalate (Terylene). *Transactions of the Faraday Society*, 1950, 459.
17. Lightfoot, S.; Xu, G.,Polymer –Plastics Technology and Engineering, 1993, 21-31.
18. Park, C. H.; Hara, M.; Akazaki, M., *IEEE Transactions on Electrical Insulation*, 1982, 17, 546.
19. Inuishi, Y.; Powers, D. A. *J. Appl. Phys.* 1957, 28, 1017.
20. Jow, T. R.; Cygan, P. J. *J. Appl. Phys.* 1993, 73, 5147.
21. Chen, G.; Fu, M.; Liu, X. Z.; Zhong, L. S. *J. Appl. Phys*. 2005, 97.
22. S. J. Laihonen, U. Gäfvert, T. Schütte and U. W. Gedde in *Proc. on IEEE Conf. on Electr. Insul. Dielectr. Phenomena (CEIDP)*, Boulder, USA, 2004, 563-567.
23. S. J. Laihonen, U. Gäfvert, T. Schütte and U. W. Gedde, *IEEE Transactions on Dielectrics and Electrical Insulation*, 2007, 263-274.

24. Diaham, S., S. Zelmat, M.-L. Locatelli, S. Dinculescu, M. Decup, and T. Lebey. "Dielectric Breakdown of Polyimide Films: Area, Thickness and Temperature Dependence." *IEEE Transactions on Dielectrics and Electrical Insulation IEEE Trans. Dielect. Electr. Insul.* 17.1, 2010, 18-27.
25. R. Bartnikas, and R.M. Eichorn, Engineering Dielectrics Volume IIB Electrical Properties of Solid Insulating Materials: Measurement Techniques, ASTM, Baltimore, 1983.
26. Chen, G.; Zhao, J. W.; Li, S. T.; Zhong, L. S. *Appl. Phys. Lett*. 2012, 100.
27. Hourquebie, P.; Marsacq, D.;Vallayer, B.;Olmedo, L., *IEEE Annual Report-Conference on Electrical Insulation and Dielectric Phenomena,* 1996.
28. Liu, N.; Chen, G.; Xu, Y., *High Voltage Engineering*, 2015, 1154-1166.
29. McKeown, J. *J. Proceedings of the Institution of Electrical Engineers*-London 1965, 112, 824.
30. Appelhans, L.N., "Dielectric Breakdown of Mylar and Doped Mylar Films" (SAND2013-8680), 2013.
31. Appelhans, L.N., *Belcher, C.B., Dielectric Breakdown in Mylar , Breakdown in Mylar and Doped Mylar*, Sandia Internal Memo, Sandia National Laboratories, September 2015.
32. D.K. Davies, *J. Phys. D. Appl. Phys.,* 5, 162 (1972).
33. Wexler, A., Hasegawa, S., "Relative Humidity-Temperature Relationships of Saturated Salt Solutions in the Temperature Range 0C to 50C" *Journal of Research of the National Bureau of Standards*, 1954, 21.
34. Walgenwitz, B., Tortai, J., Bonifaci, N., Denat, A., Self-Healing of Metallized

Polymer Films of Different Nature. *International Conference on Solid Dielectrics, 2004.*

35. J. Kammermaier, *G.* Rittmayer and S. Birkle, "Modeling of plasma-induced self-healing in organic dielectrics", *J. Appl. Phys.*, 1989, 1594-1609.
36. Hossain, M. M. Effect of humidity on the breakdown strength and diffusion characteristics of polymer film. *Bulletin Of Materials Science*, 1993, 699-707
37. Miyairi, K., Influence of Water on the Electric Breakdown of Polyethylene Terephthalate Films. *Japanese Journal Of Applied Physics*, 1981 , 2325-2328.
38. Bischoff, G. C.; Edwards, L. R. SAND 90-2362C, Sandia National Laboratories, 1990.
39. Appelhans, L. N.; Lifke, D. M.; Dirk, S. M.; Kristensen, R., Sandia Internal Memo, Sandia National Laboratories, September 25, 2012.
40. Appelhans, L. N.; Rutherford, B. M., Sandia Internal Memo, Sandia National Laboratories, August 11, 2013.
41. Edwards, L. R., Sandia Internal Memo, Sandia National Laboratories, 1993.
42. Chen, G.; Xu, Z. *J. Appl. Phys*. 2009, 106.
43. Raju, G., Dielectrics in Electric Fields, Marcel Dekker, Inc., New York, 2009.M
44. Mylar Physical-Thermal Properties Product Information Sheet, DuPont Teijin Films, 2003.
45. Zebouchi, N.; Malec, D. *J. Appl. Phys.*, vol. 83, pp. 6190-1692, 1998.
46. Jabarin, S.; Lofgren, E. *Polymer Engineering and Science,* vol. 26, pp.620-625, 1986.

47. Miyairi, K. (1981). Influence of Water on the Electric Breakdown of Polyethylene Terephthalate Films. *Japanese Journal Of Applied Physics, 20*(12), 2325-2328. doi:10.1143/JJAP.20.2325
48. Hudson, R. A. *British Plastics* 1953, *26*, 6.
49. Plawsky, J. L.; Borja, J.; Williams, B.; Riley, M. J.; Gill, W. N. *IEEE Transactions on Electron Devices* 2011, *58*, 4354.
50. Appelhans, L.N., *Study of Dielectric Breakdown in Mylar,* Sandia Internal Memo, Sandia National Laboratories, July 2014.
51. Klein, R. J.; Schroeder, J. L.; Cole, S. M.; Belcher, M. E.; Cole, P. J.; Lenhart, J.L. *Polymer* **2008**, *49*, 2632-2635.
52. Laihonen, S. J.; Gustafsson, A.; Gafvert, U.; Schutte, T.; Gedde, U. W. *IEEE Transactions on Dielectrics and Electrical Insulation* **2007**, *14*, 263.
53. Chen, G.; Tanaka, Y.; Takada, T.; Zhong, L., *IEEE Transactions on Dielectric and Electrical Insulation*, vol 11 pp.113-121, 2004.
54. Kurtz, S. R. *Applied Physics Letters* 1983, *43* (12), 1132.
55. Noguchi, K.; Okamoto, Y.; Sekii,Y, *2008 Annual Report Conference on Electrical Insulation Dielectric Phenomena*,2008.